THE UNIVERSITY OF CHICAGO

THE ARCHITECTURE OF RAD51 AND DMC1 IN MEIOTIC RECOMBINATION COMPLEXES

A DISSERTATION SUBMITTED TO

THE FACULTY OF THE DIVISION OF THE BIOLOGICAL SCIENCES

AND THE PRITZKER SCHOOL OF MEDICINE

IN CANDIDACY FOR THE DEGREE OF

DOCTOR OF PHILOSOPHY

DEPARTMENT OF MOLECULAR GENETICS AND CELL BIOLOGY

BY

MICHAEL SCOTT BROWN

CHICAGO, ILLINOIS

MARCH 2016

Table of Contents

List of figures

List of tables

Acknowledgements

Many thanks are owed to the people who directly contributed to this thesis or made a more personal impact on me during my graduate career. First, I would like to thank my advisor Doug Bishop for giving me the opportunity to do science every day and think broadly for the last six years. I am particularly thankful for his patience during the times when results were scarce. Second, I am grateful for everyone who has spent time in the lab over the years. It's been a great place to work. In particular, I need to thank Ling Chan for her friendship, guidance, and wisdom. I owe a debt of gratitude to Veronica Cloud, Jennifer Grubb, and Ling Chan for teaching me everything I needed to know in the lab and to Jennifer Grubb and Lawanda Stewart for doing a lot of day-to-day work that allowed me to concentrate on science. Third, I would like to acknowledge Annie Zhang, Matt Goodsmith, Andoni Garcia, Ivy Fitzgerald, Ben Glick, Mike Rust, Nerraj Joshi, Valentin Börner, Ling Chan, and Jennifer Grubb for their collaborative efforts. Fourth, I am thankful for the guidance of my committee members Jon Staley, Ben Glick, and Alex Ruthenburg. Finally, I am especially grateful for the support of my friends and family. In particular, I could never thank Tori enough for carrying me through grad school with her unwavering love and support.

Abstract

DNA double strand break (DSB) repair is essential to meiotic chromosome segregation. Rad51 and Dmc1 are DNA strand exchange proteins that cooperate in meiotic homologous recombination. Both proteins share very similar capabilities *in vitro*, but are functionally differentiated *in vivo*. Dmc1 is the catalytic recombinase; Rad51 plays a non-enzymatic accessory role, promoting Dmc1 assembly and directing recombination partner choice. The molecular architecture underlying this cooperation and functional differentiation is unknown. To better understand the mechanistic relationship between these meiotic recombinases, the structures of Rad51 and Dmc1 complexes were extensively characterized cytologically.

Rad51-Dmc1 co-foci commonly occur in pairs, separated by distances of up to 400 nm. Observations from *spo11* hypomorphic tetraploids, *spo11* mutants heterozygous for a VDE cut site, cytologically marked DSB hotpots, and spatial simulations suggest that a pair of Rad51-Dmc1 co-foci represent a single meiotic DSB. Co-focus pairing occurs at distances similar to that which separates sister chromatids but requires neither strand exchange nor synapsis. These results suggest that: 1. both Rad51 and Dmc1 co-occupy both ends of a meiotic DSB and 2. the two ends of a DSB are spatially separated.

Super-resolution direct stochastic optical reconstruction microscopy (dSTORM) reveals that Rad51 and Dmc1 filaments are extremely short and clustered *in vivo*. Meiotic Rad51 and Dmc1 super-resolution (sr) foci are little more than 100 nm long, corresponding to filaments a mere 40 protomers long or shorter. Additionally, multiple Rad51 and Dmc1 filaments likely occupy a single ssDNA tract. Careful controls demonstrated that these structural attributes are not artifacts of the imaging procedure and led to the correction of an artifact generated during

super-resolution image reconstruction. These results suggest that multiple, short Rad51 and Dmc1 filaments co-occupy a single tract of ssDNA.

In an effort to observe DNA recombination complexes in living cells, Rad51, Dmc1, and Rad52 were fused to fluorescent proteins or tetracysteine tags. The functionality of these proteins was characterized in mitotic and meiotic cells. Comparison of different cytological preparations suggests that the majority of recombination complexes are too small to be observed above background fluorescence in live cells. These results call into question the "recombination factory" paradigm and provide tools for future live cell imaging studies.

Chapter 1

Introduction

*This chapter is a slightly modified version of a published review: Brown, MS, Bishop, DK. 2015. DNA strand exchange and RecA homologs in meiosis. *Cold Spring Harb. Perspect. Biol.* 7:a016659. I wrote an initial draft that Doug Bishop supplemented and revised.

1.1 Chapter overview

Homology search and DNA strand exchange reactions are central to homologous recombination in meiosis. During meiosis, these processes are regulated such that the probability of choosing a homolog chromatid as recombination partner is enhanced relative to that of choosing a sister chromatid. This regulatory process occurs as homologous chromosomes pair in preparation for assembly of the synaptonemal complex. Two strand exchange proteins, Rad51 and Dmc1, cooperate in regulated homology search and strand exchange in most organisms. Here we summarize studies on the properties of these two proteins and their accessory factors. In addition, we review current models for the assembly of meiotic strand-exchange complexes and the possible mechanisms through which the interhomolog bias of recombination partner choice is achieved.

1.2 Introduction

Meiotic recombination creates genetic diversity and forms physical connections between homologous chromosomes, called chiasmata, that allow proper bipolar spindle attachment and thereby promote reductional chromosome segregation. Like recombinational repair in mitotic

cells, the core of the meiotic recombination pathway is the homology search for a recombination partner that results in the formation of heteroduplex DNA segments in which bases from the Watson strand of one chromatid are paired with bases from the Crick strand of the other. Meiotic recombination follows pre-meiotic S-phase such that the maternal and paternal chromosomes are both present as a pair of two identical sister chromatids. For recombination to execute its meiotic functions (pairing and crossing over), a region of DNA from one chromatid must form heteroduplex with the corresponding allelic DNA sequence on one of the two homolog chromatids, rather than the corresponding sequence on the sister chromatid.

Meiotic recombination is initiated by DSBs formed by the Spo11 transesterase and its many co-factors (Fig 1.1) (Hunter, 2007; Lam and Keeney, 2015). The pair of DNA ends formed by Spo11 are nucleolytically processed, yielding 3' single stranded tails. Recombinosomes assemble *de novo* by binding 3' single strand tails and then carry out homology search and DNA strand exchange. Initial homology recognition and strand exchange forms a displacement loop (D-loop) that is inferred to be unstable *in vivo.* D-loops can form by invasion of a homolog chromatid or a sister; however, while invasion of the sister can lead to DSB repair, it cannot produce a chiasma—the physical connection between homologs required for reductional segregation. The nascent D-loop formed by strand exchange has one of two fates. First, after extension of the invading end by polymerase, a D-loop can be dismantled, leading to DSB repair by the synthesis-dependent strand annealing mechanism (Fig 1.1 Dii,Div). In this case, the product of the recombination event is a non-crossover recombinant (NCO), i.e. a product in which the chromosome arms that flank the site of recombination retain their starting configuration. The second potential fate of a nascent D-loop is stabilization to form a long-lived intermediate called a single end invasion (SEI). SEIs usually go on to engage or "capture" the

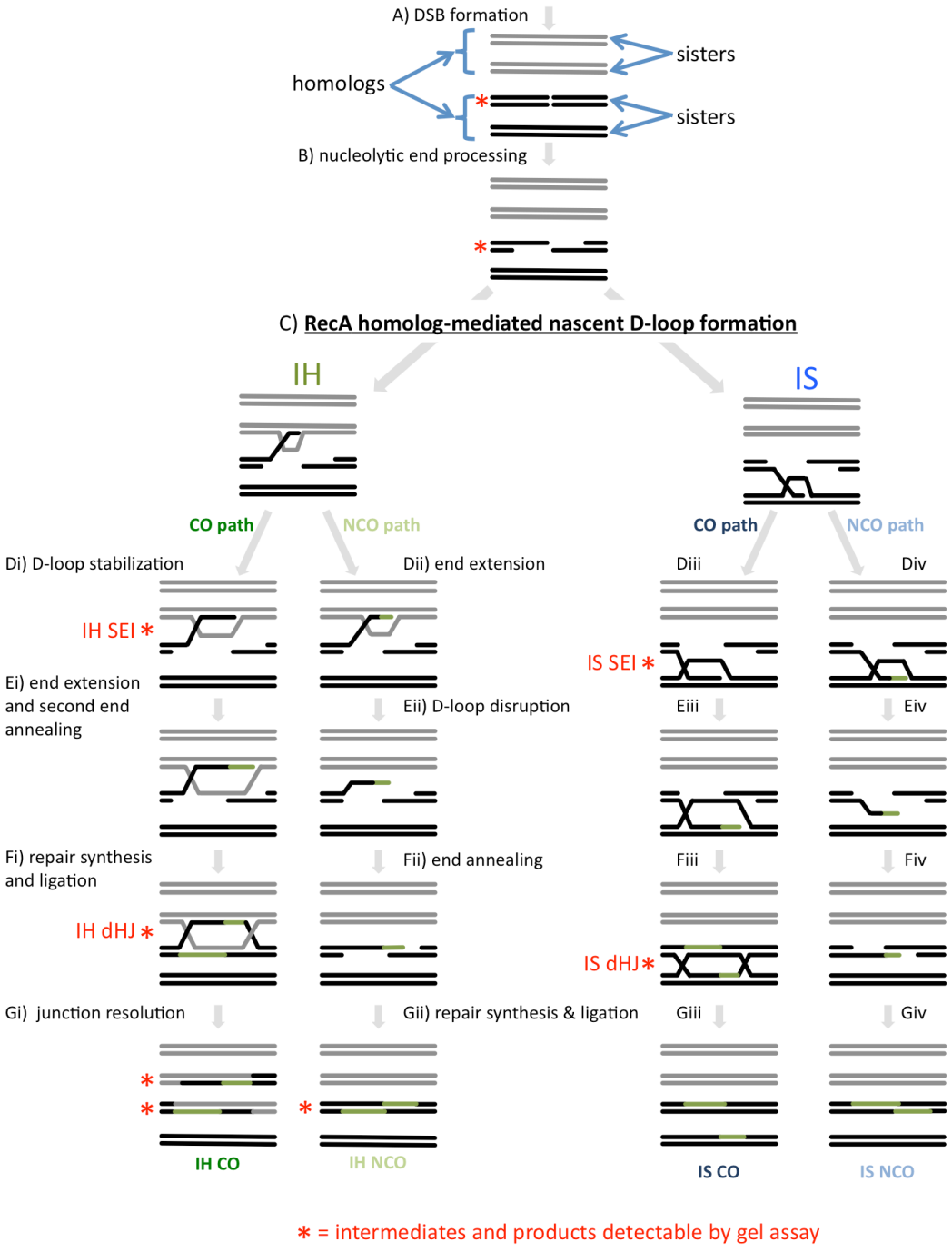

Figure 1.1 Meiotic recombination pathways. Four distinct recombination pathways can repair a meiotic DSB. Both strands of all 4 sister chromatids are shown with black and gray lines representing the two homologous chromosomes. Red asterisks indicate recombination intermediates and products that can be observed by Southern blots. (**A**) Meiotic recombination is initiated by the programmed introduction of DSBs. (**B**) 5' to 3' nucleolytic resection generates 3' ssDNA tails on both sides of the DSB. (**C**) RecA homologs locate an intact repair template on a

Figure 1.1 cont. homologous chromatid or the sister chromatid and catalyze strand exchange, generating a nascent D-loop intermediate. This D-loop structure is not stable enough to be observed in physical assays. (**Di**) IH COs are formed when the nascent strand invasion of a homologous chromatid is stabilized. The resulting JM is called an IH SEI. (**Ei**) Restorative DNA synthesis from the invading 3' end (shown in green) extends the D-loop, allowing annealing of the 2nd end of the DSB. (**Fi**) Further DNA synthesis and ligation of the remaining nicks generates an IH dHJ. (**Gi**) Resolution of the IH dHJ generates an IH CO in which the flanking DNA sequences are reciprocally exchanged. (**Dii-Gii**) IH NCOs are formed by an SDSA mechanism when an IH nascent JM is not stabilized. (**Dii**) DNA synthesis extends the 3' end of a nascent D-loop. (**Eii**) The D-loop is disrupted. (**Fii**) This extended 3' end anneals to the ssDNA tract on the opposite end. (**Gii**) Following further DNA synthesis and ligation, an IH NCO is formed. There is no reciprocal exchange of flanking regions in this recombination product. (**Diii-Giii**) Beside the choice of repair template, an IS CO is formed through the same biochemical steps as an IH CO. (**Div-Giv**) Similarly, an IS NCO forms through the same SDSA steps as an IH NCO.

opposite or "second" DNA end from the same DSB, either by single strand annealing or an independent strand invasion (Fig 1.1 Di,Diii). Capture of the opposite DSB end then leads to formation of another meta-stable intermediate, the double Holliday junction (dHJ). Most dHJs are resolved to form reciprocal crossover products (COs) leading to formation of chiasmata.

This review is focused on the activity of DNA strand-exchange proteins in forming D-loops and on factors that regulate that activity. Space limitations prevent us from discussing every significant finding. We therefore focus on studies in budding yeast for which *in vivo* analysis of recombination intermediates is most advanced, although a number of important findings from other organisms are also discussed. We also recommend previous reviews on this subject by Zickler, Kleckner, and Hunter (Hunter, 2007; Zickler and Kleckner, 1999).

1.3 Meiotic strand exchange proteins

Most eukaryotic organisms possess two structural and functional homologs of the bacterial strand-exchange protein RecA, Rad51 and Dmc1, which cooperate during meiotic recombination. Rad51 is the only RecA-like strand-exchange protein that contributes to mitotic

recombination, but it also functions during meiotic recombination. Dmc1's function is meiosis-specific. The *RAD51* and *DMC1* genes diverged following a gene duplication that occurred around the time of divergence of the pro- and eukaryotic kingdoms (Ramesh et al., 2005; Stassen et al., 1997). Most organisms that undergo meiosis fall into one of two categories with respect to Rad51 and Dmc1. The first category has orthologs of both Rad51 and Dmc1; in these organisms both proteins are involved in meiotic recombination and required for the pairing and synapsis of homologs. The second category of organisms has Rad51, but lacks Dmc1. Organisms that possess both Rad51 and Dmc1 include budding and fission yeast, plants, and mammals. The "Rad51-only" group of organisms includes *Drosophila melanogaster*, *Caenorhabditis elegans*, and the fungus *Sordaria macrospora*. *D. melanogaster* and *C. elegans* are both capable of pairing and synapsing homologs in the absence of recombination (Dernburg et al., 1998; McKim et al., 1998; Villeneuve and Hillers, 2001). *S. macrospora* is a counterexample in that it lacks Dmc1, but depends on Rad51 for homolog alignment and synapsis (Storlazzi et al., 2003). Phylogenetic studies show that "Rad51-only" organisms arose relatively recently by loss of the *DMC1* gene rather than by divergence prior to the duplication from which it arose (Ramesh et al., 2005). Genes coding for key Dmc1 accessory factors, including the *HOP2* and *MND1* genes, are also absent in the lineages that have lost Dmc1, suggesting that the function of the three proteins is interdependent (Ramesh et al., 2005; Villeneuve and Hillers, 2001). Keeping this history in mind may be useful in understanding the functional specialization of the two proteins and the mechanism(s) through which Dmc1-specific functions have been bypassed in "Rad51-only" species.

Rad51 and Dmc1 were first identified in budding yeast. The *DMC1* gene was discovered on the basis of its meiosis-specific expression (Bishop et al., 1992)[NB: Dmc1 officially stands

for disrupted meiotic cDNA, but the name was also intended as an homage to the rap group RUN DMC.] Sequencing of a *DMC1* cDNA revealed 26% amino acid identity with RecA. Dmc1 is called Lim15 in *Lilium longiflorum* and *Coprinus cinereus* (Hotta et al., 1995; Kobayashi et al., 1994).

The *RAD51* gene was discovered, along with the other members of the *RAD50-57* series of genes, on the basis of its role in repairing DNA damage caused by ionizing radiation (Game and Mortimer, 1974; Game et al., 1980). These genes were also shown to be required for production of viable spores. The structural similarity between Rad51 and RecA was discovered by cloning and sequencing members of the *RAD52* epistasis group of recombination genes. This directed effort was based on the assumption that RecA's structure and function would be conserved in evolution (Shinohara et al., 1992). The "core" domain of Rad51 was found to be 30% identical to RecA. Budding yeast Rad51 and Dmc1 are 45% identical to one another; however, the N- and C- termini of the three proteins are unrelated. The name Rad51 is used to refer to orthologs in most species, but the *Drosophila* protein is called SpnA and the *S. pombe* protein Rhp51 (Jang et al., 1994; Staeva-Vieira et al., 2003).

Budding yeast *dmc1* mutants are blocked at the strand-exchange step of recombination and accumulate processed DSBs (Bishop et al., 1992; Schwacha and Kleckner, 1997). Homolog pairing and assembly of synaptonemal complexes are also defective. Most *dmc1* mutant cells arrest in meiotic prophase due to checkpoint activation. Budding yeast *rad51* mutants also accumulate DSBs, although the amount of residual recombination is greater in *rad51* than in *dmc1* mutants and a subset of cells progress through meiosis and form spores (Bishop et al., 1992; Shinohara et al., 1992; 1997). However, the spores produced by *rad51* mutants are dead due to inefficient DSB repair. If the checkpoint mechanism that causes prophase arrest in *dmc1*

mutants is inactivated, *dmc1* mutant cells execute meiotic divisions in the presence of unrepaired DSBs and form dead spores (Lydall et al., 1996).

Either Rad51 or Dmc1 alone is capable of repairing meiotic DSBs; however, both RecA homologs are required to efficiently produce viable spores (Bishop et al., 1992; Shinohara et al., 1992; Tsubouchi and Roeder, 2006). A recent study has clarified these roles by demonstrating that while Rad51 is essential for efficient meiotic recombination, its strand-exchange activity is dispensable (Cloud et al., 2012). In accord with the dispensability of Rad51's strand exchange activity, this function is specifically inhibited during meiosis by direct binding of a protein called Hed1 (Busygina et al., 2008; Tsubouchi and Roeder, 2006). Therefore, Dmc1 is the essential DNA strand-exchange factor for meiotic interhomolog recombination, while Rad51 performs a critical regulatory role (discussed below).

1.4 Biochemical comparison of Rad51 and Dmc1 activity

The biochemical properties of Rad51 are reviewed in detail elsewhere (Morrical, 2015); we will therefore limit this discussion to biochemical studies of Dmc1's properties and compare them with those of Rad51.

Biochemical studies of Dmc1 have, by and large, revealed striking similarities between its activity and that of Rad51 (Baumann et al., 1996; Hong et al., 2001; Li et al., 1997; Sung, 1994). Both proteins have the ability to promote homology search and strand invasion/assimilation in the displacement loop (D-loop) assay. Both bind ATP via a Walker box motif and are weak DNA-dependent ATPases, with k_{cat}'s of around 1.0 min^{-1} or less. Both proteins oligomerize on both ssDNA and dsDNA forming right-handed nucleoprotein filaments (Bugreev et al., 2005; Lee et al., 2005; Ogawa et al., 1993; Sauvageau et al., 2005; Sehorn et al.,

2004; Sheridan et al., 2008). The DNA in these filaments is underwound and extended 1.5 fold resulting in a conformation with 18 nt (or bps) and 6 protomers per helical turn. The filament has a helical pitch of 10 nm. It should be noted that two structural studies suggested Dmc1 might incorporate a different number of nucleotides per helical turn than Rad51 (Lee et al., 2005; Okorokov et al., 2010). However, more recent EM analysis provided definitive support for the canonical right-handed helical structure (Sheridan et al., 2008; Yu and Egelman, 2010).

In addition to a high affinity DNA binding site (site I), which is responsible for binding of protomers to form nucleoprotein filaments, RecA has a second low affinity binding site (site II) that binds and extends dsDNA during the homology search (Chen et al., 2008b; Danilowicz et al., 2012; Mazin and Kowalczykowski, 1996; 1998). In RecA, site II also associates with the displaced ssDNA strand following strand exchange. Although studied in less detail than in RecA, site II appears to be conserved in Rad51 and Dmc1 (Cloud et al., 2012; Danilowicz et al., 2013).

Both Rad51 and Dmc1 promote D-loop formation by first assembling into nucleoprotein filaments on ssDNA and then searching for homology in duplex DNA. However, both proteins nucleate filaments on dsDNA more rapidly than does RecA, and this dsDNA binding activity inhibits D-loop formation *in vitro*. As a result, D-loop reactions typically must be staged by allowing Dmc1-ssDNA filaments to form prior to addition of dsDNA substrates (Gupta et al., 1997; Hong et al., 2001; Sung and Robberson, 1995).

Although the activity of these proteins in the D-loop reaction is quite limited in the presence of ATP and Mg^{2+} (0.5 to 4%), substituting the non-hydrolyzable analogue AMP-PNP for ATP, or substituting Ca^{2+} for Mg^{2+} can stimulate D-loop formation around 10-fold, to levels closer to those observed with RecA (around 50%) (Bugreev and Mazin, 2004; Bugreev et al., 2005; Hong et al., 2001; Lee et al., 2005). Both of these conditions block ATP hydrolysis and

stabilize the 100 nm pitch of the filament, which is active in homology search and strand exchange. These findings also show that, like the reaction promoted by RecA, the homology search and strand exchange processes promoted by Rad51 and Dmc1 do not depend on the proteins' ability to hydrolyze ATP. Strand exchange is driven by product stability (Menetski et al., 1990; Peacock-Villada et al., 2012; Wittung et al., 1997).

Importantly, addition of certain accessory factors dramatically enhances the strand-exchange activities of both Rad51 and Dmc1 under conditions that are thought to be physiologically-relevant, involving Mg^{2+} and ATP as cofactors (Benson et al., 1998; New et al., 1998; Petukhova et al., 1998; 2005; Shinohara and Ogawa, 1998). Although non-physiologically high Ca^{2+} concentrations (low millimolar) have often been utilized to increase strand exchange efficiency (see above), a recent study demonstrates that micromolar Ca^{2+} promotes robust Dmc1 activity provided Mg^{2+} is also present at physiological concentrations (Chan et al., 2014). A crystal structure of an archael homolog of Dmc1 includes Ca^{2+} and Mg^{2+} bound to different sites in each protomer, and the same study showed Ca^{2+} stabilizes an active filament conformation (Qian et al., 2006). Thus, Ca^{2+} and Mg^{2+} are also likely to bind different sites in Dmc1.

One striking difference in the properties of Dmc1 and Rad51 is that Dmc1 has a much greater tendency to form octomeric ring structures in solution (Passy et al., 1999; Sehorn et al., 2004; Sheridan et al., 2008). The only crystal structure of Dmc1 at present is of the octomeric ring form, leading to the proposal that toroids might be the active form of the protein (Kinebuchi et al., 2004). However, the proposal is likely to be incorrect given that the same conditions which stimulate Dmc1 D-loop activity also stimulate the assembly of helical filaments on DNA (Lee et al., 2005; Sehorn et al., 2004). Thus, the functional significance of Dmc1's strong tendency to form toroids, if any, remains to be determined.

Another set of studies comparing the activities of Dmc1 and Rad51 found that the two proteins were similar to one another, and to RecA, in that the strand exchange reaction represents a second, kinetically-distinct phase that occurs after formation of a less stable homology-dependent ternary intermediate (Gupta et al., 2001). Furthermore, the efficiency of strand exchange displayed similar sensitivity to the GC content of substrates. These similarities suggest that the structure of the filament scaffold on which the core homologous recombination reaction occurs, and the general properties of the DNA-DNA interactions that occur on that scaffold, are quite similar for Rad51 and Dmc1. This conclusion, along with the other similarities between Rad51 and Dmc1 described above, implies that interactions with specialized cofactors are likely to be important for functional specialization of the two proteins *in vivo*.

Although the activities of Rad51 and Dmc1 have been found to be similar in many respects, an intriguing difference has been reported for the fission yeast orthologs involving the ability of these proteins to promote reciprocal strand exchange in 4-strand branch migration reactions (Murayama et al., 2011). A circular plasmid containing a single strand gap was tested for formation of joint molecules with a homologous linear duplex. One version of the linear duplex ended at the site of the 5' end of the ssDNA gap, the second version at the 3' end of the gap (Fig 1.2A). The first of these substrates can only initiate a 4-strand reaction in the 5' to 3' direction, the second only in the 3' to 5' direction. Rad51 and Dmc1 showed opposite substrate requirements for formation of 4-stranded joint molecules. Rad51 showed activity only for the 3' to 5' substrate, Dmc1 only for the 5' to 3' substrate. A key issue regarding the interpretation of these results comes from the fact that meiotic recombination involves intermediates with 3' single stranded tails (Bishop et al., 1992; Sun et al., 1991). Dmc1-mediated exchange in the 5' to 3' direction could extend hybrid DNA by invasion of duplex and

subsequent branch migration to a 3' end. Once the 3' end is reached, however, strand exchange is expected to cease; there is no obvious mechanism though which further branch migration could extend hybrid into a region of duplex such that a 4-strand reaction would ensue (Fig 1.2 A). The same study that showed directional preferences in the 4-strand reaction also used linear substrates to analyze the directionality of 3-strand reactions and found no directional preference for Rad51 vs. Dmc1 (Murayama et al., 2011) (Fig 1.2 B). Two possible roles for the 4-strand reaction promoted by Dmc1 were proposed; removal of Spo11-linked oligonucleotides from 3' ends, and extension of D-loops by assembly of Dmc1 on the displaced ssDNA strand. We note that it is also possible that the results of 4-strand reactions reflect different directionalities of Rad51 and Dmc1 polymerization on DNA. This idea is suggested to us by analogy to RecA, which both polymerizes and promotes branch migration with a 5' to 3' bias (Lindsley and Cox, 1990; Register and Griffith, 1985; Roca et al., 1990). The possibility is interesting in light of our current model for Rad51-Dmc1 cooperation in which Dmc1 filaments are seeded at the end of Rad51 filaments (see below). If Dmc1 filaments elongate 5' to 3', they would tend to extend to the 3' end of ssDNA tracts, while the Rad51 filaments would tend to extend towards ssDNA-dsDNA junctions (Fig 1.2 C). Furthermore, if Rad51 nucleates at a random position along a ssDNA tract, and polymerizes away from the 3' end, the maximum length of a subsequent Dmc1 filament will be predetermined. Thus, depending upon the position of Rad51 filament initiation, the relative lengths of Rad51 and Dmc1 filaments could differ from one event to the next (Fig 1.2 C).

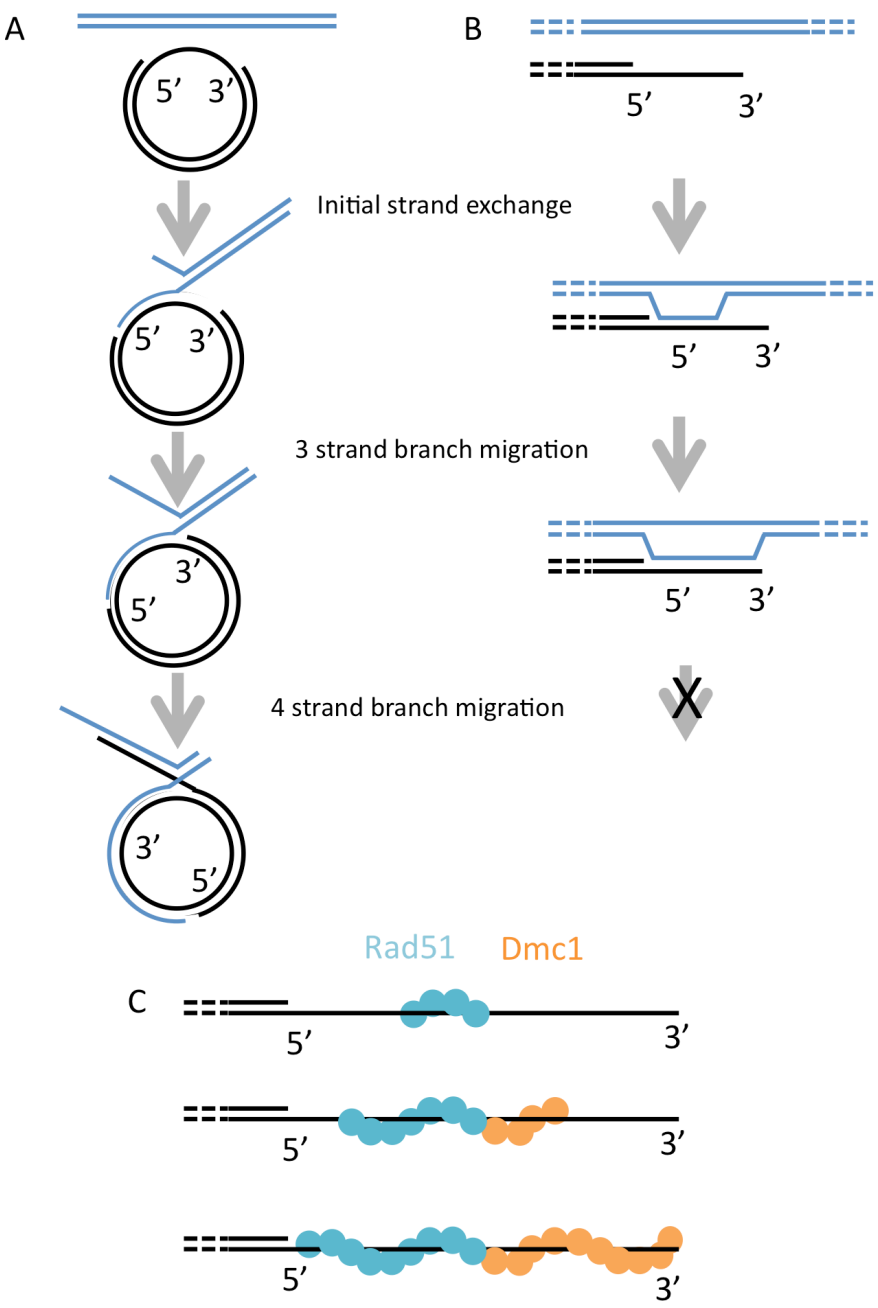

Figure 1.2 Directionality of Dmc1- vs. Rad51-mediated branch migration. (**A**) Diagramatic representation of the 4-strand reaction using substrates that can undergo conversion from 3-strand branch migration reactions to 4-strand reactions. The left side of the linear duplex substrate (blue) is homologous to the ssDNA gap on the circular substrate. Strand exchange initiates in the ssDNA gap, branch migration extends the tract of heteroduplex to the ssDNA-dsDNA junction at the 3' end of the ssDNA region. Then further 5'-3' branch migration results in reciprocal stand exchange via the 4 strand reaction. (**B**) Inferred consequence of 5'-3' branch migration on D-loops formed *in vivo*. Ends at DSB sites are processed to have 3' overhanging ssDNA tails. Branch migration is expected to proceed to the 3' end, but not be able to carry out a

Figure 1.2 cont. 4-strand reaction because an end has been reached. (**C**) Model for strand exchange filament elongation on 3' ssDNA tails. Rad51 (blue) nucleates filament formation. Dmc1 filaments (orange) are seeded at the end of a Rad51 filament. The direction of filament elongation is proposed to be the same as the direction of branch migration for the 4-strand reaction. Thus, the Rad51 filament is elongated in the 3'-5' direction, the Dmc1 filament elongated in the 5'-3' direction. This will tend to completely coat the entire ssDNA region, and perhaps lead to extension of the Rad51 filament into the flanking dsDNA.

Another study of human proteins examined the activity of the DNA translocase Rad54 on D-loops formed by Rad51 or Dmc1. Dmc1-associated D-loops were found to be more resistant to Rad54-mediated dissociation than were Rad51-associated D-loops (Bugreev et al., 2011). This result was interpreted to imply that the D-loops formed by Dmc1 are more stable than those formed by Rad51, and Dmc1-mediated stabilization of D-loops was interpreted to reflect a role for Dmc1 in channeling D-loop intermediates to the crossover rather than the non-crossover pathway. Although the experimental results of the study are convincing, the authors' interpretation of the results should be viewed with caution. Notably, this analysis did not take into account specificity of accessory factors for function with Rad51 vs. Dmc1. Biochemical and genetic observations indicate that, in spite of a high degree of functional overlap, Tid1/Rdh54 displays a marked preference for Dmc1 while Rad54 functions more efficiently with Rad51 (Dresser et al., 1997; Nimonkar et al., 2012; Shinohara et al., 2000). Thus, Rad54 is not a "neutral" reagent for comparing the stability of Rad51- vs. Dmc1-formed D-loops. It should also be noted that genetic studies indicate the biological function of Rad54 and Tid1/Rdh54 is to enhance the efficiency of the crossover pathway rather than channel intermediates away from it, as Mazin and colleagues suggested (as discussed in more detail below).

1.5 Cytological localization of Rad51 and Dmc1

The functional cooperation of Rad51 and Dmc1 during meiotic recombination raises the question of how the two RecA homologs are arranged at a DSB. The first cytological characterization of Rad51 and Dmc1 in budding yeast demonstrated that each formed a focal staining pattern in which the foci largely colocalized (Bishop, 1994). Focus formation depends on DSBs. This and other findings indicate that foci mark sites of ongoing recombination. Colocalization of Rad51 and Dmc1 foci, coupled with the functional cooperation of these RecA homologs in promoting the normal interhomolog bias of recombination, suggests that Rad51 and Dmc1 often reside at the same DSB site. However, Rad51 and Dmc1 foci do not precisely colocalize; rather, pairs of Rad51 and Dmc1 foci tend to be partially offset, lying side-by-side (Shinohara et al., 2000). This separation is consistent with 2-hybrid studies indicating that the two RecA homologs display strong homotypic interaction, and little heterotypic interaction (Dresser et al., 1997; Masson et al., 1999; Tarsounas et al., 1999). Cytological evidence for neighboring pairs of Rad51-Dmc1 homotypic filaments led to speculation that Rad51 might form a filament on one end of the DSB while Dmc1 forms a filament on the other (Shinohara et al., 2000). This speculation contributed to formal models in which the two ends of a DSB have distinct activities during recombination (Hong et al., 2013; Hunter and Kleckner, 2001; Hunter, 2007; Kim et al., 2010; Lao et al., 2008; Neale et al., 2005). Furthermore, a recent study of Rad51-Dmc1 staining patterns in *Arabidopsis* was interpreted as being consistent with the asymmetric loading model; Dmc1 foci were seen to lie adjacent to Rad51 foci (Kurzbauer et al., 2012). However, the asymmetric loading model does not easily accommodate our recent finding that Rad51 serves as an accessory factor for Dmc1-mediated D-loop formation both *in vivo* and *in vitro* (see below): Rad51 would need to stimulate Dmc1 filament assembly “in trans”, i.e. on

the end opposite to that which it is bound. If, rather than loading on just one side, loading of Rad51 occurs on both sides of a DSB, the overlapping or side-by-side Rad51-Dmc1 foci would be explained if the end of a homofilament of Rad51 served as a seed for initiating polymerization of a homofilament of Dmc1 (Fig 1.2 C, 1.3 C). This model predicts that each DSB instigates assembly of a pair of Rad51 filaments, each of which stimulates assembly of a Dmc1 filament. Consistent with this idea, our unpublished studies in budding yeast provide evidence that side-by-side Rad51-Dmc1 foci come in pairs (MSB, J. Grubb, and DKB unpublished).

It should also be noted that the longest dimension of the majority of Rad51 and Dmc1 structures visualized by conventional microscopy is usually shorter than the resolution limit of visible light (about 200 nm)(Bishop, 1994). Thus, immunostaining foci are resolution-limited "airy disks". Given that Rad51 and Dmc1 function by forming filaments on DNA, these filaments must usually be substantially shorter than 200 nm. If one assumes foci represent the helical nucleoprotein filaments described above, i.e. with one 10 nm helical turn containing 18 nt, the length of ssDNA within a diffraction limited focus is less than 400 nt. Thus, either filaments adopt a compressed configuration in cytological preparations, or they contain DNA tracts of less than 400 bases. This is also true of the majority of Rad51 staining structures observed in association with mitotic DNA damage repair (Bishop et al., 1998; Gasior et al., 2001; Haaf et al., 1995)

1.6 Accessory factors for Dmc1-mediated recombination

1.6.1 Mei5-Sae3

Dmc1's activity depends on the Mei5 and Sae3 proteins in budding yeast. Homologs of Mei5 and Sae3 are called Swi5 and Sfr1, respectively, in fission yeast and vertebrates. Mei5 and

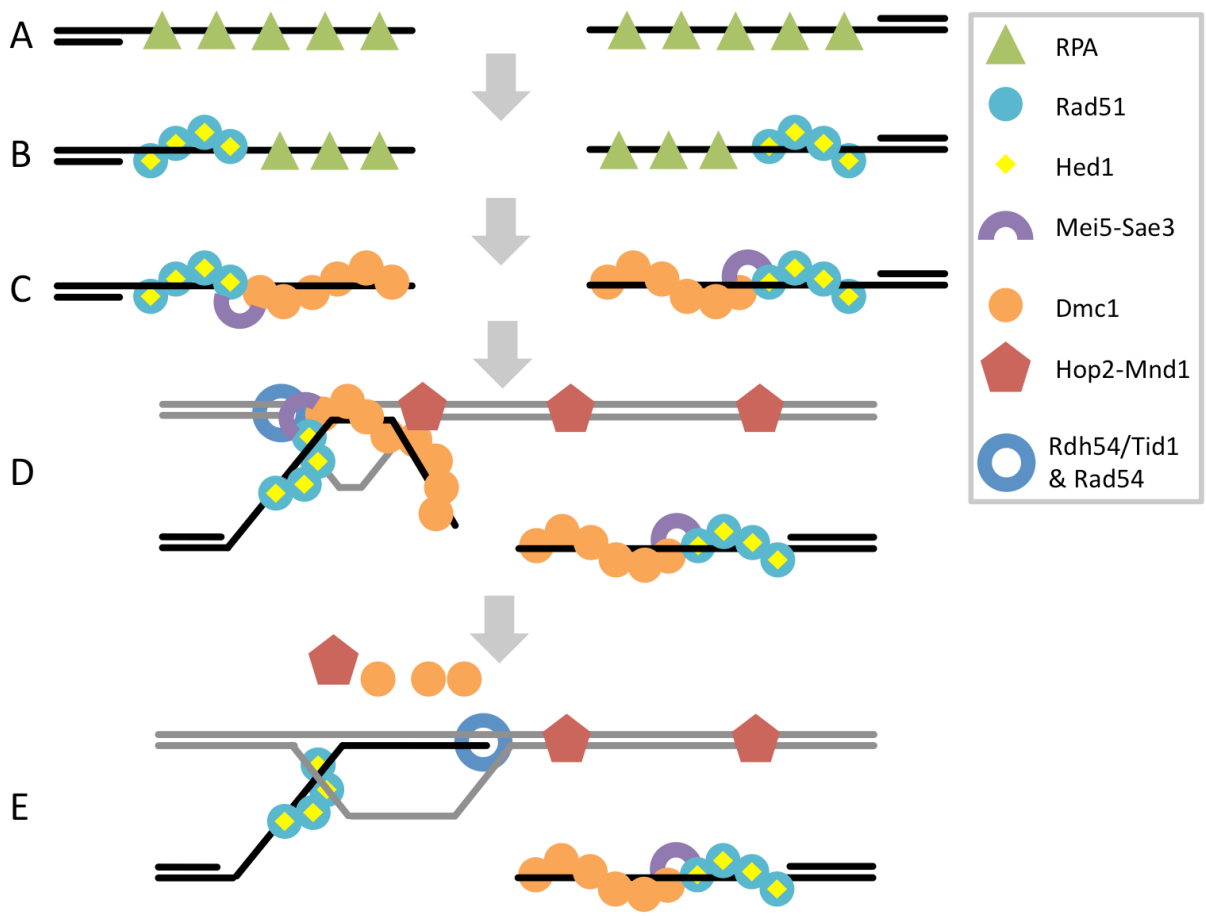

Figure 1.3 Working model for assembly and function of Rad51-Dmc1 recombinosomes. (**A**) RPA binds to ssDNA regions formed by nucleolytic resection of DNA ends. (**B**) Rad51, with the aid of mediator proteins (not shown), displaces RPA. Rad51 is prevented from forming D-loops by the inhibitory protein Hed1. (**C**) Mei5-Sae3 promotes initiation of Dmc1 filaments at the end of a Rad51 filament. Once initiated, Dmc1 filaments elongate on DNA by homotypic protomer-protomer interactions. (**D**) Dmc1 carries out a homology search culminating in formation of a segment of heteroduplex DNA. Efficient formation of D-loops by Dmc1 requires interaction of the searching filament with a complex of Hop2-Mnd1 bound to the target dsDNA. (**E**) The Rdh54/Tid1 translocase, or the Rad54 translocase, binds the Rad51 filament and translocates along the heteroduplex, simultaneously displacing Dmc1 and extending the heteroduplex tract to the 3' end. The end is thus rendered accessible for initiation of DNA synthesis.

Sae3 bind directly to one another to form a complex important for recruitment of Dmc1 to recombinosomes *in vivo* (Hayase et al., 2004; Tsubouchi and Roeder, 2004). Mei5 and Sae3 form immunonstaining foci that colocalize with each other and with foci formed by Dmc1.

Formation of Mei5-Sae3 foci is not observed in *dmc1* mutants indicating that normal association of Dmc1 and Mei5-Sae3 with chromatin is interdependent. Consistent with a role for Mei5-Sae3 in Dmc1 function, *mei5* and *sae3* mutants display clear phenotypic similarities to *dmc1* mutants including failure to repair meiotic DSBs, accumulation of Rad51 foci, defective assembly of synaptonemal complexes, and uniform meiotic arrest in prophase (Hayase et al., 2004; Tsubouchi and Roeder, 2004). In addition, Mei5-Sae3 foci do not form in a *rad51* mutant where weakly-staining Dmc1 foci are assembled (Hayase et al., 2004). Together these findings suggest that Mei5-Sae3 promotes Dmc1 assembly downstream of Rad51 loading, a conclusion supported by biochemical observations described below.

The finding that Mei5-Sae3 is required for Dmc1 focus formation *in vivo* suggested that it might directly stimulate assembly of Dmc1 nucleoprotein filaments. A common characteristic of proteins that mediate nucleoprotein filament assembly is that they can overcome the inhibitory effects of RPA bound to ssDNA (Gasior et al., 2001; San Filippo et al., 2008). RPA is a highly expressed protein that binds specifically to ssDNA. RPA is essential for replication and also plays critical roles in recombination, as reviewed in detail in this volume (Zelensky et al., 2014). Factors that promote the assembly of strand exchange proteins on RPA coated tracts of ssDNA are called recombination mediator proteins (for a more complete discussion of mediators, see (Zelensky et al., 2014)). The results of biochemical studies in budding yeast, fission yeast, and mouse indicate that Mei5-Sae3 and its homologs are capable of mediating Rad51 and Dmc1 filament formation.

Biochemical characterization of budding yeast Mei5 and Sae3, shows that the two proteins co-purify as a single complex (Ferrari et al., 2009; Hayase et al., 2004), as is also the case for orthologs in fission yeast and mammals (Kokabu et al., 2011; Say et al., 2011; Yuan and

Chen, 2011). The complex binds both ssDNA and dsDNA via contacts with Mei5 (Say et al., 2011). Electophoretic mobility shift assays show that binding of Mei5-Sae3 to ssDNA is preferred over dsDNA (Ferrari et al., 2009; Say et al., 2011). In addition, preferential binding to dsDNA-ssDNA forks has been observed and suggested to direct mammalian RAD51 or DMC1 filament assembly to the dsDNA-ssDNA junctions formed by nucleolytic 5' end resection (Say et al., 2011). However, the *in vivo* relevance of this fork-binding activity remains to be tested. It should also be noted that the intrinsic DNA binding activity of budding yeast Mei5-Sae3 is not sufficient for its stable association with recombination sites during meiosis because, as previously mentioned, *dmc1* mutants are severely defective for formation of Mei5-Sae3 foci (Hayase et al., 2004; Tsubouchi and Roeder, 2004). Similarly, Swi5-Sfr1 focus formation in mitotically cycling *S. pombe* cells requires Rhp51, the pombe Rad51 homolog (Akamatsu et al., 2007). In addition to binding DNA via Mei5, the Mei5-Sae3 complex has been shown to bind directly to three proteins: Rad51 and Dmc1 (both via the N-terminus of Mei5) and RPA (Ferrari et al., 2009; Hayase et al., 2004; Say et al., 2011).

Budding yeast Mei5-Sae3 has recombination mediator activity: it suppresses the inhibitory effect of adding RPA to D-loop reactions prior to addition of Dmc1 (Ferrari et al., 2009). Although budding yeast Mei5-Sae3 only stimulates Dmc1 activity (Ferrari et al., 2009; Say et al., 2011), the Swi5-Sfr1 heterodimer from fission yeast can enhance the activity of both Rad51 and Dmc1 *in vitro* (Haruta et al., 2006; Kurokawa et al., 2008). Similarly, *S. pombe* and human Mei5-Sae3 orthologs stimulate Rad51 *in vivo* (Akamatsu et al., 2007; Yuan and Chen, 2011). Thus, the specificity of Mei5-Sae3 for stimulating Dmc1 seen for budding yeast *in vivo* does not appear to be a conserved feature.

The requirement for both Rad51 and Mei5-Sae3 in Dmc1 focus formation suggested that Rad51 might function with Mei5-Sae3 to stimulate Dmc1 filament assembly (Bishop, 1994; Hayase et al., 2004; Tsubouchi and Roeder, 2004). This possibility is supported by the observation of robust simulation of Dmc1's D-loop activity by a combination of Rad51 and Mei5-Sae3 (Cloud et al., 2012). This synergistic effect of combining Rad51 and Mei5-Sae3 was observed under more physiological conditions than those used to detect mediator activity in the absence of Rad51 (high Mg^{2+} and low Ca^{2+} concentration as opposed to high Ca^{2+} only). The role of Rad51 in stimulating Dmc1 assembly may normally occur via nucleation of a Dmc1 homopolymer on the end of a growing Rad51 filament, a scenario that would explain the side-by-side localization pattern of Rad51 and Dmc1 foci (Fig 1.3 C). Furthermore, genetic observations suggest that Rad51 can contribute to Dmc1 focus formation in a *rad52* mutant background, in which cytologically visible Rad51 foci do not form (Bishop, 1994; Gasior et al., 1998; Gasior, 1999). This suggests that Rad51 can stimulate Dmc1 assembly without itself forming an extensive polymeric complex on DNA. Perhaps a minimal core complex composed of Rad51, Mei5, and Sae3 is sufficient to stimulate Dmc1 filament nucleation on ssDNA, or to stabilize such filaments once they form. Biochemical studies designed to determine the influence of Rad51, Mei5, and Sae3 on Dmc1 filament assembly are needed.

Overall, the biochemical properties of Mei5-Sae3 and its orthologs suggest that the protein has three related functions: assembly/stabilization of active Rad51 filaments, assembly/stabilization of Dmc1 filaments, and promoting the ability of Rad51 to enhance Dmc1 filament assembly/stabilization. All three of these activities are likely to be mechanistically related. Iwasaki and colleagues proposed that *S. pombe* Swi5-Sfr1 stabilizes filaments by binding to the helical groove, where its elongated form could bridge adjacent protomers of Rad51

(Kokabu et al., 2011). Structural analysis of *S. pombe* Swi5-Sfr1 revealed it to be an elongated and kinked alpha helical coiled-coil structure (Kokabu et al., 2011; Kuwabara et al., 2010; 2012) that could fit in the groove of a Rad51 or Dmc1 filament. If the protein does bind in the groove, it will be of interest to determine how such binding can occur without disruption of Rad51- (or Dmc1-) mediated homology search and strand exchange activities, which occur within the groove (Haruta et al., 2008; Kokabu et al., 2011; Kuwabara et al., 2012). Following Iwasaki's suggestion, an attractive possibility to explain the role of Mei5-Sae3's role in promoting Rad51-dependent Dmc1 activity is that it stabilizes protein-protein contacts between adjacent Rad51 and Dmc1 protomers by forming a bridge at the junction between end-to-end Rad51 and Dmc1 homofilaments on the same piece of ssDNA (Fig 1.3 C).

The meiotic function of Mei5-Sae3 homologs in other organisms might not be entirely conserved with *S. cerevisiae*. At the time of writing, there is no information on the meiotic functions of the mammalian complex (called Swi5-Sfr1 or Swi5-Mei5). Mutant analysis of meiotic recombination in *S. pombe* indicates that Swi5-Sfr1 is specifically required for interhomolog JM formation (but not for intersister JM formation) (Hyppa and Smith, 2010). However, the role of this putative interhomolog-specific Swi5-Sfr1 function appears to be distinct from that of Mei5-Sae3 in *S. cerevisiae* meiosis, because is seems to act through Rad51 and not Dmc1 at DSB hotspots (Hyppa and Smith, 2010). Yet, JM formation at DSB cold spots requires Rad51, Swi5-Sfr1, and Dmc1 (Hyppa and Smith, 2010); and Swi5-Sfr1 acts as a mediator of Dmc1 function *in vitro* (Haruta et al., 2006). These observations leave open the possibility that *S. pombe* Swi5-Sfr1 acts analogously to *S. cerevisiae* Mei5-Sae3 in wild type *S. pombe*.

1.6.2 Hop2-Mnd1

A second critical accessory factor in meiotic strand invasion and exchange is the Hop2-Mnd1 heterodimer. The *HOP2* gene was found in a screen for mutants defective in meiotic gene conversion (Leu et al., 1998). The *MND1* gene was identified among genes that are specifically expressed in meiosis as being required for DSB repair, JM formation, and chromosome segregation (Gerton and DeRisi, 2002; Rabitsch et al., 2001). Interaction between Hop2 and Mnd1 proteins was discovered following the demonstration that high copy numbers of *MND1* can suppress phenotypes associated with a non-null allele of *HOP2* (Tsubouchi and Roeder, 2002). Hop2 has been shown to bind Mnd1 in crude extract pull down experiments (Tsubouchi and Roeder, 2002) as well as by copurification (Chen et al., 2004; Petukhova et al., 2005; Pezza et al., 2006; 2007). Furthermore, molecular genetic and biophysical studies have established that the two proteins interact via coiled-coil motifs to form a tightly-bound heterodimeric complex with a stoichiometry of 1:1 (Pezza et al., 2006; Tsubouchi and Roeder, 2002). Small angle X-ray scattering analysis suggests that the heterodimer has a kinked, elongated V shape with the N-termini of both Hop2 and Mnd1 at the termini of the V (Zhao et al., 2014). Correspondingly, *hop2* and *mnd1* single mutant phenotypes are very similar to *hop2 mnd1* double mutant phenotypes: all show uniform prophase arrest in budding yeast with unrepaired DSBs and non-homologous pairing/synapsis (Chen et al., 2004; Gerton and DeRisi, 2002; Henry et al., 2006; Rabitsch et al., 2001; Tsubouchi and Roeder, 2002; Zierhut et al., 2004). Defects in meiotic recombination have also been reported for single mutants in mouse, Arabidopsis, and fission yeast (Domenichini et al., 2006; Kerzendorfer et al., 2006; Nabeshima et al., 2001; Panoli et al., 2006; Petukhova et al., 2003; Saito, 2004; Schommer et al., 2003; Vignard et al., 2007). Together these findings suggest that the major functional form of Hop2 and Mnd1 is the

heterodimeric form, although certain results involving the mouse homologs raise the possibility that Hop2 can contribute recombinogenic activity in the absence of Mnd1 both *in vitro* and *in vivo* (Pezza et al., 2006; 2014).

Additional findings led to the view that Hop2-Mnd1 functions to promote Dmc1-mediated homology search and strand exchange in budding yeast. First, there are strong phenotypic similarities between *dmc1*, *hop2*, and *mnd1* single mutants, and *dmc1 mnd1* or *dmc1 hop2* double mutant resemble *dmc1* single mutants (Henry et al., 2006; Tsubouchi and Roeder, 2002; Zierhut et al., 2004). Second, overexpression of *RAD51* was shown to bypass the arrest conferred by *mnd1* or *hop2* mutants, as was previously shown to be the case for *dmc1* mutants (Tsubouchi and Roeder, 2002; Zierhut et al., 2004) (see discussion below). Third, other mutations previously identified as being required for the uniform arrest observed in *dmc1* mutants were shown to also be required for arrest conferred by *hop2* or *mnd1* mutants (Henry et al., 2006; Tsubouchi and Roeder, 2002; Zierhut et al., 2004). Mutations that bypass arrest include those that block checkpoint signaling and axial element assembly (as described below in the section on "recombination partner choice"). Although no significant colocalization between Hop2-Mnd1 and Dmc1 has been observed (as discussed further below), Dmc1 foci and DSBs persist indefinitely in *hop2* and *mnd1* mutants suggesting Dmc1 is unable to promote JM formation in the absence of Hop2-Mnd1 *in vivo* (Gerton and DeRisi, 2002; Lao et al., 2013; Leu et al., 1998; Tsubouchi and Roeder, 2002; Zierhut et al., 2004). These findings support the hypothesis that Hop2-Mnd1 plays a specific role in promoting interhomolog recombination by functioning as a Dmc1 cofactor. The fact that Dmc1 foci form normally in the absence of Hop2-Mnd1 suggests that Hop2-Mnd1 acts on Dmc1 after the Mei5-Sae3 complex exerts its influence (Hayase et al., 2004; Tsubouchi and Roeder, 2002; Vignard et al., 2007; Zierhut et al., 2004).

Initial biochemical studies of budding yeast Hop2-Mnd1 showed the protein stimulates Dmc1 D-loop activity only 3-fold (Chen et al., 2004). However, this study was flawed because the Hop2 protein used lacked its normal C-terminal, which is coded by a third exon in the *HOP2* gene (Chan et al., 2014). The third exon had not been discovered at the time the expression construct used in the earlier experiments was built. Importantly, wild type Hop2-Mnd1 stimulates Dmc1 activity 30-fold or more. This dramatic stimulation was also found for the mouse and fission yeast proteins (Enomoto et al., 2006; Petukhova et al., 2005; Ploquin et al., 2007). Thus, Hop2-Mnd1 can be viewed as an essential co-factor for Dmc1's homology search and strand exchange functions *in vivo* and *in vitro*.

A number of different biochemical interactions have been proposed to play a role in the stimulation of Dmc1's strand invasion activity by Hop2-Mnd1. Direct interaction of Hop2-Mnd1 with Dmc1 has been observed by surface plasmon resonance (Petukhova et al., 2005). This direct interaction is likely to be responsible for the Hop2-Mnd1-mediated stabilization of ssDNA-Dmc1 filaments that has been observed *in vitro* (Pezza et al., 2007; Zhao et al., 2014). However, Hop2-Mnd1 binds DNA directly, preferring dsDNA to ssDNA (Chen et al. 2004; Enomoto et al. 2006). Furthermore, the finding that pre-incubation of duplex DNA with Hop2-Mnd1 provides optimal stimulation of yeast Dmc1 suggested that either non-specific dsDNA capture or alteration of the structure of duplex target might be important for the mechanism of stimulation (Chan et al., 2014; Chen et al., 2004). Indeed, affinity capture and co-sedimentation experiments using the mouse and human orthologs of Hop2-Mnd1 and Dmc1, respectively, have provided evidence for homology-independent capture of dsDNA by ssDNA-Dmc1 filaments (Pezza et al., 2007). A similar activity of Hop2-Mnd1 has been seen with ssDNA-Rad51 filaments (Chi et al., 2007). In addition, Hop2-Mnd1 has been shown to dramatically alter the structure of duplex

DNA via single molecule analysis which revealed that Hop2-Mnd1 can promote extensive condensation of duplex DNA (Pezza et al., 2010). These findings led to the hypothesis that Hop2-Mnd1 stimulates Dmc1-mediated homology searching by promoting non-specific binding of duplex by ssDNA-Dmc1 filaments followed by condensation of dsDNA in a manner that increases the rate of homology search (Pezza et al., 2010) (Fig 1.4 E).

Although Hop2-Mnd1 can stimulate certain Rad51 activities *in vitro*, it is unclear at present if this activity plays a significant role *in vivo* (Petukhova et al., 2005). One report suggested that *Arabidopsis* Mnd1 is capable of enhancing Rad51-mediated intersister repair in a *Dmc1*$^{-/-}$ mutant (Vignard et al., 2007), but a more recent and extensive study came to the opposite conclusion (Uanschou et al., 2013). Similarly, there are conflicting reports concerning the radiation sensitivity of somatic cells in *Mnd1*$^{-/-}$ mutants (Domenichini et al., 2006; Kerzendorfer et al., 2006). In budding yeast, Hop2 and Mnd1 are not required for Rad51-mediated meiotic recombination in the *dmc1 hed1* double mutant background (Lao et al., 2013). Furthermore, neither budding yeast Hop2-Mnd1 nor fission yeast Swi5-Sfr1 stimulates Rad51's D-loop activity *in vitro* (Chan et al., 2014; Ploquin et al., 2007). Finally, no evidence of Hop2-Mnd1 stimulation of Rad51 activity has been reported for *Hop2*$^{-/-}$ or *Mnd1*$^{-/-}$ knockout mice (Petukhova et al., 2003). Thus, further evidence is required to determine if Hop2-Mnd1 influences Rad51 activity *in vivo*. If it does, the function is likely to be a more recent evolutionary invention than the role of Hop2-Mnd1 in controlling Dmc1's activity.

Cytological characterization of Hop2-Mnd1 indicates that the protein associates with chromosomes independently of other components of the meiotic recombinosomes. Hop2 and Mnd1 localize to chromosomes in a dense focal staining pattern (Leu et al., 1998; Tsubouchi and Roeder, 2002; Zierhut et al., 2004). Surprisingly, Hop2-Mnd1 foci show key differences

compared to those formed by other proteins that play direct roles in D-loop formation. First, Hop2-Mnd1 foci form independently of DSBs (Leu et al., 1998; Tsubouchi and Roeder, 2002; Vignard et al., 2007; Zierhut et al., 2004). Second, in contrast to other accessory proteins, Hop2-Mnd1 foci do not show high levels of colocalization with Rad51 or Dmc1 (Tsubouchi and Roeder, 2002; Vignard et al., 2007; Zierhut et al., 2004). These findings led to the suggestion that Hop2-Mnd1 might influence the activity of recombinosomes indirectly via control of chromosome pairing interactions. This idea was supported by the finding that mutation of the *S. pombe* homolog of Hop2 (Meu13) reduced chromosome pairing somewhat in a *spo11* mutant background and that *S. cerevisiae hop2* mutants build synaptonemal complexes between non-homologous chromosomes (Nabeshima et al., 2001; Tsubouchi and Roeder, 2003). However, biochemical evidence for direct interaction between Hop2-Mnd1 and strand exchange proteins (Petukhova et al., 2005), as well as evidence showing that Hop2-Mnd1 can stimulate strand exchange in purified systems (Chan et al., 2014; Chen et al., 2004; Enomoto et al., 2006; Petukhova et al., 2005; Ploquin et al., 2007), suggest Hop2-Mnd1 functions directly at sites of meiotic recombination *in vivo*. The simplest explanation for the absence of significant colocalization between Dmc1 and Hop2-Mnd1 is that the dsDNA binding activity of Hop2-Mnd1 accounts for the presence of DSB-independent foci, and only a small fraction of Hop2-Mnd1 foci are associated with DNA recombination intermediates at any given moment, i.e. the preponderance of Hop2-Mnd1 complexes are not engaged with Dmc1 (and/or Rad51) may obscure the relatively small subset of complexes that are.

1.6.3 Tid1/Rdh54 and Rad54

The DNA translocase enzymes Rad54 and Tid1/Rdh54 both play a role in meiotic recombination. They possess a potent dsDNA-dependent ATPase activity and function as molecular motors, translocating along dsDNA. Although multiple mechanisms of translocase action have been proposed, it is important to emphasize that both translocases positively regulate meiotic recombination including crossing over (Ceballos and Heyer, 2011) (also reviewed in (Daley et al., 2014)). A *tid1* single mutant displays a substantial delay in forming JM crossover intermediates, but high levels of CO products are eventually formed (Shinohara et al., 1997; 2000; 2003b). A *rad54* mutant displays normal CO levels, but reduced spore viability (Schmuckli-Maurer and Heyer, 2000; Shinohara et al., 1997). Importantly, *rad54 tid1* double mutants rarely produce spores, and those produced are mostly inviable (Shinohara et al., 1997). Furthermore, recombinant products fail to form, DSBs persist, and end hyperresection occurs demonstrating a substantially redundant role for Rad54 and Tid1 in promoting both crossover and non-crossover recombination (Shinohara et al., 1997). In addition to this role in DSB repair, Rad54 and Tid1 have another role in preventing the sequestration of Rad51 and Dmc1 in non-recombinogenic complexes by displacing the proteins from dsDNA (Holzen et al., 2006; Shah et al., 2010).

The same dsDNA translocation activity can account for Rad54 and Tid1's roles in both promoting productive recombination and preventing non-recombinogenic complex formation. Biochemical studies have demonstrated that Rad54 is capable of stripping Rad51 from the heteroduplex formed at sites of strand invasion (Kiianitsa et al., 2006; Wright and Heyer, 2014). Given their partial redundancy and similar phenotypes *in vivo*, it seems likely that Tid1/Rdh54 and Rad54 function similarly. Thus, the translocases are probably recruited to the ends of Dmc1

and Rad51 filaments—whether recombinogenic or non-recombinogenic—and mediate their disassembly. In the case of recombinogenic filament disassembly, homology between the donor and acceptor chromatids would allow the translocase to act as a "heteroduplex pump" which mechanistically couples the extension of heteroduplex DNA, to stabilize the nascent joint molecule, with removal of RecA homolog protomers from the heteroduplex DNA product (Li and Heyer, 2008; Wright and Heyer, 2014) (Fig 1.3 D,E). Finally, the DNA translocases may also contribute to the efficiency of repair by virtue of their nucleosome remodeling activity, which could also act to stabilize D-loops (Alexeev et al., 2003; Hicks et al., 2011; Zhang et al., 2007).

1.6.4 MEIOB and SPATA22

Recently, genetic studies in mice identified two proteins, MEIOB and SPATA22, that are critical for fertility (Ishishita et al., 2013; La Salle et al., 2012; Luo et al., 2013; Souquet et al., 2013). MEIOB is of particular interest as it contains a so-called OB fold, which is common to proteins that bind specifically to tracts of ssDNA, including RPA. Indeed, biochemical experiments show that MEIOB binds ssDNA (Luo et al., 2013; Souquet et al., 2013). A truncated form of the protein was also found to have ssDNA-specific 3' exonuclease activity (Luo et al., 2013). Immunostaining studies show that both proteins display very high levels of interdependent co-localizing foci, which also co-localize with RPA. *Meiob*$^{-/-}$ single mutants display evidence of DNA damage accumulation and fail to form MLH1 foci (Luo et al., 2013; Souquet et al., 2013), which mark positions of crossovers in wild type cells (Anderson et al., 1999). RAD51 and DMC1 foci form in these mutants, but two studies reported that the foci do not persist as long as in wild type (Ishishita et al., 2013; Souquet et al., 2013). These results

implicate MEIOB and SPATA22 as components of the meiotic recombinosome that play a role during the RAD51/DMC1-dependent stage of recombination.

1.7 Regulation of recombination template choice during meiotic recombination

In diploids, each meiotic DSB could form a D-loop with any of three intact repair templates, one on the sister chromatid and two on the pair of homolog chromatids (Fig 1.1). Yet, meiotic DSBs are preferentially repaired using a homolog chromatid; interhomolog bias (IH bias) in budding yeast yields a 5:1 ratio of interhomolog to instersister JM species, exceeding the 2:1 ratio expected by random choice between the three available intact chromatids. This is in stark contrast with mitotic DSB repair which shows strong intersister (IS) bias (Bzymek et al., 2010; Jackson and Fink, 1985; Kadyk and Hartwell, 1992; Schwacha and Kleckner, 1994).

Southern blotting assays that allow detection of DNA intermediates and products of meiotic recombination have facilitated the study of IH bias in fungi (Cao et al., 1990; Cromie et al., 2006; Schwacha and Kleckner, 1994). In budding yeast, Southern blots of 2-D gels revealed that two JM intermediates—the single end invasion (SEI) and the double Holliday Junction (dHJ)—are biased towards the homolog chromatid rather than the sister chromatid (Hunter and Kleckner, 2001; Schwacha and Kleckner, 1995). In addition to these CO intermediates, 1-D gel electrophoresis variations can reveal both IH CO and NCO product levels. However, these physical assays cannot detect nascent D-loops—the last common intermediate between CO and NCO pathways—and are similarly unable to detect IS CO and NCO products. Additionally, assumptions are required to determine the lifetimes of intermediates. Despite these significant limitations, JM analysis via 2-D gels has driven our current understanding of the mechanism of partner choice in meiosis.

Using the 2-D gel assay, a number of proteins have been implicated by genetic analysis as being required for the 5-fold homolog bias observed in budding yeast *in vivo* (Hunter, 2007). Positive regulators of homolog bias include the RecA homologs Rad51 and Dmc1 (Schwacha and Kleckner, 1997), as well as DNA damage checkpoint signaling proteins (Grushcow et al., 1999; Shinohara et al., 2015; Thompson and Stahl, 1999), including components of the checkpoint clamp, the clamp loader, and the ATR/Mec1 checkpoint kinase. In budding yeast, the checkpoint clamp is composed of Rad17, Mec3, and Ddc1; the clamp loader is a derivative of the RFC complex that contains the checkpoint specific subunit Rad24 (Hochwagen and Amon, 2006). Also critical for IH bias is a set of proteins that are associated with the axial/lateral elements of the synaptonemal complex. These proteins include Red1 and Hop1, two abundant proteins that are thought to be structural components of axial/lateral elements of the SC, as well as Mek1, a key meiotic kinase whose activity depends on Red1 and Hop1. Importantly, Red1, Hop1, and Mek1 are downstream components of a DSB-dependent checkpoint signal in which Mec1- and Tel1-mediated phosphorylation of Hop1 is translated into a DSB-proximal Mek1 signal (Carballo et al., 2008; Niu et al., 2005; Wan et al., 2004). Finally, cohesin has been proposed to be a negative regulator of meiotic IH bias (Kim et al., 2010).

The identification of these players led to a number of molecular models of IH bias, although the critical aspects of the mechanism remain unclear. A key point of discussion has been whether homolog bias results from negative regulation of IS recombination or positive regulation of IH recombination (Callender and Hollingsworth, 2010; Hong et al., 2013). However, the two possibilities are not mutually exclusive and a number of results suggest that both modes of regulation are involved.

1.7.1 Rad51 and Dmc1 must cooperate to impose interhomolog bias of template choice

Although mutation of Dmc1 was shown to result in a strong block to meiotic recombination, it was later shown that this strong block requires Hed1, a protein capable of inhibiting the activity of Rad51 (Tsubouchi and Roeder, 2006). If Hed1 is eliminated, Rad51 is capable of promoting DSB repair. This Dmc1-independent activity of Rad51 results in eventual completion of the meiotic program for most cells and generation of tetrads in which about 65% of spores are viable. Among these spores, the frequency of IH recombination is only modestly reduced relative to that observed in wild type. These and earlier observations suggested that Rad51 is capable of substituting for Dmc1 or that Dmc1 play a relatively minor role in supporting Rad51's strand exchange activity, with Hed1 acting to prevent Rad51 from acting until Dmc1 is incorporated into recombinosomes. However, analysis of recombination intermediates showed that interhomolog bias is drastically diminished when Rad51 is activated to take the place of Dmc1 (Hong et al., 2013; Lao et al., 2013). This defect in interhomolog interactions is manifested by defects in the formation of interhomolog joint molecules, chromosome pairing and synapsis, and exit from prophase (Lao et al., 2013). Given that nearly normal levels of crossovers do eventually form in *dmc1 hed1* in spite of an extreme deficiency in interhomolog bias, it is clear that homeostatic mechanisms compensate, albeit incompletely, for the deficiency. Two mechanisms explain this compensation (Lao et al., 2013). First, a larger fraction of IH interactions results in formation of a CO as opposed to an NCO recombinant (Lao et al., 2013; Martini et al., 2006). Second, additional DSBs are inferred to form when homolog pairing/synapsis is inefficient and prophase is extended (Argunhan et al., 2013; Gray et al., 2013; Lao et al., 2013; Thacker et al., 2014). As a consequence of these two compensatory processes, normal or near-normal levels of COs eventually form in *hed1 dmc1* mutants. Thus, as in

organisms that lack a Dmc1 ortholog, budding yeast Rad51 can promote high levels of IH recombination in budding yeast, albeit with greatly reduced efficiency. However, homolog bias requires Dmc1.

Additional evidence that Dmc1 and Rad51 cooperate in meiosis comes from analysis of the *rad51* mutant, where Dmc1 can still form immunostaining foci and promote strand-exchange, albeit inefficiently (Schwacha and Kleckner, 1997; Shinohara et al., 2003a). The Dmc1 foci formed in *rad51* mutants are 3-fold dimmer on average than those formed in wild type suggesting that they reflect incomplete filament elongation (Bishop, 1994; Shinohara et al., 2003a). However, as seen when Rad51 catalyzes recombination in the absence of Dmc1, interhomolog bias is lost when Dmc1 catalyzes recombination in the absence of Rad51 (Schwacha and Kleckner, 1997).

Additionally, the formation of axial associations, that connect aligned but unsynapsed, homologs in budding yeast *zip1* mutants, requires both Rad51 and Dmc1 (Rockmill et al., 1995). Yet, despite the ability of either Rad51 or Dmc1 to catalyze strand invasion independently, the strand invasion activity of Rad51 is dispensable during meiosis (Cloud et al., 2012); a separation of function mutant that retains the ability to form helical filaments, but is deficient in D-loop formation, has normal IH bias and forms normal levels of recombination products. Thus, the RecA homologs normally cooperate during meiosis: Dmc1 catalyzes strand invasion and Rad51 directs this invasion towards a homolog chromatid.

Rad51 and Dmc1 appear to similarly cooperate in plants (Couteau et al., 1999). Like *S. cerevisiae*, Dmc1 appears to be the catalytic recombinase in *A. thaliana* meiosis, because a Rad51-GFP fusion supports normal meiosis despite being deficient in mitotic DNA repair (Cloud et al., 2012; Da Ines et al., 2013). Also similar to budding yeast, formation of wild type levels of

Dmc1 foci requires Rad51 (Kurzbauer et al., 2012; Vignard et al., 2007). Interestingly, the Rad51-independent assembly of Dmc1 foci is suppressed by ATR kinase in *A. thaliana* (Kurzbauer et al., 2012). It is currently unclear if a similar mode of regulation is present in other organisms. *rad51*, *dmc1*, and *rad51 dmc1 A. thaliana* mutants all display aberrant homolog alignment and synapsis (Couteau et al., 1999; Kurzbauer et al., 2012; Li et al., 2004; Vignard et al., 2007). However, in contrast to the arrest of budding yeast *dmc1* mutants, plant *dmc1* mutants progress and repair all meiotic DSBs via Rad51-mediated IS repair (Couteau et al., 1999; Vignard et al., 2007). This finding is consistent with the apparent absence of a Hed1 homolog in plants. It is possible that local assembly of Dmc1 inhibits Rad51's intersister repair activity in plants, as appears to be the case in budding yeast (Cole, 2014; Hong et al., 2013; Lao et al., 2013; Liu et al., 2014).

Despite the overwhelming evidence of cooperation between Rad51 and Dmc1, there are examples where the two RecA homologs appear to contribute different functions based on the location of a DSB. In *A. thaliana*, Dmc1-mediated recombination can promote centromere pairing independently of Rad51, while both Rad51 and Dmc1 are required for IH recombination and pairing of chromosome arms (Da Ines et al., 2012). In *S. pombe*, IH recombination at DSB hotspots appears to be independent of Dmc1; however, at DSB coldspots, both Rad51 and Dmc1 are required for IH JM formation (Hyppa and Smith, 2010). It should be noted that, in contrast to *S. cerevisiae*, there appears to be no IH bias at hotspots in *S. pombe* (Cromie et al., 2006; Hyppa and Smith, 2010); however, it is unclear if and how the lack of IH bias is connected to differential use of Dmc1 at DSB hotspots and coldspots. In both of these cases, at least one mode of IH recombination still requires both Rad51 and Dmc1.

1.7.2 Evidence for negative regulation of intersister recombination

A number of observations indicate that cells can negatively regulate IS recombination, leading to the proposal that homolog bias results from a kinetic impediment or barrier to sister chromatid recombination (BSCR; Fig 1.4 A). Key observations have utilized *dmc1* mutants, which assemble Rad51 complexes but fail to repair DSBs (Bishop, 1994; Bishop et al., 1992). In the absence of *red1* or *mek1* activity, *dmc1* mutants efficiently repair DSBs almost exclusively using the sister chromatid through a Rad51/Rad54-dependent pathway, suggesting the relaxation of a Red1-Mek1-imposed constraint on IS recombination (Niu et al., 2005; 2009; Schwacha and Kleckner, 1997). As mentioned above, a similar result pertains when a direct inhibitor of Rad51's activity, Hed1, is mutated in the absence of Dmc1: homolog bias is reduced 25-fold relative to that in wild type cells (Hong et al., 2013; Lao et al., 2013). Notably, Dmc1 itself also blocks Rad51's ability to promote IS recombination given that a *hed1* single mutant has only a modest reduction in homolog bias relative to a *hed1 dmc1* double mutant (Hong et al., 2013; Lao et al., 2013). Importantly, *red1*, *mek1*, and *hed1* single mutants also display defects in homolog bias, indicating that they play important roles during wild type meiosis (Hong et al., 2013; Kim et al., 2010; Lao et al., 2013; Rockmill and Roeder, 1990; 1991). Thus, Red1, Mek1, and Hed1 are all required to block Rad51-mediated IS recombination in *dmc1* mutant cells; while Red1, Mek1, and Dmc1 all act to limit Rad51's IS activity in the absence of Hed1.

Importantly, the BSCR is not specific to Rad51-mediated events. In addition to blocking Rad51-mediated events in a *dmc1* mutant, Mek1 appears to partially inhibit Dmc1-mediated IS DSB repair during haploid meiosis in a mutant in which Rad51 activity is diminished and no homologous chromatid is available (Callender and Hollingsworth, 2010). While the nature of this BSCR is still uncertain, Red1 clearly controls Mek1 kinase activity and specific inhibition of the

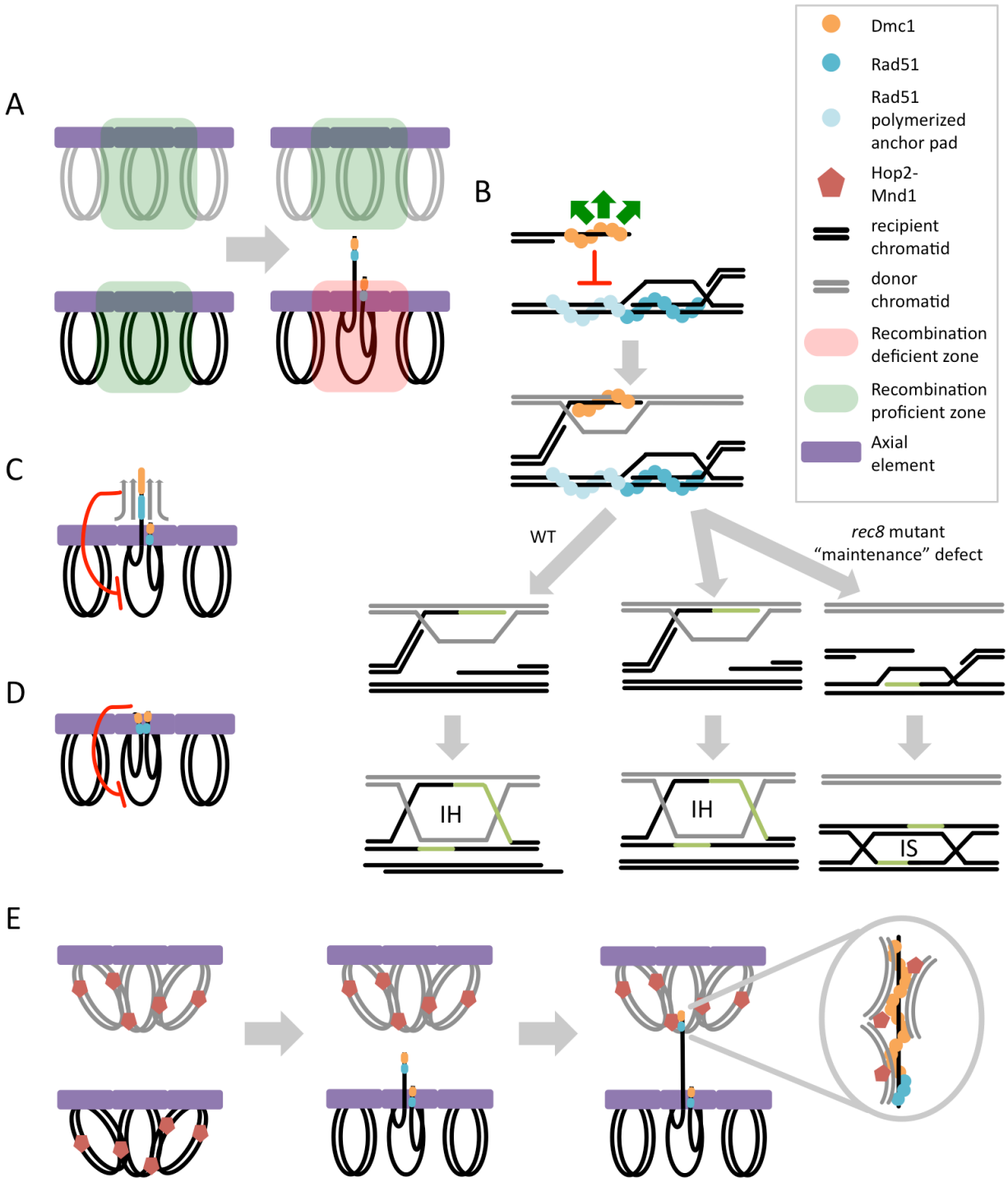

Figure 1.4 IH bias models. (**A**) Barrier to sister chromatid recombination (BSCR). In response to DSB formation, a local recombination deficient zone (red) is created on the recipient homolog. Since there are no DSBs at the allelic position on the homolog, the donor homolog remains a recombination proficient zone (green). (**B**) Anchor pad model. The Rad51 filament (blue) end of the DSB invades the sister chromatid. Further Rad51 polymerization beyond the D-loop (light

Figure 1.4 cont. blue) creates an "anchor pad" that blocks invasion of the sister chromatid by the Dmc1 end of the DSB. Left with no other choice, the Dmc1 end invades a homologous chromatid. In WT cells, this IH nascent interaction proceeds to an IH dHJ. In *rec8* cells, the nascent IH interaction has an equal probability of forming an IH or an IS dHJ. Note that the version of the model shown has Rad51 and Dmc1 loaded on opposite DSB ends (Hong et al. 2013). However, the model could be modified to account for loading of the two RecA homologs on both ends, (**C**) Steric hindrance model 1. A scaffold structure, dependent upon Rad51, projects the Dmc1 filament away from the recipient homolog axis. The scaffold precludes invasion of the sister chromatid. (**D**) Steric hindrance model 2. The DSB ends are held in close proximity to the recipient homolog axis, while the sister chromatid loop is distant from the axis. (**E**) Hop2-Mnd1 creates recombination proficient zones distant from DSBs. Hop2-Mnd1 associates with chromatin non-specifically, locally clustering DNA. A DSB on the recipient homolog results in local depletion of Hop2-Mnd1. Aided by Hop2-Mnd1-mediated clustering of chromatin, the Dmc1 filament is able to simultaneously sample discontinuous regions of chromatin for homology, but precluded from searching in the vicinity of the DSB due to the lack of Hop2-Mnd1. Note that, except for the cartoon of the anchor pad model in B), Rad51 and Dmc1 are both shown on both ends of a DSB. However, the originally proposed version of the anchor pad model (Hong et al. 2013) could be modified to account for symmetric RecA homolog loading.

Mek1 kinase, using an ATP analog sensitive *mek1-as* allele, strongly suggests that target phosphorylation is responsible for Mek1's role in homolog bias (Wan et al., 2004).

Three substrates of Mek1 kinase have been reported to date. First, Mek1 self-activates its kinase activity by autophosphorylation on threonine 327 (Niu et al., 2007). Second, Mek1-dependent phosphorylation occurs at threonine 11 of histone H3 (Govin et al., 2010). Although subsequent work showed that H3 is a direct substrate of Mek1, no overt recombination phenotypes have been found to be associated with a mutant form of H3 that cannot be phosphorylated (S. Keeney, personal communication). Finally, Mek1 phosporylates Rad54 on threonine 132. This modification of Rad54 can inhibit its activity *in vitro* and *in vivo* (Busygina et al., 2008; Niu et al., 2005; 2009). Nonetheless, it is currently unclear whether phosphorylation of Rad54 by Mek1 contributes to IH bias in wild type cells. This is because single mutant strains harboring the non-phosphorylatable allele of the *RAD54* gene, *rad54-T132A,* produce IH recombinants with normal efficiency, and also form viable meiotic products. Thus,

phosphorylation of Rad54 is unlikely to be a primary mechanism for promoting homolog bias. Two-dimensional gel analysis of IH bias in the *rad54-T132A* single mutant would address this outstanding question.

It is possible to infer that Mek1 phosphorylation of substrates other than Rad54 contributes to IH bias (Niu et al., 2009). One key observation is that the Rad51-repressive activity of Hed1 is largely, although not completely, Mek1-dependent (Lao et al., 2013; Niu et al., 2007). However, there were no reports implicating Hed1 as a substrate of Mek1 at the time this review was prepared.

Mek1-mediated repression of Rad51's strand exchange activity via Hed1 may be lifted late in meiosis, during a "clean up" phase in which a mitotic-like IS repair pathway ensures that all DSBs are repaired (Sheridan and Bishop, 2006). Consistent with this late idea, in *C. elegans*, IH recombination is shut down late in meiosis and IS recombination predominates (Rosu et al., 2011). In addition to contributing to the BSCR, Mek1 activity is also inferred to be a positive regulator of IH recombination (discussed below), further emphasizing the fact that additional Mek1 substrates remain to be discovered.

1.7.3 Evidence for positive regulation of interhomolog recombination

Since Dmc1 directly catalyzes homology search and strand invasion, the incorrect choice of recombination partner in *rad51* mutants implies that IH bias is positively imposed during normal meiosis, overruling the default propensity for IS recombination (Cloud et al., 2012; Schwacha and Kleckner, 1997). Furthermore, mutant analysis suggests that Mek1 kinase activity may confer two distinct regulatory effects on Dmc1's IH strand exchange activity. First, completely eliminating Red1 or Mek1 function using null mutations blocks Dmc1-dependent JM

formation (Hong et al., 2013). Second, low levels of Red1 function allow Dmc1-mediated joint molecule formation, but do not support IH bias (Schwacha and Kleckner, 1997). Thus, in addition to negatively regulating Rad51's activity via Hed1, Mek1 acts as a positive regulator of Dmc1's JM forming activity.

In addition to the positive regulation of Dmc1's activity by Rad51 and Mek1 signaling, a recent study concluded that local regulation of the meiosis-specific cohesin component Rec8 positively regulates IH recombination (Hong et al., 2013; Kim et al., 2010). Specifically, cohesin is inferred to direct recombination between sisters and the Rad51-Mek1 ensemble removes this constraint to IH recombination. This study distinguished two classes of homolog bias mutants, a highly-defective class with IH:IS dHJ ratios of 1:5 or less (wild type bias is 5:1) and a second class, that results in the less severe IH:IS dHJ ratio of *exactly* 1:1. Mutants lacking a RecA homolog, Red1, or Mek1 represent the first class, while mutants lacking Rec8 constitute the second class. Importantly, *rec8 red1, rec8 rad51,* and *rec8 hed1 dmc1* mutants all display the less severe 1:1 IH:IS defect of the *rec8* single mutant rather than the more severe defects of *red1, rad51,* or *hed1 dmc1* mutants (Hong et al., 2013; Kim et al., 2010). These results support the inference that Rec8 negatively regulates IH recombination and Red1-Mek1 signaling overcomes this negative effect to enhance the efficiency of IH recombination.

1.7.4 Recombination between sisters is not completely blocked in DMC1$^+$ meiosis

Although IS repair of DSBs is completely blocked in *dmc1* mutants, IS recombination does occur during normal meiotic recombination. DSBs formed at hemizgyous loci—where repair is only possible via IS recombination—are efficiently repaired during otherwise wild type meiosis (Goldfarb and Lichten, 2010). Interestingly, the timing of DSB repair was equivalent

whether the DSB occurred in a homozygous or hemizygous region; however, the rate of this IS repair at both homozygous and hemizygous loci is increased in *mek1* mutants. To account for these findings, a kinetic model of IH bias was proposed in which the relative rates of IS and IH strand exchange are skewed to favor IH recombination (Goldfarb and Lichten, 2010). Specifically, Mek1 signaling imposes a kinetic brake on IS recombination and the degree of this negative regulation determines the relative rates at which IH and IS repair proceed. Similarly, in haploid yeast engineered to enter meiosis—where every DSB lacks a homologous chromatid repair template—there is a Mek1-dependent delay in IS recombination (Callender and Hollingsworth, 2010; De Massy et al., 1994). Thus, regardless of the presence of a non-sister chromatid, Mek1 limits the rate of IS recombination. In addition to controlling the relative rates of IH and IS recombination, Mek1 signaling modulates CO vs. NCO repair choice (Goldfarb and Lichten, 2010). The increased rate of intersister DSB repair at hemizygous sites in a *mek1* mutant is not associated with a corresponding increase in IS JMs, suggesting increased use of an NCO pathway. This emphasizes the need for caution in relying solely on IH:IS JM ratios to characterize partner choice defects, since these measures only detect CO intermediates.

1.7.5 Both DNA ends often form D-loops independently of one-another

Hunter and colleagues reported that multi-chromatid joint molecule (mcJM) intermediates, comprising 3 and 4 interconnected chromatids, occur during normal meiotic recombination and that these structures accumulate to high levels in mutants that lack the JM disrupting helicase Sgs1 (Oh et al., 2007). Invasion of both homolog and sister chromatids within the same mcJM is consistent with the inference that IS recombination occurs frequently during normal meiosis (above), and that a given DNA end may engage more than one chromatid before

a DSB is eventually repaired (McMahill et al., 2007). The existence of mcJMs further suggests that both ends created by a DSB are capable of promoting homology search and strand exchange. This possibility is consistent with the loading of Dmc1 on both DNA ends (as discussed above) rather than Rad51 being the sole strand exchange protein located on one of the two ends. Another implication of these findings is that IH bias may involve processes that preferentially stabilize nascent IH interactions, possibly dependent on chromosome pairing and/or synapsis (Börner et al., 2004; Lao and Hunter, 2010).

1.7.6 Partner choice in organisms with DSB-independent synapsis

Although most organisms require recombination to properly align and synapse homologs, *D. melanogaster* and *C. elegans* synapse homologs independent of DSBs (Dernburg et al., 1998; McKim et al., 1998). In these organisms—which lack Dmc1, Hop2, and Mnd1— the stable, co-linear juxtaposition of homologs in the context of the synaptonemal complex could constitute a distinct mechanism of IH bias in which the spatial proximity of homolog chromatids to a DSB increases the likelihood of IH recombination, perhaps approaching the 2:1 IH:IS ratio predicted from random invasion of one of the three available chromatids. Consistent with this idea, IH CO recombination in these organisms is absolutely dependent on synapsis (MacQueen et al., 2002; Page and Hawley, 2001). Furthermore, DSBs—manifested as cytologically visible γ-H2AX or Rad51 foci—appear to form after full synapsis in these organisms (Colaiacovo et al., 2003; Jang et al., 1994).

1.8 Models for interhomolog bias

1.8.1 The anchor pad model

The analysis of Rec8 function described above led to the development of a model for the mechanism of IH bias (Fig 1.4 B) (Hong et al., 2013; Kim et al., 2010). This model breaks IH bias into two distinct phases: "establishment" and "maintenance." Establishment is the process through which a homologous chromatid is chosen as the initial recombination partner. Technically exquisite 2-D gel analysis, in which both IS and IH SEIs were distinguished, showed that *rad51*, *hed1 dmc1*, *red1*, and *mek1* mutants are defective for establishment of IH bias, forming high levels of IS SEIs rather than IH SEIs (Hong et al., 2013; Kim et al., 2010). The maintenance phase is proposed to occur at the SEI-to-dHJ transition. *rec8* single mutants are inferred to properly establish IH bias at the SEI stage, but subsequently manifest a *precise* 1:1 ratio of IH:IS dHJs (Hong et al., 2013; Kim et al., 2010). This 1:1 dHJ ratio was argued to reflect defective processing of an "ends-apart" recombination intermediate in which one DSB end forms an IH SEI, and the opposite end forms a homology-dependent complex with the sister chromatid. This putative homology-dependent IS complex was presumed to be undetectable by the current 2-D gel method. The 1:1 dHJ ratio seen in *rec8* mutants was thus explained by disruption of the ends-apart intermediate as the SEI-to-dHJ transition occurs. If maintenance is normal, the IS complex is preferentially lost and the IH SEI is converted to an IH dHJ. In the *rec8* mutant, the mechanism which selectively disrupts the IS complex is defective such that the IH SEI and the IS complex are lost with equal probability, leading to subsequent formation of an IS or an IH dHJ, respectively. The putative IS connection is given the name "anchor pad." During normal (*REC8*$^{+}$) meiosis, the anchor pad blocks the opposite (partner) DSB end from a homology-dependent interaction with the sister by seeding polymerization of the strand exchange

nucleoprotein filament beyond the 3' end of the IS complex (which we presume would be a nascent D-loop) into the adjacent duplex DNA region. This elongated filament could block invasion of the sister by the opposite DSB end, leaving the homolog chromatids as the only available partners for that end. This model has yet to be supported by evidence for the existence of anchor pads.

1.8.2 Homology-independent steric hindrance models

Other models to explain IH bias propose that recombinosomes are subject to steric hindrance that reduces access to the target DNA sequence on the sister chromatid. One proposal suggested that the homology search activity of Dmc1 filaments is confined by an extended structure or scaffold which projects the active portion of the filament away from the axial element on which the scaffold is assembled (Sheridan and Bishop, 2006) (Fig 1.4 C). The integrity of this structure was proposed to require local assembly of Rad51 as well as phosphorylation of a nearby Mek1 substrate. Ultrastructural studies in *Allium*, showing recombinosomes associated with proteinacious bridges between co-aligned axial elements, are consistent with this idea (reviewed by (Zickler and Kleckner, 1999). However, it is not known if these extended structures form prior to the homology search or not. Another model involving steric hindrance proposes that recombinosomes are locally tethered to the axial/lateral element (Blat et al., 2002; Hunter, 2007) (Fig 1.4 D). Such confinement could preclude interaction with corresponding sequences on a sister chromatid which are physically separated from the axis in loop regions. The model rests on the assumption that both DSB ends remain associated with the axis during the homology search.

1.8.3 Activation of strand exchange in DSB-distal regions

Klein and colleagues proposed a model in which Mnd1 (and by extension, Hop2) mediates IH bias by creating recombination-proficient donor templates (Zierhut et al., 2004) (Fig 1.4 E). This model was based on the fact that Mnd1 forms immunostaining foci independently of, and spatially separated from, DSBs (as discussed above). Mnd1 was proposed to bind to chromatin non-specifically, which is now understood to reflect the dsDNA binding activity of the Hop2-Mnd1 heterodimer, and then to be locally displaced (or inactivated) from DSB proximal regions, which would include the target sequence on the sister chromatid. Consequently, Mnd1-dependent activation of strand exchange is only possible with homolog templates, where Mnd1 has not been displaced. The biochemical results described above lead us to propose an updated version of this model in which homolog bias results from local activation of Dmc1's D-loop activity by Hop2-Mnd1, together with rapid displacement of Hop2-Mnd1 from DSB-proximal regions during the time between DSB formation and the completion of recombinosome assembly (Chan et al., 2014).

It should be noted that the models presented above are compatible with one another and IH bias could involve aspects of more than one of these hypothetical mechanisms.

1.9 Concluding remarks

In conclusion, recent progress has identified many, perhaps all, of the proteins that carry out the search for DNA homology and catalyze DNA strand exchange during meiotic recombination. Many of these proteins appear to modulate mitotic-like DNA repair pathways, contributing meiosis-specific functions that promote the invasion of a homolog rather than the sister chromatid. These studies have generated a number of hypotheses to explain the mechanism

of IH bias. However, critical evidence for any of the models is still lacking. Of particular importance will be the improvement of methods to detect all joint molecule species, especially those that go on to form NCO recombinants. Other key questions include: does local regulation of Rec8 occur at DSB sites and, if so, how does this contribute to IH bias? Does an IS anchor pad form as a required intermediate on the pathway to IH JM formation? More generally, how are the activities of the two ends of a given DSB differentiated? Is activation of Mek1 kinase normally limited to DSB proximal regions? Does inhibitory phosphorylation of Rad54 by Mek1 normally play any role in normal IH bias? What are all the Mek1 substrates that play a role in IH bias and how does phosphorylation contribute to those roles? Does local, DSB-dependent redistribution or inactivation of Hop2-Mnd1 dictate template choice? What is the 3D structure of the recombinosome? How does that structure contribute to regulation of recombinosome function? By what mechanisms do organisms that lack Dmc1 promote IH recombination? We expect answers to many of these questions in the near future.

Chapter 2

Materials and Methods

* Mike Rust wrote section 2.8 on the dSTORM artifact. Ivy Fitzgerald and Ben Glick contributed GFP constructs. Matt Goodsmith performed some of the GFP experiments. Annie Zhang performed the *in vitro* filament assembly experiment.

2.1 Strain construction

Tetracysteine-tagged Rad51 and Dmc1 constructs were constructed by overlap PCR and subcloned into pNRB 4. TC_6 (CCPGCC) or TC_{12} (FLNCCPGCCMEP) tags were fused to the N- or C-terminus. N-terminal fusions were followed by a TGSSG linker (Wurm et al., 2010), and C-terminal tags were fused directly to the end of the open reading frame. Specifically, wild type genomic DNA was amplified first with primers (FlAsH/ReAsH 1 + FlAsH/ReAsH 5) or (FlAsH/ReAsH 9 + FlAsH/ReAsH 11) for *DMC1* or *RAD51* construction, respectively. This PCR product was then used as a template for two reactions with the following primer pairs:

- *TC_{12}-RAD51*: (FlAsH/ReAsH 9 + FlAsH/ReAsH 22) and (FlAsH/ReAsH 23 + FlAsH/ReAsH 16)
- *RAD51-TC_6*: (FlAsH/ReAsH 9 + FlAsH/ReAsH 33) and (FlAsH/ReAsH 32 + FlAsH/ReAsH 16)
- *DMC1-TC_6*: (FlAsH/ReAsH 1 + FlAsH/ReAsH 29) and (FlAsH/ReAsH 28 + FlAsH/ReAsH 7)

DMC1-TC_{12}: (FlAsH/ReAsH 1 + FlAsH/ReAsH 31) and (FlAsH/ReAsH 30 + FlAsH/ReAsH 7)

DMC1 constructs were then completed by overlap PCR with primers (FlAsH/ReAsH 1 +

FlAsH/ReAsH 7) followed by tailing PCR with primers (FlAsH/ReAsH 39 + FlAsH/ReAsH 38). Similarly, *RAD51* constructs were completed by overlap PCR with primers (FlAsH/ReAsH 9 + FlAsH/ReAsH 16) followed by tailing PCR with primers (FlAsH/ReAsH 37 + FlAsH/ReAsH 36). Finally, these PCR products were subcloned into pNRB 4 at KpnI and XbaI sites. *DMC1* and *RAD51* plasmids were sequenced and linearized with HindIII or EcoNI, respectively, before transformation into DKB 197 or 577. Following selection for URA+, appropriate targeting was confirmed by PCR.

msGFP-tagged Rad51 and Dmc1 constructs were constructed by Ivy Fitzgerald. SGSGSSGSSGS and GSSGSSGSSGSS linkers separated N- and C-terminal msGFP fusions from Rad51 or Dmc1. Following transformation with KanMX4-marked PCR products, targeting was confirmed by PCR and ORFs were sequenced. Rad52-EGFP and -msGFP strains were constructed and sequenced by Ben Glick. The 1- or 3- DSB strains were constructed by Matt Goodsmith via transformation of DKB 4758 (generous gift from Jim Haber; YCSL004) with a RAD52-EGFP::KanMX4 construct. This DNA fragment was prepared from pNRB569 following digestion with MfeI and EcoRI. pNRB 569 was constructed by inserting a RAD52-EGFP PCR product into pNRB 658 via a two-step sequential ligation protocol at SalI and NdeI sites.

The cytological landmark strain was constructed by combining the *HIS4::LEU2* DSB hotspot (Hunter and Kleckner, 2001), a *tetO* array, a *lacO* array, YFP-TetR, and 3xHA-LacI via genetic crosses (Joshi et al., 2015).

lacO and *tetO* arrays were inserted into *Chr III*, centromere proximal and distal to the *HIS4::LEU2* DSB hotspot, respectively, using the cloning-free method (Rohner et al., 2008). Specifically, the *ARS304* and *ARS308* array-targeting plasmids, pNRB 571 and pNRB 590 respectively, were constructed by TA-cloning tailed-PCR products amplified from pNRB 302

using primers 5'ARS304-Forward and 5'ARS304-Reverse or CENgasTar Forward and CENgasTar Reverse. First, the targeting construct was integrated via transformation. Then, linearized pSR10/pNRB 577 (277x *lacO* array/*TRP1*$^{+}$) or pSR11/pNRB 578 (119x *tetO* array/*TRP1*$^{+}$) was transformed, replacing the targeting module (Rohner et al., 2008).

Fusion proteins designed to bind the *tetO* and *lacO* arrays were constructed by standard molecular methods. *YFP-TetR::LEU2* (pNRB 667) was constructed by overlap PCR and inserted into pNRB 567 via EcoRI and BamHI sites. After linearization of the plasmid with EcoRV, it was integrated at *LEU2*. *3xHA-LacI::LYS2* (pNRB 677) was constructed by overlap PCR and inserted into pNRB 592 via EcoRI and SphI sites. After linearization with StuI, it was integrated at *LYS2*.

Tetraploid *spo11* hypomorphic strains were constructed by mating a *SPO11/spo11-Y135F* a/Δ diploid with a *spo11-Y135F/spo11-Y135F* α/Δ diploid (Storchová et al., 2006). The a/Δ and α/Δ diploids were obtained by gene targeting with DNA constructs designed to delete the *MATα* or the *MATa* locus, respectively. Specifically, primers MAT1 and either MAT3 or MAT2 were used to amplify the *hphNT* fungicide resistance cassette from pNRB 598 and add homology arms. *MATα /Δ* and *MATa /Δ* transformants were verified by mating type tests.

For the *spo11* VDE cut site heterozygote experiment, DKB 4571 was constructed by mating of YOC 3524 and YOC 3525 (Fukuda et al., 2003), provided by the Ohya Lab. DKB 5369 was constructed by transformation of YOC 3524 and YOC 3525 with a PCR product designed to introduce an *mnd1* mutation followed by mating. Specifically, genomic DNA from DKB 5115 (*mnd1*) was amplified with MND1F and MND1R.

DKB	genotype
5166	*MATa/matα::hphNT1/matα::hphNT1/MATα, ho::hisG/"/", ura3/"/", trp1::hisG/"/", leu2::hisG::YFP-TetR::LEU2/leu2::hisG/"/", lys2::LacI-HA3::LYS2/lys2/"/", SPO11/SPO11-Y135F-HA3-His6::KanMX4/"/", his4X::LEU2-(Nbam)-URA/his4XB/"/", ARS 304::tetO Array (TRP+)/ARS 304::KanMX4 target construct/ARS 304/", ARS 308::lacO Array (TRP+)/ARS 308::KanMX4 target construct/ARS 308/"*
5169	5166 except *zip1::LYS2/"/",* the *tetO* and *lacO* arrays are located at *ARS 308* (with *tetO* on the *HIS4::LEU2* containing chromosome), and *ARS 304::KanMX4 target construct* is present on both array containing chromosomes
5115	5166 except *mnd1::KANMX6/"/"*
4571	*MATa/MATα, ho::LYS2/ho::hisG, leu2/", ura3/", lys2/", trp1/TRP1, spo11::CgLEU2/", VMA1-201/VMA1-202*
5369	4571 except *mnd1::KANMX6/"*
5333	*MATa/MATα, ho::LYS2/ho::hisG, leu2::hisG/", ura3/", lys2/", trp1::hisG/TRP1, spo11::hisG-URA3-hisG/"*
5423	*MATa/MATα, ho::hisG/", his4XB/", lys2/", ura3/", trp1::hisG/", leu2::hisG/"*
5374	5423 except *zip1::LYS2/"*
5378	5423 except *mnd1::KANMX6/"*
5453	5423 except *dmc1::KANMX4/"*
5916	*MATα, CAN1*, *his3-11*, *his3-15*, *leu2-3*, *leu2-112*, *trp1-1*, *ura3-1*, *srs2::KANMX4*, 2μ (URA3, pGAL1::RAD51)
3213	*MATa, CAN1, his3-11, his3-15, leu2-3, leu2-112, trp1-1, ura3-1, SML1*
5003	3213 except *RAD52-EGFP*
5005	3213 except *RAD52-msGFP*
5477	*MATα, DELho, DELhml::ADE1, DELhmr::ADE1, ade1-110, leu2,3-112, lys5, trp1::hisG, ura3-52, ade3::GAL10:HO, Rad52-EGFP::KanMX*
5479	*MATα, DELho, DELhml::ADE1, DELhmr::ADE1, ade1-110, leu2,3-112, lys5, trp1::hisG, ura3-52, ade3::GAL10:HO, Chr.VI 97749 nt::HPH:Hocs, Chr.II 252kb::HOcs-URA3, Rad52-EGFP::KanMX*
577	*MATa, ho::LYS2, ura3, rad51Δ::hisG, leu2::hisG, his4x, ade2::LK*
197	*MATα, ho::LYS2, lys2, ura3, leu2::hisG, arg4-Bgl, his4B::LEU2, dmc1Δ::ARG4*
4156	*MATa/MATα, ho::LYS2/", lys2?/lys2?, ura3/", leu2::hisG/", his4B::LEU2/his4x, arg4-bgl/ARG4, rad51Δ::hisG::Rad51-WT::URA3/"*
4111	*MATa/MATα, ho::LYS2/", lys2/", ura3/", leu2::hisG/", his4B::LEU2/his4x, arg4-Bgl/ARG4, rad51Δ::hisG/"*
3852	*MATa/MATα, ho::LYS2/", lys2?/lys2?, ura3/", leu2::hisG/LEU2, HIS4/his4X, rad51Δ::hisG::TC6-Rad51::URA3/"*
4031	*MATa/MATα, ho::LYS2/", lys2/", ura3, leu2::hisG/", his4B::LEU2/his4x, arg4-Bgl/ARG4, rad51Δ::hisG::Rad51-TC6::URA3/"*
4107	*MATa/MATα, ho::LYS2/", lys2/", ura3/", leu2::hisG/", his4B::LEU2/his4x, arg4-Bgl/ARG4, rad51Δ::hisG::TC12-Rad51::URA3/"*
3946	*MATa/MATα, ho::LYS2/", lys2/", ura3/", leu2::hisG/leu2::hisG?, HIS4/his4B::LEU2, arg4-Bgl/", dmc1Δ::ARG4::Dmc1-WT::URA3/"*
3948	*MATa/MATα, ho::LYS2/", lys2/", ura3/", leu2::hisG/leu2::hisG?, HIS4/his4B::LEU2, arg4-Bgl/", dmc1Δ::ARG4::Dmc1-TC6::URA3/"*
4029	*MATa/MATα, ho::LYS2/", lys2/", ura3/", leu2::hisG/", arg4-Bgl/", HIS4/his4B::LEU2, dmc1Δ::ARG4::Dmc1-TC12::URA3*
4780	*MATa/MATα, ho::hisG/", his4X::LEU2-(Nbam)-URA3/HIS4::LEU2-(Nbam), lys2/", ura3/", leu2::hisG/",*
4617	4780 except *msGFP-Rad51::KanMX4/"*
4782	4780 except *msGFP-Rad51::KanMX4/Rad51*
4776	4780 except *Rad51-msGFP::KanMX4/"*
4774	4780 except *Rad51-msGFP::KanMX4/Rad51*
4839	4780 except *msGFP-Dmc1::KanMX4/"*
4945	4780 except *Dmc1/msGFP-Dmc1::KanMX4*
4888	4780 except *Dmc1-msGFP::KanMX4/"*
4946	4780 except *Dmc1-msGFP::KanMX4/Dmc1*

Table 2.1 Yeast strains. All strains are of the SK-1 background, except DKB 5916, 3213, 5003, and 5005 which are W303 derivatives. Note that the *HIS4::LEU2* DSB hotspot in DKB 5166 is located on the same chromosome and in between the *lacO* and *tetO* arrays.

primer	sequence (5'-->3)
MAT1	CGAAACCCAGTTTTTGATTTGAATGCGAGATAAACTGGTATTCTTCCGTCCCAAAACCTTCTCA
MAT2	CATACCCAAACTCTTACTTGAAGTGGAGTAATGCCACATTTCTTTGCCATCAGCGACATGGAGGC
MAT3	GTTGCGCGAAGTAGTCCCATATTCCGTGCTGCATTTTGTCCGCGTCAGCGACATGGAGGC
5'ARS304-Forward	AGTTAAATTATCCAATTCCAAATTCTAGGGACGGTTTCCAAGCGGATGCCGGGAGCAGAC
5'ARS304-Reverse	GTTATAATTGTGTAAAAGGGCACAGTCAATGAGTAGTAGAGTGAGCTGATACCGCTCGCC
CENgasTar Forward	CTAACACTTGTCAAACAGAATATAAGGATTACTTGTCTTCAGCGGATGCCGGGAGCAGAC
CENgasTar Reverse	CGCCATGCCATGTTTATGAAATGTATAGGTACTGTACTATGTGAGCTGATACCGCTCGCC
MND1 R	CGGCTAATCTGCAAGCTCTATGCCT
MND1 F	ACCTAAGCCTCTTCTCACGAAGGCA
FlAsH/ReAsH 1	TGCTGCTCCTCCTCC
FlAsH/ReAsH 5	GGCTATTATAAACGCTATAATAACTGACG
FlAsH/ReAsH 7	CTCAATTTTATATAC
FlAsH/ReAsH 9	ACTTAGCAGCTTCCCGATTTAAT
FlAsH/ReAsH 11	GGGTACTGCCTGATTTTAACAAAG
FlAsH/ReAsH 16	GGGTGACAGACAATA
FlAsH/ReAsH 20	ACTGGTAGTAGCGGTTGTTGTCCAGGTTGTTGTTCTCAAGTTCAAGAA
FlAsH/ReAsH 21	ACAACAACCTGGACAACAACCGCTACTACCAGTCATATGACGATAACA
FlAsH/ReAsH 22	TGGTTCCATACAACAACCTGGACAACAATTTAGAAAACCGCTACTACCAGTCATATGACGATAACA
FlAsH/ReAsH 23	ACTGGTAGTAGCGGTTTTCTAAATTGTTGTCCAGGTTGTTGTATGGAACCATCTCAAGTTCAAGAA
FlAsH/ReAsH 24	ACAACAACCTGGACAACAACCGCTACTACCAGTCATATTTGTTCAAAT
FlAsH/ReAsH 25	ACTGGTAGTAGCGGTTGTTGTCCAGGTTGTTGTTCTGTTACAGGAACT
FlAsH/ReAsH 26	TGGTTCCATACAACAACCTGGACAACAATTTAGAAAACCGCTACTACCAGTCATATTTGTTCAAAT
FlAsH/ReAsH 27	ACTGGTAGTAGCGGTTTTCTAAATTGTTGTCCAGGTTGTTGTATGGAACCATCTGTTACAGGAACT
FlAsH/ReAsH 28	TGTTGTCCAGGTTGTTGTTAGTTTTTGTATACT
FlAsH/ReAsH 29	ACAACAACCTGGACAACAGTCACTTGAATCGGT
FlAsH/ReAsH 30	TTTCTAAATTGTTGTCCAGGTTGTTGTATGGAACCATAGTTTTTGTATACT
FlAsH/ReAsH 31	TGGTTCCATACAACAACCTGGACAACAATTTAGAAAGTCACTTGAATCGGT
FlAsH/ReAsH 32	TGTTGTCCAGGTTGTTGTTAGGTATTTGGTCTC
FlAsH/ReAsH 33	ACAACAACCTGGACAACACTCGTCTTCTTCTCT
FlAsH/ReAsH 34	TTTCTAAATTGTTGTCCAGGTTGTTGTATGGAACCATAGGTATTTGGTCTC
FlAsH/ReAsH 35	TGGTTCCATACAACAACCTGGACAACAATTTAGAAACTCGTCTTCTTCTCT
FlAsH/ReAsH 36 R	AGCAT TCTAGA GGGTGACAGACAATACGAAA
FlAsH/ReAsH 37 F	AGCAT GGTACC ACTTAGCAGCTTCCCGATTT
FlAsH/ReAsH 38 R	AGCAT TCTAGA CTCAATTTTATATACGCATATGCA
FlAsH/ReAsH 39 F	AGCAT GGTACC TGCTGCTCCTCCTC
RAD52.FOR	TACCAGGCACAATCCATTAGGCAC
Rad52_R_5	TCCAGTGTCGAC ATCTATTGTTTTTCCGAGTTGCCAT

Table 2.2 Oligonucleotides

2.2 Meiotic time courses

Sporulation was induced as previously described (Bishop, 1994). Sporulation was monitored by observing the number of DAPI-staining bodies in ethanol-fixed cells at varying points throughout the time course.

2.3 *RAD51* overexpression experiment

For Fig 3.11Q-T, *RAD51* was overexpressed from a 2-micron plasmid (Shah, 2008; Shah et al., 2010). Cells were grown overnight in galactose-supplemented media lacking uracil. The culture was diluted to an OD^{600} of about 0.1, allowed to double, and resuspended in glucose-supplemented media lacking uracil. Samples were collected at zero- and four-hour time points. The aberrant, often elongated, Rad51 and RPA structures observed required both *RAD51* overexpression and *srs2* mutation.

2.4 Irradiation experiments

Cells were grown overnight, diluted to an OD^{600} of about 0.1, and allowed to double. The cultures were transferred to conical tubes and irradiated on ice with variable amounts of gamma rays from a ^{60}Co source. For survival assays, 10^0-10^6 serial dilutions were prepared and plated on YPDA. For cytological assays, irradiated cells were returned to flasks and grown for 45 minutes, before cytological samples were prepared or live cells were observed.

2.5 DSB induction experiment

One mL of overnight YPDA culture was used to inoculate 25 mL YEP-lactate culture. These over day starter cultures were diluted into fresh YEP-lactate for overnight growth. When

cultures reached an OD^{600} of around 1.0, galactose was added to a final concentration of 2%. Samples were collected for imaging at zero and four hours.

2.6 Cytological sample preparation and immunostaining

Chromosome spreads were prepared by the lipsol method (Grubb et al., 2015). 4 mM PMSF was added to spheroplast suspensions and the solutions used for spreading. Rabbit anti-Rad51 (#159 or 158), goat or guinea pig anti-Dmc1 (#189, 190, or 174), chicken anti-GFP (Invitrogen A10262; #177), goat anti-Zip1 (Santa Cruz, sc-15632; #120), rabbit anti-Red1 (Roeder lab; #143), and rabbit anti-Rec8 (Shinohara lab; #185) antibodies were utilized at 1:1000 dilutions. Mouse anti-HA (Santa Cruz, sc-7392; #17) was used at 1:100. Secondary antibodies were generally used at 1:1000 with the following order of preference: Alexa fluor 488, 594, 647, and 750. This order of preference reflects the decreasing resolution attainable with longer wavelengths using widefield microscopy. Alexa fluor 750 was utilized at 1:100 because the LacI-3xHA signal was weak.

For dSTORM microscopy, spreads were performed on 22 x 22 #1.5 coverslips. Samples were blocked with 3% BSA in TBS. Primary and secondary antibodies were used at 1:1000 to balance signal strength with background. Higher concentrations appear to result in substantial levels of punctate, background signal without altering the appearance of the primary structures. More stringent washes were also used to reduce this type of background. Following primary and secondary staining, coverslips were washed five times in TBS + 0.05% Trition X-100. Alexa fluor 647 was the super-resolution dye. Alexa fluor 488 was sometimes included as a second color for widefield imaging only. DAPI was never used to counterstain nuclei. Coverslips were stored in TBS in six-well dishes prior to mounting and imaging.

For two-color STED, Alexa fluors 594 and 647 were used. All primary and secondary antibodies were used at 1:100. These coverslips were mounted in Prolong Diamond and allowed to cure at room temperature for five days prior to imaging.

For Fig 3.5A-D, *in vitro* Rad51 assembly reactions were performed as previously described (Cloud et al., 2012) with the following exceptions. The assembly reaction included 0.5 nM 2.7 kb linear dsDNA (1.35 μM bp) generated by asymmetric PCR of pRS306 with one biotinylated primer, 1.6 μM Rad51, and 1 μM Hed1 to stabilize the filament (Busygina et al., 2012). The reaction was fixed with 3% PFA prepared in reaction buffer and then added to previously prepared coverslips coated with streptavidin by a modified version of a previously established protocol (Joo and Ha, 2012). Slides were stained for dSTORM as described above.

Whole cell samples were prepared and stained as previously described (Rua et al., 2004). For live cell imaging experiments, cells were concentrated (10-50 times) by centrifugation and kept on ice. Immediately prior to imaging, 4-5 microliters of cells were placed on a slide and covered with a standard coverslip. This small volume generally prevents cells from moving too much but only allows imaging for about 10-15 minutes because of the speed of evaporation from the edges.

2.7 Microscopy

Images were acquired on a Zeiss Axiovision 4.6 microscope at 100X magnification and adjusted for brightness and contrast on ImageJ/FIJI software. For all two-color experiments, proper registration of image pairs obtained with different filter sets was confirmed using fluorescent beads (Molecular Probes, L-5241).

For dSTORM, coverslips were mounted on a depression well slide filled with 10 mM MEA (prepared in PBS) and sealed with a two-part curable rubber product called "Body Double" (Smooth-On, Inc). Image sequences were acquired on a Leica SR GSD 3D microscope in 2D epifluorescence mode. Depletion with the 642 laser at 100% power was performed until the frame correlation dropped below 0.05, then acquisition commenced at 60% laser power. At least 25,000 frames were acquired. Images were reconstructed with the QuickPALM plugin (Henriques et al., 2010) on FIJI using: an input pixel size of 100 nm, a reconstruction pixel size of 20 nm, a minimum SNR of 5.00, minimum symmetry of 0%, local threshold of 25%, maximum iterations per frame of 1000, and 50 threads. Also, a FWHM of 2 pixels was used to eliminate an artifact in which a large fraction of adjacent structures appear to be connected by a thin, sparsely populated thread (see below). This artifact is due to the almost simultaneous blinking of two adjacent fluorophores resulting in a "mis-called" event half way between two diffraction-limited blinks (Fig 3.6). A 0.75 pixel Gaussian blur was applied to each micrograph before analysis.

2-color STED micrographs were acquired with the help of Robert Davison (Lecia) on a Lecia SP8 scanning confocal microscopy with 3D gated STED. The 775 nm depletion line was utilized to create super-resolution images of Alexa Fluor 594 and 647 stained Rad51 and Dmc1. In my hands, the core-owned SP5II STED-CW microscope's 592 nm depletion line cannot achieve super-resolution in two different colors. The use of two fluorophores with a large Stoke's shift and subsequent definition of narrow collection windows (to prevent overlapping signals) severely limits the observable signal. The extremely high laser powers necessary to boost the signal resulted in melted coverslips.

2.8 dSTORM reconstruction artifact

2.8.1 Strategy for reducing artifacts in super-resolution microscopy

In preliminary analyses of super-resolution data sets, we observed that nearby pairs of punctate structures sometimes appeared to be connected by thin threads of localizations. We suspected that these thread-like objects might be artifacts of image analysis that do not reflect the underlying structure in the cell. Algorithms used to analyze dSTORM and other single-molecule localization data sets must make statistical calls to estimate which parts of the data set correspond to isolated fluorescent molecules. An important source of error is the common scenario where two nearby molecules are both emitting in the same frame. When the image of one of the emitting molecules is dim (for example, because it either switched into a dark state or into a fluorescent state in the middle of the frame), analysis software may treat the two molecules as single emitter, resulting in an artifactual localization that tends to lie along the line joining the two molecules. Although such mis-localization events have been described previously (van de Linde et al., 2010), their manifestation as thread-like structures has to our knowledge never been reported.

Image analysis algorithms use statistical tests to reject artifactual localizations by comparing data to an idealized point-spread function based on the expectation for a single fluorescent molecule. These algorithms contain tunable parameters that set thresholds for when a candidate localization will be rejected, e.g. the width or the ellipticity of the fluorescent spot. Here, we describe a general method that can be used to test for artifactual structures in a reconstructed image. The method involves creating several reconstructions by running a single-molecule localization algorithm on the same data set with various values of threshold parameters

(e.g. spot width). These reconstructed images are then compared against each other. The intuitive expectation behind this procedure is that, while making a threshold parameter more stringent will cause some true single emitters to be rejected (type I errors), cases with multiple emitters will be correctly rejected more efficiently. Thus, one expects artifactual structures to fade relative to true structures as parameter stringency is increased (Fig 3.6). Finally, we note that most artifactual localization problems originate with nearby emitters overlapping in time, so that any algorithm will become less susceptible to artifacts as the density of fluorophore switching events (per unit area per frame) decreases.

2.8.2 Difficulties with appropriately setting the spot width threshold

When applying the above strategy, we found that in order to reduce the thread-like artifactual localizations to an acceptable level, we often had to set the spot width threshold to a value that seemed physically unreasonable. For example in QuickPALM, we had to set the FWHM (full width at half-maximum) parameter to 2 px to get satisfactory results, while the actual FWHM of isolated fluorescent spots in our images was 3.7 ± 0.44 px corresponding to 370 nm (n=50 spots, measured manually).

We experienced a similar problem with multiple commercially available analysis packages, but chose to investigate the QuickPALM plug-in in depth because the source code for this algorithm is publicly available. The point-spread function of a diffraction-limited microscope projected onto one dimension can often be well approximated by a Gaussian:

$$I(x) = I_{\max} e^{\frac{-x^2}{2\sigma^2}}$$

Where σ is the standard deviation. The FWHM of this Gaussian is:

$$FWHM_{\text{Gauss}} = 2\sqrt{2\ln 2}\sigma \approx 2.355\sigma$$

The QuickPALM algorithm estimates spot width not by the standard deviation but by the mean absolute deviation, that is $MAD = \langle |xI(x)| \rangle$.

$$MAD_{\text{Gauss}} = \frac{2}{\sigma\sqrt{2\pi}} \int_0^\infty dx\, x\, e^{-\frac{x^2}{2\sigma^2}} = \frac{2}{\sqrt{2\pi}}\sigma$$

The QuickPALM algorithm implements a width cut-off by comparing 2.355·*MAD* to the user input FWHM. Since, for a Gaussian, *MAD* differs from σ by a factor $2/\sqrt{(2\pi)} \approx 0.798$, the result is that the effective FWHM being tested against will be ≈25% larger than the intended FWHM input by the user.

The simplest workaround for this discrepancy is to decrease the FWHM parameter in the QuickPALM input by a factor of ~0.8 relative to empirical estimates. Note that larger (uncorrected) values of the FWHM parameters result in substantial artifactual structures in our data (Fig 3.6). We tested some other commercial super-resolution analysis packages and found that they produced the same artifactual thread-like structures (although we could not subject the reconstructions to the same kind of parameter sampling in those packages). It is therefore possible that similar discrepancies exist in other algorithms.

2.9 Analysis and simulations

Custom written ImageJ macros designated *4-spot macro* were used to generate nearest neighbor distributions for widefield micrographs. Specifically, the (x,y) coordinates of focal centroids were determined manually with the ImageJ multipoint selection tool within the context of the macro. Note that Rad51 and Dmc1 foci were assumed to be diffraction limited spots (a valid assumption based on dSTORM micrographs). Thus, focus centroids as close as about 150 nm were often recognized as being distinct based on the fine appearance of staining structures (elongation vs perfectly circular focus, appearance of two maxima, etc), despite the fact that they

were closer together than the resolution limit (around 250 nm). The nearest neighbor distributions were generated by coalescing output from the ImageJ macro using Excel. dSTORM reconstructions were scored in FIJI. The elliptical selection tool was fit to each observed sr focus. The (x,y) coordinates and various other descriptors of the ellipses were measured. Nearest neighbor distributions were determined in Excel workbooks.

For the Zip1 foci nearest neighbor experiment, the (x,y) coordinates of both Rad51 and Zip1 foci were determined in early prophase nuclei. Nuclei were selected for having both Rad51 and Zip1 staining, but only nuclei with a completely punctate Zip1 staining pattern were chosen for analysis. Scoring of nearest neighbor positions were performed as above.

Simulated nearest neighbor distributions were generated from a custom-written ImageJ macro that independently chooses points within a defined two-dimensional space and measures their proximity to one another. Specifically, a matched list of nuclear areas and focus numbers (from experimentally observed data) were input. For each input nucleus, 10 nuclei were simulated (50 for dSTORM nuclei). The simulated nucleus was approximated by a circle of the same area. Simulated foci were placed iteratively and randomly within the nucleus. A simulated focus was rejected if it was located closer to another simulated focus than the closest inter-focus distance observed in the experimental data set (not just the single nucleus being simulated). The simulated nearest neighbor distances were coalesced in Excel for analysis and compared to the experimental distribution.

For the *spo11* VDE cut site heterozygote experiment, unselected nuclei were scored, but only focus-positive nuclei are included in the analysis. Single foci (category I) include Rad51-only, Dmc1-only, and Rad51-Dmc1 co-foci. Similarly, paired foci include all varieties of single foci, located within 1 μm of each other (category II). The “>2 Rad51 and/or Dmc1 foci” class

(category III) includes structures where all of those foci are within 1 μm one another. The distant class (category IV) represents nuclei in which foci are separated by distances greater than 1 μm, but there are no more than 2 Rad51 or Dmc1 foci. Finally, the ">2 Rad51 and/or Dmc1 foci and distant" class (category V) consists of nuclei with two distinct cytological complexes separated by greater than 1 μm where the sum or Rad51 or Dmc1 foci is greater than two.

Scoring the cytological landmark experiment required multiple levels of filtering. First, only nuclei displaying *lacO* and *tetO* arrays were scored for experiments involving both landmarks. Meiotic proteolysis resulted in a large fraction of nuclei without *lacO* spots. Also, rare nuclei with >2 *lacO* or *tetO* spots were excluded from analysis. Furthermore, only nuclei with one Dmc1 focus within 300 nm of the point between the closest *tetO* and *lacO* foci and 0-2 Dmc1 foci within 1 μm of that Dmc1 focus were analyzed. All analysis was performed with ImageJ software.

Chapter 3

Small Rad51 and Dmc1 complexes often co-occupy both ends of a meiotic double strand break

*This chapter is a slightly modified version of a published paper: Brown, M.S., Grubb, J., Zhang, A., Rust, M.J., and Bishop, D.K. (2015). Small Rad51 and Dmc1 Complexes Often Co-occupy Both Ends of a Meiotic DNA Double Strand Break. PLoS Genet *11*, e1005653. Annie Zhang performed the *in vitro* filament assembly experiment, and Jennifer Grubb helped with strain construction.

3.1 Chapter overview

The Eukaryotic RecA-like proteins Rad51 and Dmc1 cooperate during meiosis to promote recombination between homologous chromosomes by repairing programmed DNA double strand breaks (DSBs). Previous studies showed that Rad51 and Dmc1 form partially overlapping co-foci. Here we show these Rad51-Dmc1 co-foci are often arranged in pairs separated by distances of up to 400 nm. Paired co-foci remain prevalent when DSBs are dramatically reduced or when strand exchange or synapsis is blocked. Super-resolution dSTORM microscopy reveals that individual foci observed by conventional light microscopy are often composed of two or more substructures. The data support a model in which the two tracts of ssDNA formed by a single DSB separate from one another by distances of up to 400 nm, with both tracts often bound by one or more short (about 100 nt) Rad51 filaments and also by one or more short Dmc1 filaments.

3.2 Introduction

Meiotic recombination is a highly regulated process that faithfully repairs programed DSBs, ensuring accurate reductional chromosome segregation at meiosis I (Hunter, 2007). Following pre-meiotic DNA replication, Spo11 introduces DSBs across the genome. These DSBs are nucleolytically resected, revealing 3' single strand DNA (ssDNA) tracts that are subsequently used to locate an intact, homologous double strand DNA (dsDNA) repair template. Upon completing the homology search, the ssDNA invades the intact dsDNA duplex creating a displacement-loop structure. The invading 3' end serves as a primer for restorative DNA synthesis, facilitating the completion of the DNA repair process.

During meiosis, the eukaryotic RecA homologs Rad51 and Dmc1 cooperate to promote homology search and strand exchange, the central step in homologous recombination (Brown and Bishop, 2015). Like RecA, Rad51 and Dmc1 form nucleoprotein filaments on ssDNA and catalyze strand exchange *in vitro* (Baumann et al., 1996; Hong et al., 2001; Li et al., 1997; Sung, 1994). Rad51 is responsible for catalyzing strand exchange *in vivo* in mitotically cycling cells (Shinohara et al., 1992). However, the meiosis-specific protein Dmc1 is the predominant meiotic strand exchange enzyme (Bishop et al., 1992; Cloud et al., 2012; Da Ines et al., 2013). Rad51's activity is inhibited during meiosis by the Hed1 protein (Busygina et al., 2008; Tsubouchi and Roeder, 2006). Nonetheless, Rad51 plays an important non-enzymatic role, promoting Dmc1 assembly and directing it to invade a homolog chromatid rather than a sister chromatid (Cloud et al., 2012; Hong et al., 2013; Lao et al., 2013; Schwacha and Kleckner, 1997).

Rad51 and Dmc1 form spatially associated repair complexes in accord with their genetic interaction. In spread meiotic *S. cerevisiae* nuclei, Rad51 and Dmc1 form DSB-dependent foci

(Bishop, 1994). Rad51 and Dmc1 approximately co-localize as side-by-side, partially offset "co-foci" when viewed by widefield epifluoresence microscopy (Bishop, 1994; Kurzbauer et al., 2012; Shinohara et al., 2000). Combined with the propensity of Rad51 and Dmc1 to interact homotypically but not heterotypically (Dresser et al., 1997; Masson et al., 1999; Tarsounas et al., 1999), this staining pattern led to speculation that Rad51 and Dmc1 homofilaments might occupy opposite ends of each DSB (Kurzbauer et al., 2012; Shinohara et al., 2000). This speculation, along with a number of other observations, influenced the development of models of meiotic recombination involving asymmetric loading of Rad51 and Dmc1 on opposite DSB ends (Hong et al., 2013; Hunter, 2007).

The asymmetric loading model in which Rad51 and Dmc1 homofilaments occupy opposite ends of a single DSB has awkward implications. First, the model implies that Rad51 is selectively loaded onto one member of a pair of ends, somehow avoiding the other end of each DSB. Second, Rad51 is required for normal assembly of Dmc1 (Bishop, 1994; Shinohara et al., 2003a), thus the asymmetric loading model requires Rad51 to accomplish this assembly function *in trans* on the opposite DSB ssDNA tract. Third, the asymmetric loading model implies that only the Dmc1-decorated end is capable of strand exchange, given the disposability of Rad51's catalytic activity (Cloud et al., 2012; Da Ines et al., 2013; Tsubouchi and Roeder, 2006). While the asymmetric loading model has been argued to account for the apparent differentiation of the two ends of a DSB (Hong et al., 2013; Hunter, 2007), both ends of a DSB can catalyze strand exchange as evidenced by multichromatid joint molecules that are normally disassembled by the Sgs1 helicase (Oh et al., 2007). Here we present evidence contradicting the asymmetric loading model and supporting a model in which both Rad51 and Dmc1 can and often do load on both

DSB ends. Additionally, we demonstrate that Rad51 and Dmc1 filaments are very short *in vivo* coating only about 100 nt of ssDNA.

3.3 Results

3.3.1 Rad51-Dmc1 co-foci form pairs that can be separated by up to 400 nm

When viewed by widefield microscopy, a substantial fraction of Rad51-Dmc1 co-foci appear to be arranged in pairs separated by up to 400 nm in sparsely populated regions of meiotic *S. cerevisiae* spread diploid (2N) nuclei (Fig 3.1A, arrowhead). It was unclear if this apparent pairing might simply be due to the fortuitous arrangement of unrelated foci in a crowded nucleus. To reduce the potential bias imposed by crowding, we constructed a tetraploid (4N) strain hypomorphic for *SPO11*. This tetraploid carries one wild type (*SPO11*$^{+}$) allele and three alleles that code catalytically inactive protein (*spo11-Y135F*) (Henderson and Keeney, 2004). Spo11 is the transesterase that forms DSBs (Bergerat et al., 1997; Keeney et al., 1997). As expected for a strain with reduced DSB levels and larger nuclei, the average density of Rad51 (and Dmc1) foci per unit area was lower in the *spo11* hypomorphic tetraploid than in wild type diploids. However, individual nuclei with focus densities ranging from very low to the same as that in wild type diploid nuclei were observed, likely reflecting the homeostatic control of DSB levels that eventually compensate for reduced Spo11 activity (Cole et al., 2012; Lange et al., 2011; Lao et al., 2013; Martini et al., 2006)(supported by relatively high spore viability in this strain; Table 3.1). When the analysis was restricted to tetraploid nuclei early in prophase (2.5 hr) with low densities of foci, pairs of foci separated by ≤ 400 nm could clearly be seen (Fig 3.1B-D). Thus, Rad51-Dmc1 co-foci tend to be arranged in pairs.

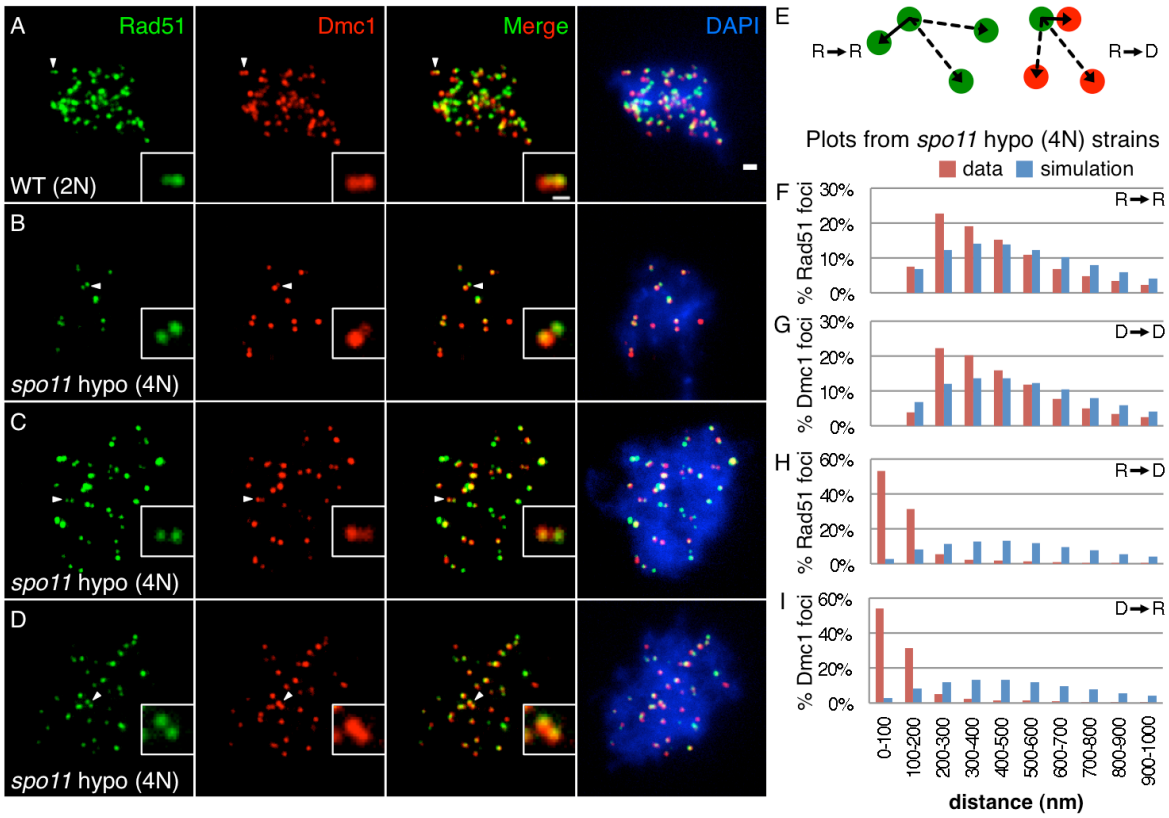

Figure 3.1 Rad51-Dmc1 co-foci occur in pairs separated by 200-400 nm. (**A**) Spread wild type diploid [WT (2N)] nucleus stained for Rad51 (green) and Dmc1 (red). (**B,C,D**) Spread *spo11* hypomorphic tetraploid [*spo11* hypo (4N)] nuclei with relatively low densities of Rad51-Dmc1 staining. Arrowheads indicate examples of paired co-foci in less densely stained areas, magnified in the insets. Scale bar = 1 μ m, 400 nm for the inset. (**E**) Schematic of distance to nearest neighbor measurement for Rad51-to-Rad51 (left) and Rad51-to-Dmc1 (right). Solid arrow represents the distance to the reference focus' nearest neighbor. Dashed arrows represent the longer distances to other foci. (**F,G,H,I**) Distribution of nearest neighbor measurements in wild type *spo11* hypomorphic tetraploid. Experimental data (red) and matched random simulations (blue) shown for (**F**) Rad51→Rad51, (**G**) Dmc1→Dmc1, (**H**) Rad51→Dmc1, and (**I**) Dmc1→Rad51. Micrographs from cultures 2.5 hours after meiotic induction. Scoring of 195 focus-positive nuclei, of all staining densities, containing a total of 13,528 Rad51 foci and 13,230 Dmc1 foci are included in the histograms.

	viable spores						
catalytically active *SPO11* alleles	0	1	2	3	4	total	n
4/4	4%	0%	8%	0%	88%	92%	24
3/4	8%	0%	0%	17%	75%	88%	24
2/4	8%	0%	0%	13%	79%	89%	24
1/4	4%	4%	4%	46%	42%	79%	24
0/4	100%	0%	0%	0%	0%	0%	22

Table 3.1 Spore viability of *spo11* hypomorphic tetraploid series. The *spo11* hypomorphic tetraploids used in the rest of the study all have one of four catalytically active *SPO11* alleles and three *SPO11-Y135F* alleles.

To quantitatively assess the prevalence of the paired co-focus architecture, the distance between each focus and its nearest neighboring focus was measured in the *spo11* hypomorphic tetraploid strains. For example, the shortest distance between the centroid of a Rad51 focus and the centroid of the nearest neighboring Rad51 focus was determined (solid lined arrow, Fig 3.1E, left). This process was repeated for each Rad51 focus in the nucleus, and such measurements from many nuclei were pooled to form a Rad51-to-Rad51 (R→R) nearest neighbor distribution (Fig 3.1F, red). The limited resolution of light microscopy makes it difficult to distinguish foci separated by distances below 200 nm, resulting in estimates of inter-focus distances that decay below 200 nm with a minimum inter-focus distance of about 150 nm in this assay (see Analysis section of Materials and Methods). To evaluate the likelihood that this distribution could be generated by the independent, random assortment of individual foci, a simulated Rad51-to-Rad51 nearest neighbor distribution was generated by randomly positioning foci within a nuclear area (Fig 3.1F, blue, see Methods). For a given distance bin, a higher frequency of experimental pairs than of simulated pairs indicates that such pairs are enriched relative to the expectation based on the random arrangement of foci.

Quantitative analysis of nearest neighbor distributions confirmed that both Rad51 and Dmc1 foci are non-randomly arranged in pairs separated by up to 400 nm (Fig 3.1F,G). This enrichment of focus pairs separated by ≤400 nm was detected in both unselected nuclei and nuclei selected for low focus density (Fig 3.2A-D). Additionally, paired foci are not simply due to local crowding, since ≤400 nm pairs are enriched in locally sparse regions (Fig 3.2E,F). This analysis cannot make strong conclusions regarding the prevalence of pairing below 200 nm (due to the diffraction limit of light). The method also has limited power to identify non-random spatial patterns at distances greater than 400 nm, because it reports only on the closest distance between structures. However, if a precise longer pairing distance were present, it could not account for more than 15% of Rad51 or Dmc1 foci because a subpopulation larger than that size would have been detected (Fig 3.1F,G). We also used the nearest neighbor methodology to assess the spatial relationship of Rad51 foci to Dmc1 foci and vice versa (Fig 3.1E, right). 84% of Rad51 foci are less than 200 nm from the nearest neighboring Dmc1 focus (Fig 3.1H). Similarly, 85% of Dmc1 foci are less than 200 nm from a Rad51 focus (Fig 3.1I). It should be noted that this analysis differs from that of measuring distances between resolved pairs of Rad51, or resolved pairs of Dmc1 foci, because the use of different fluorophores to detect Rad51 and Dmc1 allows measurement of nearest neighbor distances below the resolution limit. The distributions of Rad51-Dmc1 distances support the longstanding observation that Rad51 and Dmc1 foci colocalize imperfectly in a side-by-side configuration (Bishop, 1994; Kurzbauer et al., 2012; Shinohara et al., 2000). In the context of a ≤400 nm pair, each focus in a pair could be a Rad51-Dmc1 co-focus, a Rad51-only focus, or a Dmc1-only focus. All permutations of pair composition were observed with no apparent difference between Rad51 and Dmc1 (e.g. a Rad51 focus was paired with a co-focus equally often as a Dmc1 focus was paired with a co-focus). A

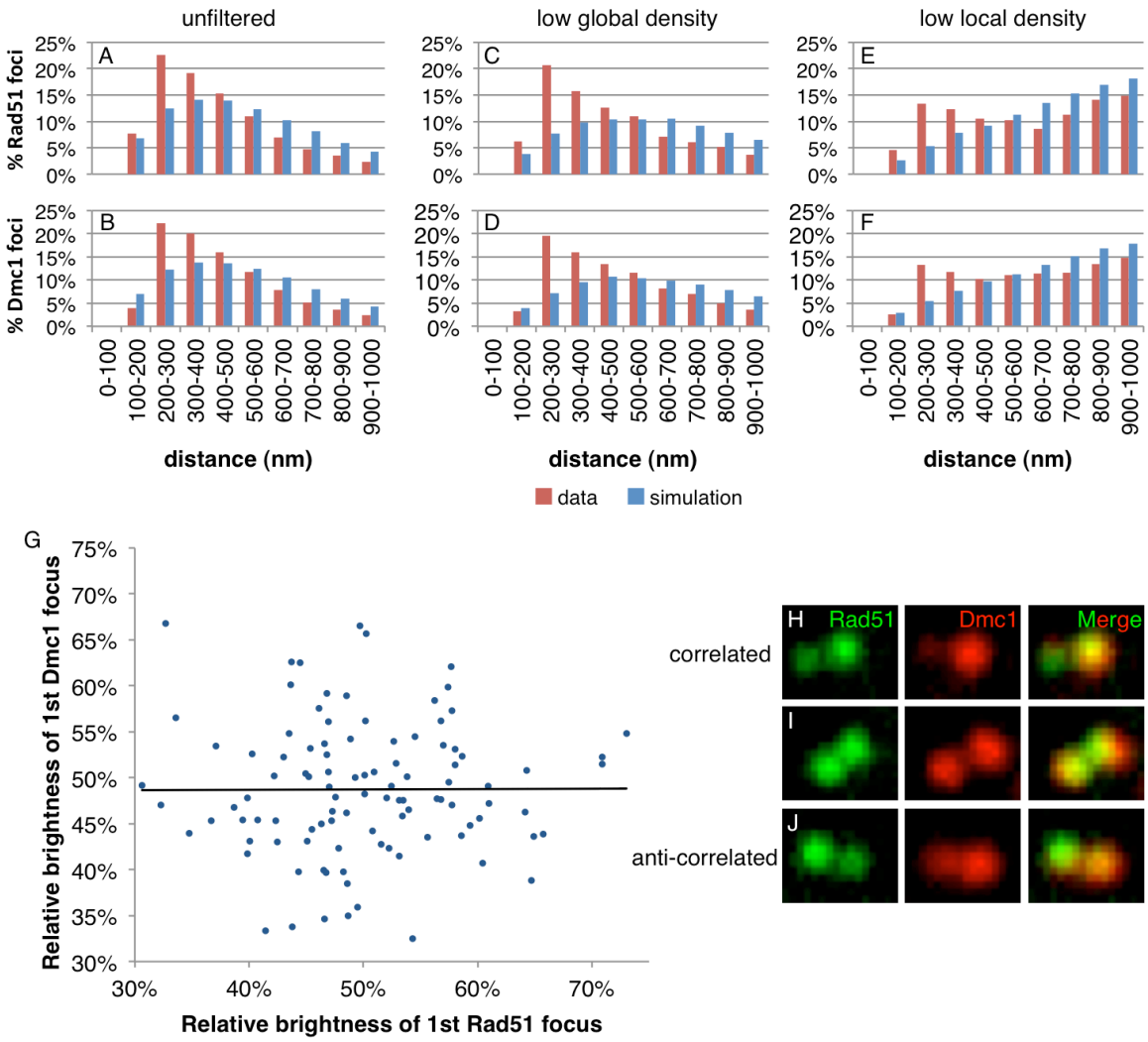

Figure 3.2 Paired Rad51-Dmc1 co-foci are not the result of focus crowding and the staining intensities of Rad51 and Dmc1 in each constituent co-focus are unrelated to the other co-focus. (**A-F**) Focus crowding does not account for pairing of Rad51 foci or pairing of Dmc1 foci. Observed (red) and simulated (blue) Rad51-Rad51 nearest neighbor distributions (**A,C,E**) and Dmc1-Dmc1 nearest neighbor distributions (**B,D,F**) in different subsets of foci from wild type *spo11* hypomorphic nuclei. (**A,B**) The raw, unfiltered set of nuclei replicated from Fig 1F,G for comparison. (**C,D**) Nearest neighbor distributions of low-density nuclei (<0.8 Rad51 or <0.8 Dmc1 foci per μ m^2 of nuclear area). (**E,F**) Nearest neighbor distributions of Rad51 or Dmc1 foci that are located in sparsely populated regions of the nucleus (exactly 1 Rad51 or Dmc1 focus within a 1 μ m horizon of the focus). Micrographs from cultures 2.5 hours after meiotic induction. Sample sizes are 13,528 (A), 4,344 (C), and 1,624 (E) Rad51 foci and 13,230 (B), 4,251 (D), and 1,714 (F) Dmc1 foci. (**G-J**) Rad51 (or Dmc1) staining intensity in one co-focus is unrelated to the staining intensity of Rad51 (or Dmc1) in the other co-focus of a pair of co-foci. (**G**) Scatterplot displaying the brightness of a Rad51 focus vs. that of its associated Dmc1 focus, in 102 pairs of co-foci from *spo11* hypomorphic tetraploids at 2.5 hr time point. The brightness of a Rad51 (or Dmc1) focus is expressed as the percentage of total Rad51 (or Dmc1) signal in

Figure 3.2 cont. the Rad51 (or Dmc1) pair. Each individual point represents one scored pair of co-foci. Linear regression revealed a best-fit line (black line) with a slope of zero, indicating no relationship. (**H-J**) Examples of paired co-foci where the brighter Rad51 focus is associated with the brighter Dmc1 focus (**H**, correlated); both Rad51 and Dmc1 foci are roughly equally bright in both co-foci (**I**); and the brighter Rad51 focus is associated with the fainter Dmc1 focus (**J**, anti-correlated). If Rad51 and Dmc1 brightness were correlated a best-fit line would have a positive slope, while a negative slope would result if they were anti-correlated.

conservative measurement indicates that at least 50% of all focus pairs contain two Rad51-Dmc1 co-foci. Furthermore, the staining intensity of Rad51 or Dmc1 within one half of a co-focus pair does not predict the staining intensity of Rad51 or Dmc1 within the other half of the co-focus pair (Fig 3.2G-J). These results suggest each Rad51-Dmc1 co-focus assembles independently of its partner co-focus.

3.3.2 Pairs of Rad51-Dmc1 co-foci form at individual meiotic DSBs

The enrichment of Rad51 (and Dmc1) pairing at distances ≤400 nm is not simply explained by the restriction of foci to positions along an underlying, but invisible, linear chromosome structure. In leptotene nuclei, Zip1 foci form along the otherwise invisible, linear chromosome axis. Yet, the Zip1 nearest neighbor distribution peaks at longer distances than the Rad51 distribution measured in the same nuclei (Fig 3.3A-E). Furthermore, the Zip1 nearest neighbor distribution resembles the distribution expected from a random arrangement of Zip1 foci (Fig 3.3E). These observations are consistent with the possibility that individual pairs of Rad51-Dmc1 co-foci represent meiotic recombination complexes associated with a single DSB.

Nuclei with a single DSB site provided evidence that each DSB often gives rise to a pair of foci. To further rule out the possibility that paired Rad51-Dmc1 co-foci represent adjacent DSBs along a single chromosome, recombination complexes were characterized in a *spo11* strain heterozygous for the VDE cut site. This background is heterozygous for a cleavage site for the

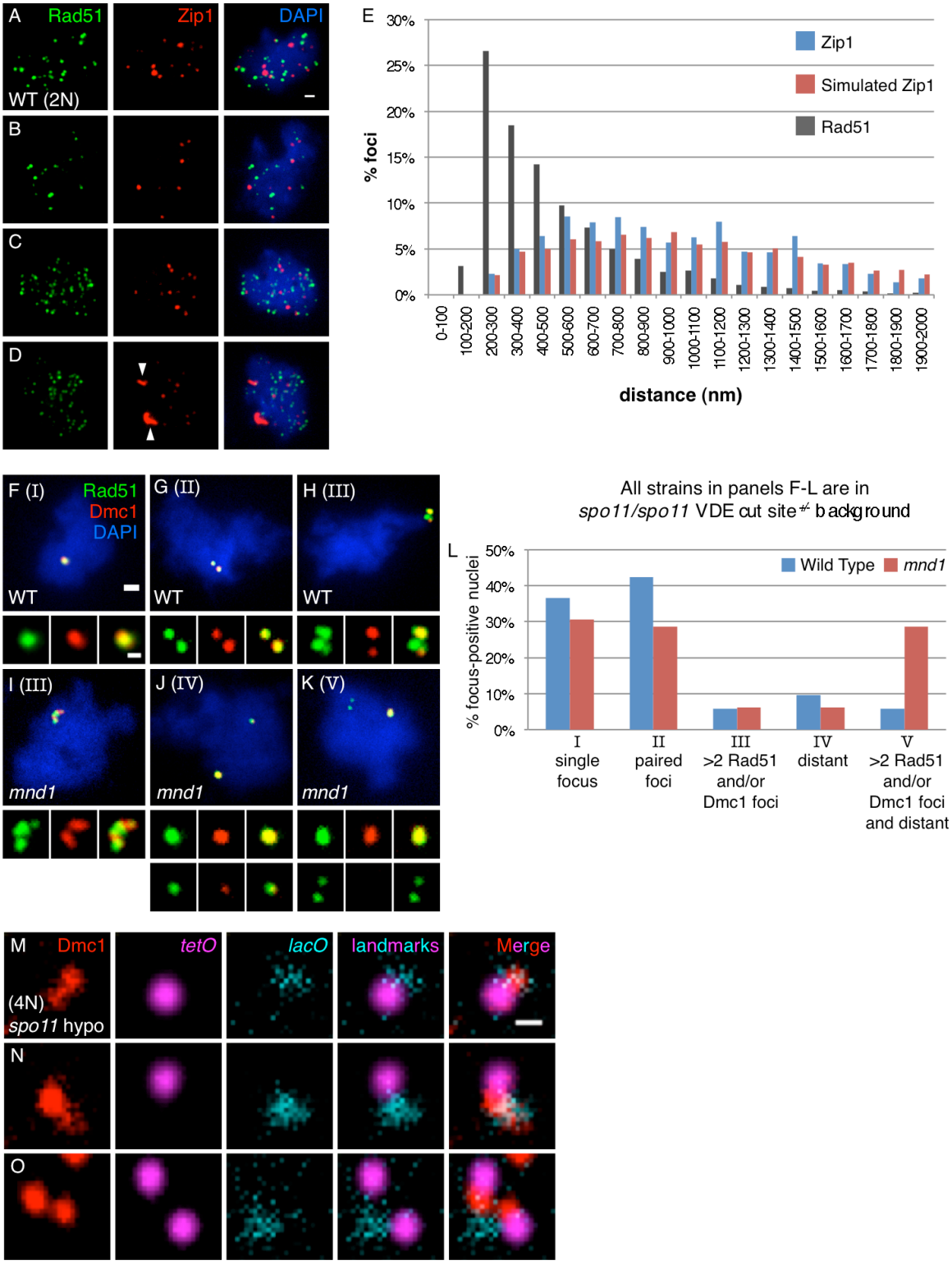

Figure 3.3 Rad51 and Dmc1 form structures inconsistent with asymmetric loading at individual meiotic DSBs. (**A-E**) Rad51 focus pairing is distinct from the spatial arrangement of Zip1. (**A-C**) Micrographs of wild type diploid leptotene (3 hr) nuclei included in the analysis in

Figure 3.3 cont. (E). Rad51 staining is shown in green, Zip1 staining in red, and DAPI in blue. (**D**) Micrograph of nucleus excluded from analysis in (E) because of non-punctate Zip1 structures (arrowheads). (**E**) Nearest neighbor distributions for Zip1 (blue), simulated Zip1 (red), and Rad51 (grey). Sample size is 86 nuclei containing 2,953 Rad51 foci and 1,041 Zip1 foci. Scale bar in panel A is 1 μ m. (**F-L**) Characterization of Rad51-Dmc1 structures in *spo11* diploids heterozygous for the VDE cut site. Rad51 staining is shown in green, Dmc1 in red, and DAPI in blue. (**F-H**) Micrographs of wild type nuclei with (**F**) a single focal structure (category I), (**G**) paired foci (category II), and (**H**) a more complicated structure (>2 Rad51 and/or Dmc1 foci; category III; categories shown in parentheses at top left of each micrograph). (**I**) Micrograph of *mnd1* strand exchange mutant with more complicated structures containing >2 Rad51 and/or Dmc1 foci in close proximity (category III). (**J**) Micrograph of spatially distinct structures each composed of a single focus (category IV) in an *mnd1* mutant. (**K**) Micrograph of a nucleus with >2 Rad51 and/or Dmc1 structures that are also spatially separated (category V) in an *mnd1* mutant. Scale bar = 1 μ m, 400 nm for inset. (**L**) Distribution of these structures in wild type and *mnd1* nuclei represented as a percentage of focus-positive nuclei. Micrographs from cultures 4.5 hours after meiotic induction. 116 wild type and 89 *mnd1* focus-positive nuclei are included. (**M-O**) Paired Dmc1 foci can be observed at the *HIS4::LEU2* DSB hotspot. Micrographs of paired Dmc1 foci near the *lacO* (*ARS 308*) and *tetO* (*ARS 304*) landmarks flanking the *HIS4::LEU2* DSB hotspot. Dmc1 is shown in Red, *tetO* in magenta, and *lacO* in cyan. Scale bar = 500 nm. (**O**) Micrograph in which sister chromatids are split as indicated by a pair of *tetO* foci. Micrographs from cultures 2.5 hours after meiotic induction.

meiosis-specific endonuclease VDE on *chromosome IV*. During meiotic prophase, both sister chromatids are eventually cleaved and repaired via recombination with a homolog chromatid, resulting in about 86% 4:0 gene conversions (Fukuda et al., 2003; Johnson et al., 2007). The kinetics of cleavage and repair at the VDE cut site have not (to our knowledge) been assayed in single cells, but at any given time 0, 1, or 2 DSBs are expected to be present. In chromosome spread preparations, VDE-dependent Rad51-Dmc1 foci were readily observed. While only 4% (2/47) of *spo11* nuclei were focus-positive, 47% (54/116) of wild type and 56% (49/88) of *mnd1* nuclei were focus-positive in the *spo11* VDE cut site heterozygote background. Nuclei with a single focus or a single pair of foci are the predominant classes observed in wild type cells (Fig 3.3F,G,L; categories I and II) representing 79% of total focus-positive nuclei. However, a more complex class of structures containing more than two Rad51 foci and/or more than two Dmc1 foci in close proximity to each other was observed in about 6% of focus-positive wild type nuclei

(Fig 3.3H,I,L; category III). Additionally, nuclei with distant cytological complexes (greater than 1 μm apart) were observed in about 15% of wild type nuclei: 9.6% contained no more than two Rad51 or two Dmc1 foci (Fig 3.3J,L; category IV) and 5.8% contained greater than two Rad51 or two Dmc1 foci (Fig 3.3K,L; category V). Importantly, 11.5% of wild type nuclei with greater than two Rad51 foci or two Dmc1 foci (categories III and V) cannot be explained by the asymmetric loading model in which two Rad51-Dmc1 co-foci—one co-focus at each of two DSBs—is the most complicated predicted structure. Moreover, a model in which both Rad51 and Dmc1 can co-occupy each of the four ssDNA tracts associated with two DSBs readily explains these data. This interpretation is further supported by the accumulation of category III and V nuclei to levels up to 39% of focus-positive cells in *mnd1* mutants defective for strand exchange (Fig 3.3I,K,L) (Gerton and DeRisi, 2002; Tsubouchi and Roeder, 2002; Zierhut et al., 2004). We interpret distant cytological complexes as likely reflecting situations in which the VDE sites on both sister chromatids are simultaneously cleaved, breaking the sister chromatid pair entirely, such that the two halves of the broken chromosome separate *in vivo* and/or during the spreading procedure. Supporting this interpretation, the incidence of distantly separated foci was greater among nuclei with more than 2 Rad51 and/or Dmc1 foci (50%) than among nuclei with only two foci (19%). Furthermore, the class of nuclei with distantly separated foci (categories IV and V) was more predominant in an *mnd1* mutant, primarily due to an increase in category V nuclei (Fig 3.3J,K,L). This observation suggests that blockage of Mnd1-mediated strand exchange results in the accumulation of DSBs leading to the complete breakage of *chromosome IV*, and loading of Rad51 and/or Dmc1 on all four associated ssDNA tracts. In conclusion, the range of structures observed in *spo11* strains heterozygous for the VDE cut site are best explained if both Rad51 and Dmc1 can load onto both ends of a single meiotic DSB.

Co-focus pairs can be seen at a strong meiotic recombination hotspot. To obtain further evidence that paired Rad51-Dmc1 co-foci form at a single DSB, we simultaneously visualized co-foci and fluorescent landmarks flanking the *HIS4::LEU2* DSB hotspot on *chromosome III*. Specifically, tandemly repeated arrays of the bacterial transcription factor binding sites *lacO* and *tetO* were integrated about 60 kb away proximal to the centromere and 37 kb away distal to the centromere, respectively, relative to the *HIS4::LEU2* DSB hotspot on *chromosome III*, in the *spo11* hypomorphic tetraploid strain with only a single chromatid bearing the *HIS4::LEU2* DSB hotspot. Expression of 3xHA-LacI and YFP-TetR allows the arrays to serve as chromosomal landmarks that can be visualized along with Rad51 or Dmc1 foci via immunostaining. Although the position of the *lacO* array was not always detectable (due to partial proteolysis of the 3xHA-LacI fusion protein as demonstrated cytologically and by western blot), a significant subset of nuclei displayed both landmarks. Considering only those nuclei that display both landmarks and a low density of Dmc1 foci in the vicinity of the landmarks, 41% (16/39) had one resolvable pair of Dmc1 foci at the hotspot (Fig 3.3M-O); the remainder had a single focus. Similarly, 39% (19/49) of selected nuclei had paired Rad51. Given previous results showing that breakage of both sister chromatids is very rare at the *HIS4::LEU2* hotspot (only 11% of tetrads show evidence of two different recombination events in a less severe *spo11* hypomorph than the one used in this study) (Zhang et al., 2011), the data provide additional evidence that a single DSB produces a co-focus pair.

3.3.3 Sister chromatids are often spatially separated

Interestingly, the *tetO* landmark signal was split in 50% or more of nuclei, indicating separation of sister chromatids 37 kb away from the *HIS4::LEU2* DSB hotspot (for example, Fig

3.3O). Although the frequency of *tetO* splitting increases after meiotic induction, the vast majority of the observed splitting is *SPO11*-independent (76% vs. 67% of total nuclei in wild type and *spo11,* respectively; n=45 nuclei for each). When there was an optically resolvable pair of split *tetO* spots, they were separated by around 400 nm (381±144; range 240-1008; 94% are between 240 and 600 nm), similar to the distance between paired Rad51 (and Dmc1) foci.

3.3.4 Rad51-Dmc1 co-focus pairing does not require strand exchange or synapsis

To probe the relationship between the paired co-focus architecture and both the progression of recombination reactions and transitions in global chromosome structure, nearest neighbor distributions were determined in strand exchange-defective (*mnd1*) and synapsis-defective (*zip1*) mutants. When strand exchange was blocked in an *mnd1* mutant (Gerton and DeRisi, 2002; Tsubouchi and Roeder, 2002; Zierhut et al., 2004), the paired character of Rad51 (and Dmc1) foci was maintained (Fig 3.4A,C,D). The pairing of Rad51 (and Dmc1) foci was also unaltered in the *zip1* mutant which blocks the progress of recombination reactions after strand exchange (Fig 3.4B-D) (Börner et al., 2004; Rockmill et al., 1995; Sym et al., 1993). In *zip1* mutants, nascent post-strand exchange intermediates promote homolog co-alignment at a distance of 400 nm or less, but the closer 100 nm alignment of lateral elements resulting from elongation of the synaptonemal complex does not occur (Sym et al., 1993). Together, these mutants suggest that the ≤400 nm paired Rad51-Dmc1 co-focus architecture does not require strand exchange and is retained until synapsis. Further analysis demonstrated that the nearest neighbor distributions of Rad51-to-Dmc1 and Dmc1-to-Rad51 distances are also unaltered in strand exchange-defective and synapsis-defective mutants (Fig 3.4E,F), suggesting that the side-

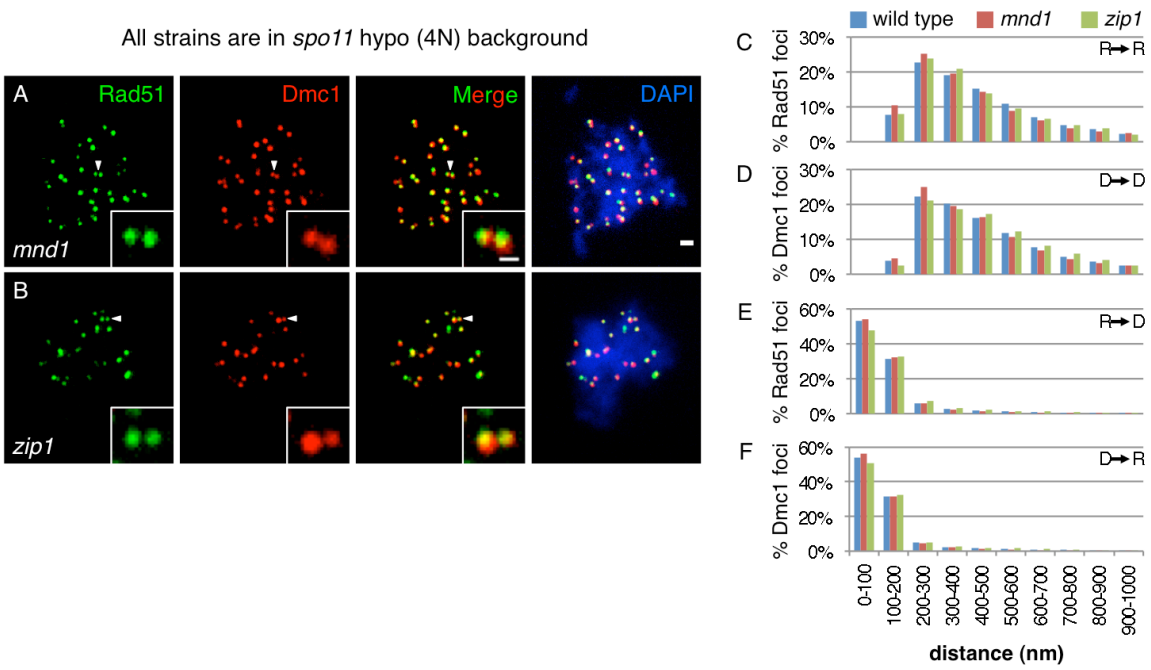

Figure 3.4 The paired architecture of Rad51-Dmc1 co-foci is independent of strand exchange and synapsis. (**A,B**) Micrographs of (**A**) *mnd1* and (**B**) *zip1* mutant nuclei in the *spo11* hypomorphic tetraploid background. Scale bar = 1 μ m, 400 nm for the inset. Rad51 staining is shown in green, Dmc1 in red, and DAPI in blue. (**C-F**) Accompanying distribution of nearest neighbor measurements as in Fig 1 for (**C**) Rad51→Rad51, (**D**) Dmc1→Dmc1, (**E**) Rad51→Dmc1, and (**F**) Dmc1→Rad51. Micrographs from cultures 2.5 hours after meiotic induction. Wild type data repeated from Fig 1 for comparison. Scoring of 70 and 44 focus-positive nuclei; 6,364 and 2,824 Rad51 foci; and 6,114 and 2,655 Dmc1 foci are included in histograms for *mnd1* and *zip1* mutants, respectively.

by-side Rad51-Dmc1 configuration is also established prior to, and persists after, strand exchange.

3.3.5 Small Rad51 and Dmc1 structures are paired at sub-diffraction distances

To characterize recombination complexes in more detail we used direct stochastic optical reconstruction microscopy (dSTORM), a method with higher resolution than standard widefield microscopy (Fölling et al., 2008; Heilemann et al., 2008). We validated our experimental system by imaging long Rad51 filaments prepared by the same method as that used previously for

analysis by electron microscopy (Ogawa et al., 1993; Sehorn et al., 2004; Sheridan et al., 2008). The Rad51 filaments were assembled on dsDNA *in vitro*, deposited on a coverslip, immunostained, and imaged. As expected, reconstructed dSTORM micrographs clearly show long Rad51 filaments often exceeding one micron in length (Fig 3.5A-D). Following indirect immunostaining, the structures observed are 70 nm wide, 60 nm wider than the underlying protein filament as a consequence of both antibody decoration and the finite resolution of the imaging method. Given this apparent filament width, only filaments longer than about 70 nm have readily identifiable long axes in dSTORM reconstructions. Such elongated filaments were readily identified. After validating our dSTORM imaging procedure, we utilized the methodology to interrogate the molecular structures underlying widefield Rad51 and Dmc1 foci *in vivo*.

Super-resolution light microscopy revealed that individual Rad51 (and Dmc1) foci observed by widefield microscopy are often composed of multiple distinct substructures. These Rad51 and Dmc1 "super-resolution foci", hereafter referred to as sr foci, appeared to be paired or to be members of small clusters separated by less than 200 nm (Fig 3.5E,F). In our initial experiments, images generated by super-resolution analysis software displayed fine threads connecting close pairs of sr foci, but further analysis showed this feature of the images was artifactual (for details see Methods and Fig 3.6). Elimination of this artifact revealed pairs or clusters of distinct staining sr foci. In accord with the visual prevalence of pairing/clustering, the 100 nm peak in the Rad51-to-Rad51 (and Dmc1-to-Dmc1) nearest neighbor distribution was enriched relative to a randomly simulated distribution (Fig 3.5I; Fig 3.7A). Furthermore, 28% of Rad51 sr foci that were within 200 nm of at least one sr focus were within 200 nm of more than one sr focus. The nearest neighbor distributions of Rad51 sr foci and Dmc1 sr foci were similar

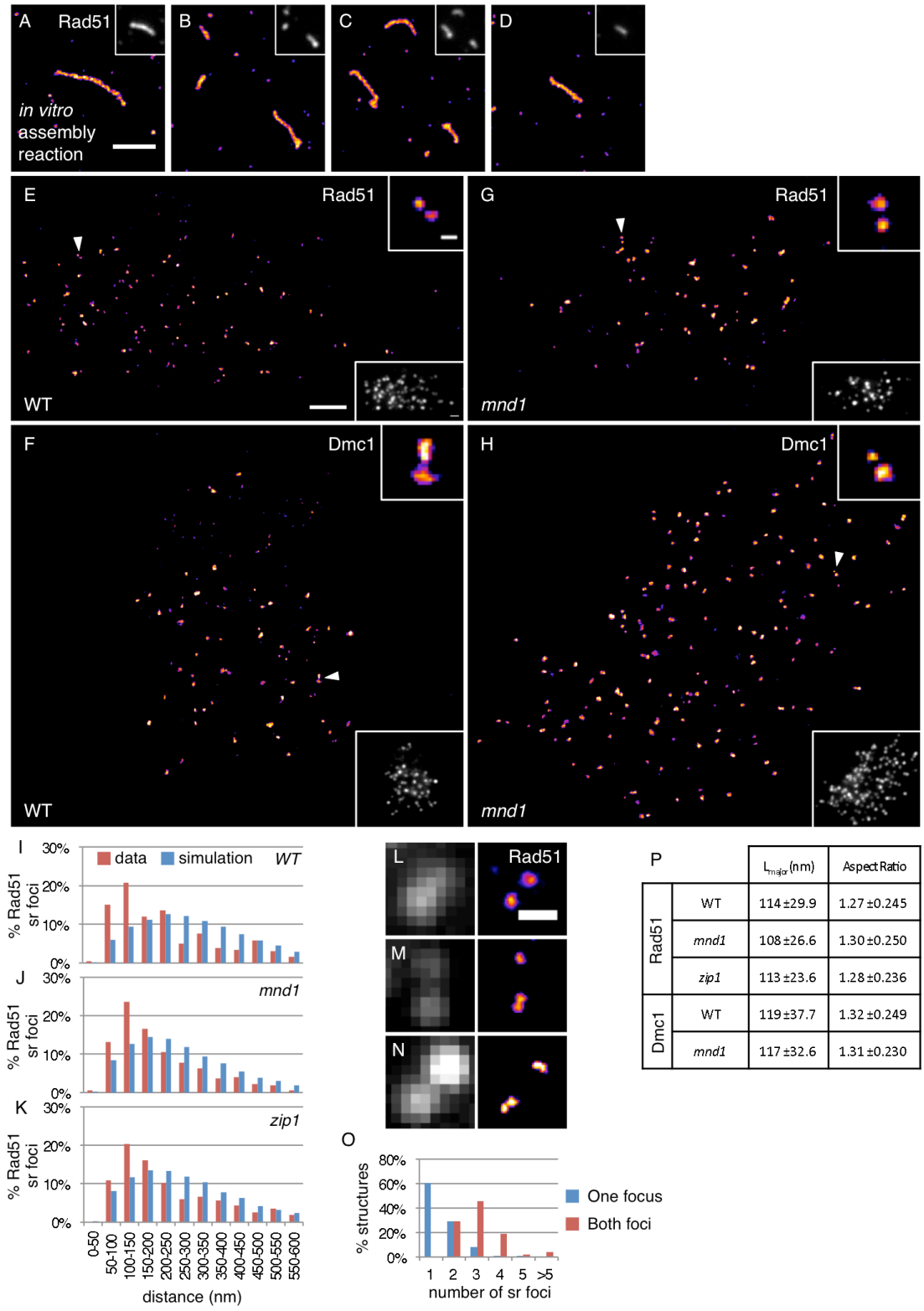

Figure 3.5 Rad51 and Dmc1 sr foci are extremely small and clustered at sub-diffraction distances. (**A-D**) dSTORM micrographs of Rad51 filaments assembled on a linear 2.7 kbp

Figure 3.5 cont. dsDNA *in vitro* in the presence of the meiotic protein Hed1. Corresponding widefield micrographs are inset at top right and the scale bars are 1 μ m wide (**E-H**) Example dSTORM and widefield (bottom right insets) micrographs of wild type nuclei stained for (**E**) Rad51 and (**F**) for Dmc1; *mnd1* nuclei stained for (**G**) Rad51 and (**H**) Dmc1. Arrowheads indicate examples of 100 nm paired Rad51 sr foci, magnified in the upper right insets. Scale bar is 1 μ m for dSTORM and widefield micrographs, 100 nm in top right insets. (**I-K**) Distributions of Rad51→Rad51 sr foci nearest neighbor measurements for (**I**) wild type, (**J**) *mnd1*, and (**K**) *zip1* mutants. Micrographs from cultures 3.5 hours after meiotic induction. (**L-O**) Each Rad51 focus in a pair of Rad51 foci imaged under widefield can contain more than one Rad51 sr focus. (**L-N**) Micrographs of paired Rad51 foci observed at widefield resolution (left) and with dSTORM (right) containing 1 and 1 (**L**); 1 and 2 (**M**); and 2 and 2 (**N**) Rad51 sr foci. Scale bar is 400 nm. (**O**) Distribution of the frequencies of Rad51 sr foci in one focus (blue) or both foci (red) in paired Rad51 foci at low resolution. 48 widefield pairs of Rad51 foci were scored. (**P**) Characterization of the dimensions of Rad51 and Dmc1 sr foci. An ellipse was fit to each sr focus. L_{major} is the length of the ellipse's long axis; aspect ratio equals L_{major}/L_{minor}. Scoring of 432, 212, and 304 sr foci from 5 wild type, 5 *mnd1*, and 5 *zip1* nuclei for Rad51 scoring; 359 and 592 sr foci from 3 wild type and 6 *mnd1* nuclei for Dmc1 scoring. Errors are S.D.

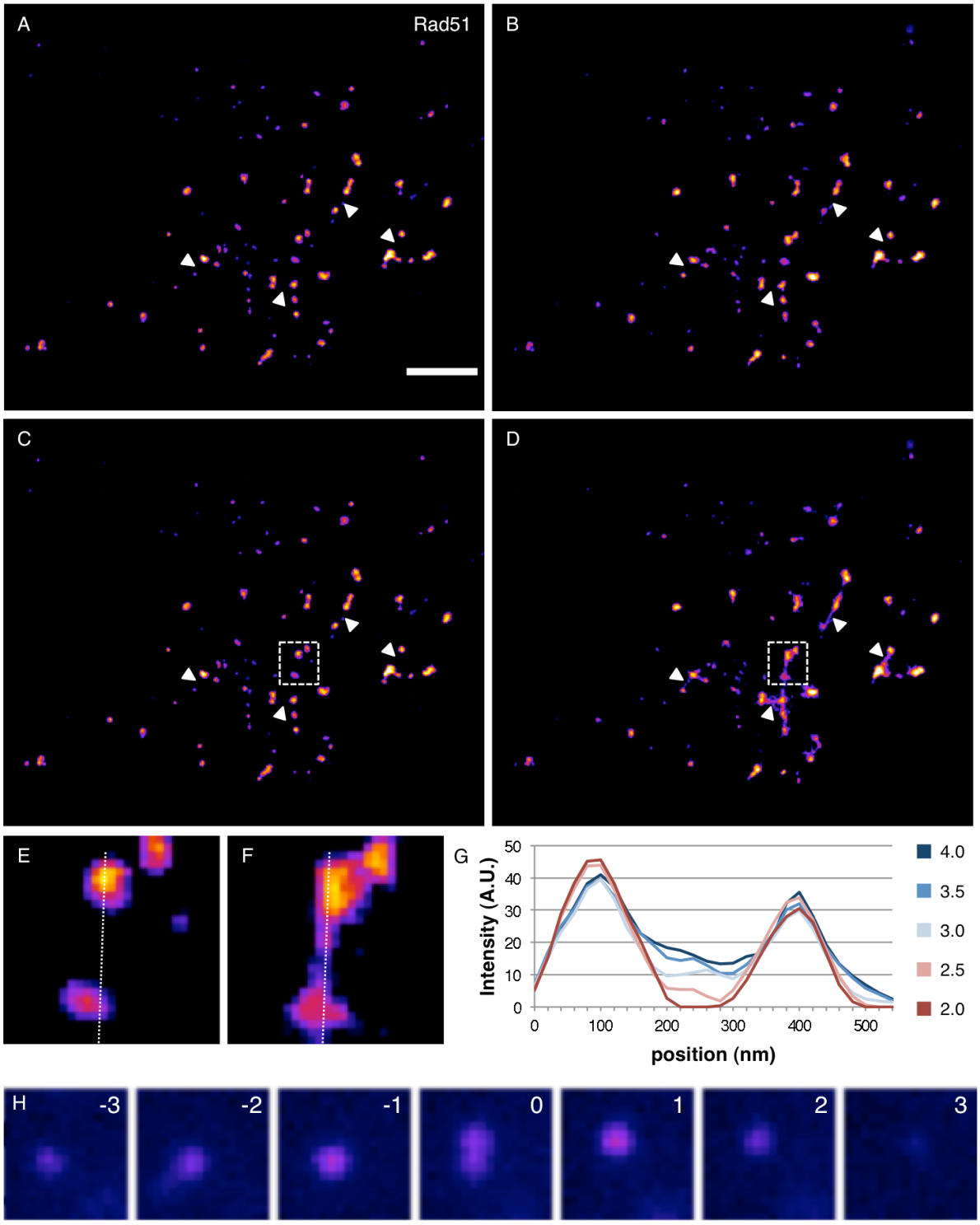

Figure 3.6 Thread-like artifact that can result from post-acquisition localization determination with dSTORM. (**A-F**) A single nucleus imaged and/or reconstructed under different conditions. Imaging was performed under 100% 642 nm laser excitation (low density blinking); later 405 nm laser was added to increase the frequency of blinking (high density

Figure 3.6 cont. blinking). The ImageJ plugin QuickPALM was used to reconstruct micrographs using a stringent or relaxed threshold (2 or 4 pixels, respectively, input into QuickPALM as the "FWHM") to localize events from raw image stacks. (**A**) Low-density blinking and stringent threshold (0.415 events/ μ m^2/sec). (**B**) High-density blinking and stringent threshold (2.09 events/ μ m^2/sec). (**C**) Low-density blinking and relaxed threshold (0.742 events/ μ m^2/sec). (**D**) High-density blinking and relaxed threshold (2.95 events/ μ m^2/sec). 33,378 and 8,375 frames were utilized for the low- and high-density reconstructions, respectively, resulting in about 51,500 "events" called in both frames (C) and (D). Arrowheads indicate the location of threads formed in (D). (**E,F**) Magnified version of boxed region in (C,D). (**G**) Statistical test for artifactual features. As the width cutoff in the image reconstruction algorithm is reduced, real features do not change in relative intensity (peaks near 100 nm and 400 nm in the line scan), but artifactual features due to multiple emitters decay (localizations near 250 nm). (**H**) Threads are the result of localizing an "event" in between two simultaneously fluorescing molecules located several hundred nanometers apart. One example "event" localized to the thread indicated in (F) is shown in frame 0 (relative frame numbers indicated in upper right). A diffraction-limited spot corresponding to a fluorophore in the bottom structure in (E,F) is fluorescing in frames -3 to 0. A separate diffraction-limited spot corresponding to a fluorophore in the top structure in (E,F) is fluorescing in frames 0 to +3. The simultaneous fluorescence of these nearby fluorophores in frame 0 results in mis-localizations that appear as a thread in between the two legitimate structures.

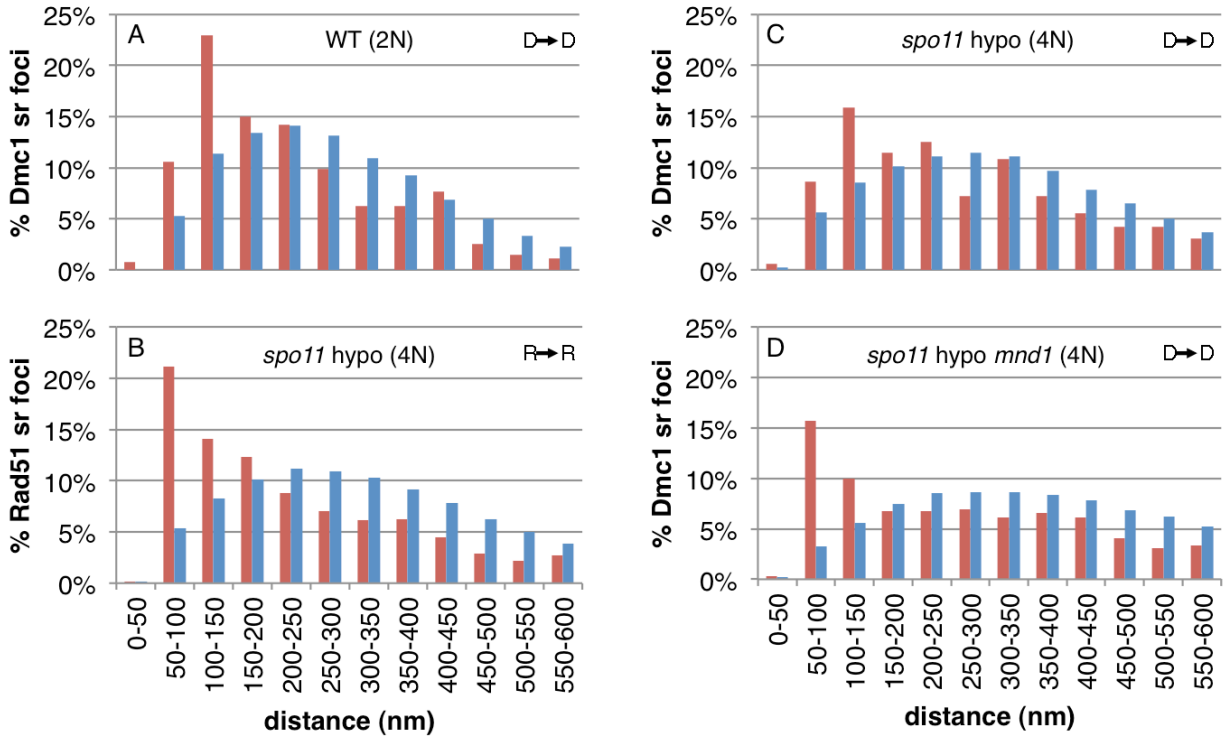

Figure 3.7 Additional nearest neighbor distributions from dSTORM data sets. Nearest neighbor distributions for (**A**) Dmc1 sr foci in WT diploids, (**B**) Rad51 sr foci in *spo11* hypomorphic tetraploids, (**C**) Dmc1 sr foci in *spo11* hypomorphic tetraploids, and (**D**) Dmc1 sr foci in *mnd1 spo11* hypomorphic tetraploids. Sample sizes are 274 Dmc1 sr foci in 4 nuclei, 1084 Rad51 sr foci in 10 nuclei, 359 Dmc1 sr foci in 3 nuclei, and 592 Dmc1 sr foci in 6 nuclei, respectively.

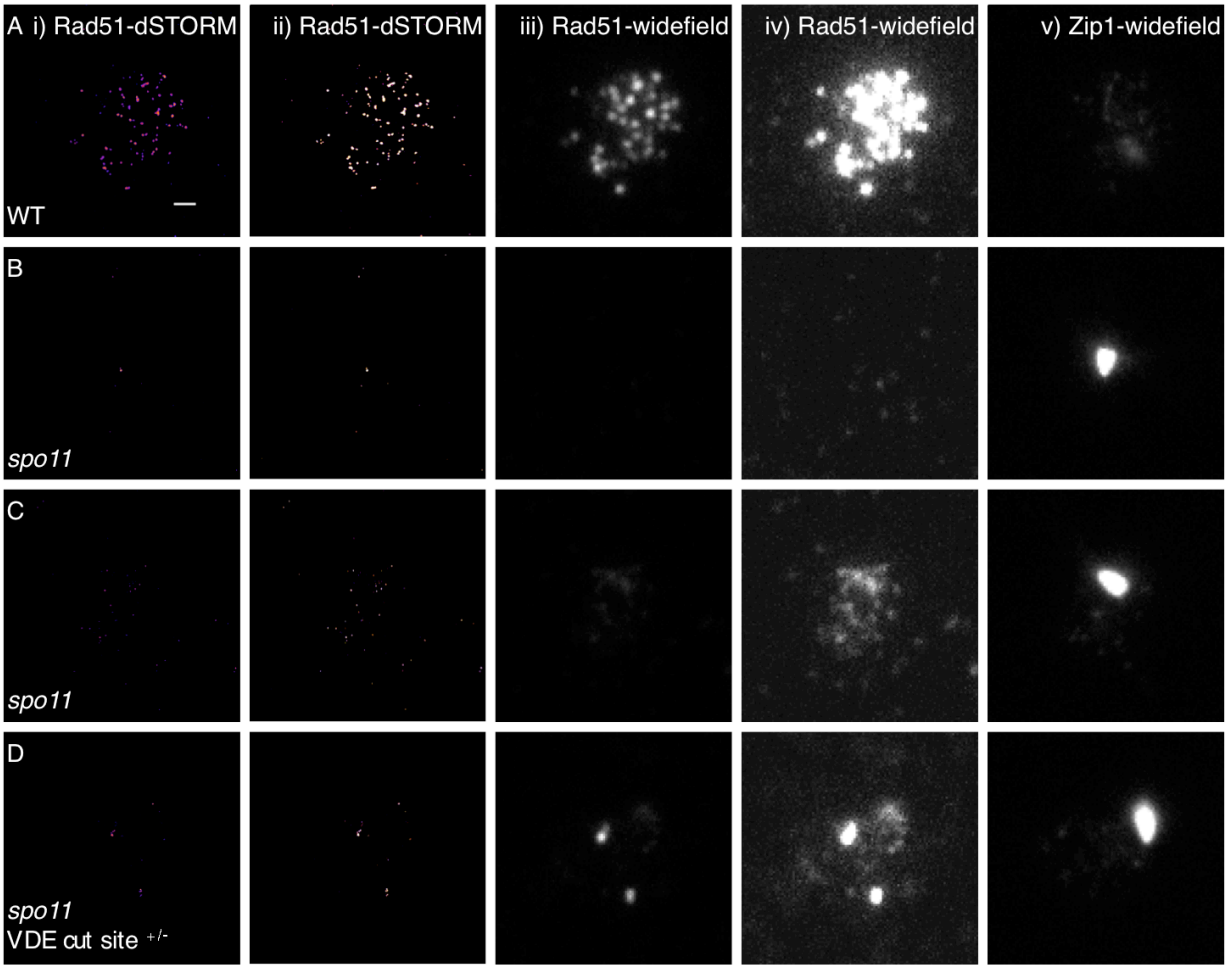

Figure 3.8 When observed by dSTORM, *SPO11*-independent Rad51 sr foci are small, faint, and less numerous than *SPO11*-dependent Rad51 structures. Micrographs of wild type (**A**), *spo11* (**B,C**), and *spo11* VDE cut site heterozygote (**D**) nuclei. The nuclei in (B) and (C) have very little and significant *SPO11*-independent Rad51 staining, respectively. Columns i) and ii) show the same dSTORM reconstruction, the latter displayed more brightly at the expense of signal saturation in some regions. Similarly, columns iii) and iv) show the same widefield micrograph of Rad51 staining displayed at two different brightness levels. Column v) shows the Zip1 staining pattern. Zip1 polycomplex served as a convenient means to locate nuclei lacking bright Rad51 staining patterns. In the micrograph of a *spo11* VDE cut site heterozygote shown in (D) the bright (VDE-dependent) and faint (VDE- and *SPO11*-independent) structures are readily distinguished. Micrographs from cultures 4 hours after meiotic induction. Scale bar is 1 μm wide.

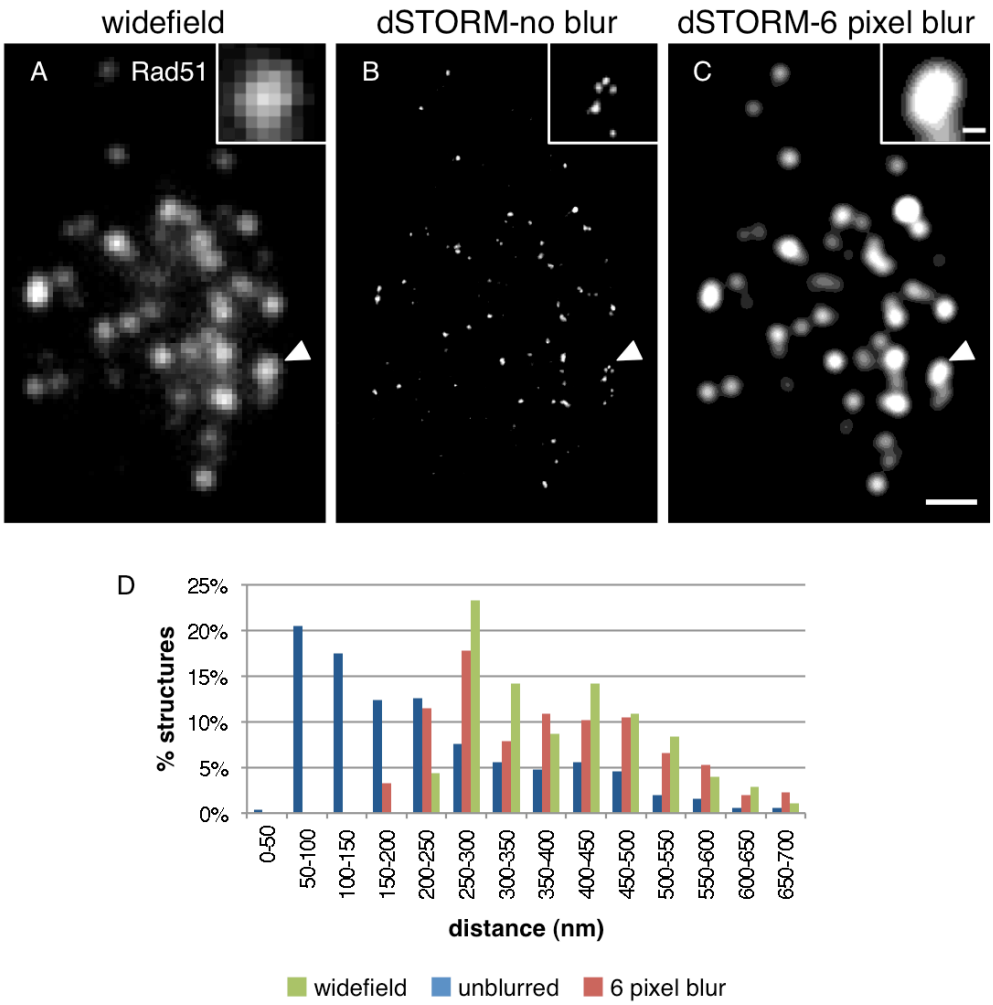

Figure 3.9 dSTORM and widefield micrographs are internally consistent. A single nucleus stained for Rad51 is imaged with (**A**) widefield microscopy and (**B**) dSTORM. The reconstructed dSTORM image is subjected to a (**C**) 6 pixel Gaussian blur, which approximates the transformation of the high resolution micrograph into the low resolution widefield micrograph. A small area (arrowhead) is magnified in insets at top right. Scale bar is 1 μ m wide (or 200 nm wide in the inset). (**D**) Rad51-to-Rad51 nearest neighbor distributions under each of the conditions are plotted. Note that the peak of the distribution is around 100 nm for the dSTORM micrograph without blur and around 300 nm for either the widefield micrograph or the blurred dSTORM micrograph.

in wild type diploids and *spo11* hypormorphic tetraploids (Fig 3.5I; 3.7A-C). Importantly, like standard resolution foci, Rad51 and Dmc1 sr foci are predominantly *SPO11*-dependent (Fig 3.8); the very faint *SPO11*-independent staining observed is likely to reflect binding of Rad51 and Dmc1 at non-DSB sites (Holzen et al., 2006). Artificially blurring dSTORM micrographs generates images that display the same nearest neighbor distributions as those obtained by the standard widefield method, indicating that the images produced by the two modalities are congruent (Fig 3.9).

Comparison of widefield and dSTORM images demonstrates that standard resolution Rad51 (and Dmc1) foci are often composed of two or more constituent sr foci. In the context of paired standard resolution Rad51 foci (see Fig 3.1), each standard resolution focus contains an average of 1.53 ± 0.78 Rad51 sr foci (Fig 3.5L-O). Additionally, nuclei with greater than four Rad51 sr foci were observed in *spo11* mutants heterozygous for the VDE cut site (Fig 3.10). These observations suggest that more than one Rad51 (and more than one Dmc1) filament can occupy a single tract of ssDNA. It should also be noted that the dSTORM results indicate that many of the "single" foci seen by widefield, i.e. foci well-separated from their nearest neighbors, represent pairs or clusters of sr foci.

Like the ≤400 nm pairs observed with widefield microscopy, the Rad51-to-Rad51 (and Dmc1-to-Dmc1) nearest neighbor distributions obtained by dSTORM imaging were unaffected in strand exchange and synapsis mutants (Fig 3.5G,H,J,K; Fig 3.7C,D). These results suggest that sr focus clusters form independently of strand exchange and persist until synapsis.

The Rad51 and Dmc1 structures observed with super-resolution microscopy are only slightly elongated (Fig 3.5E-H,P). The longest dimension of the image of Rad51 and Dmc1 sr foci in wild type nuclei is 114 ± 29.9 and 119 ± 37.7 nm, respectively. Although these distances

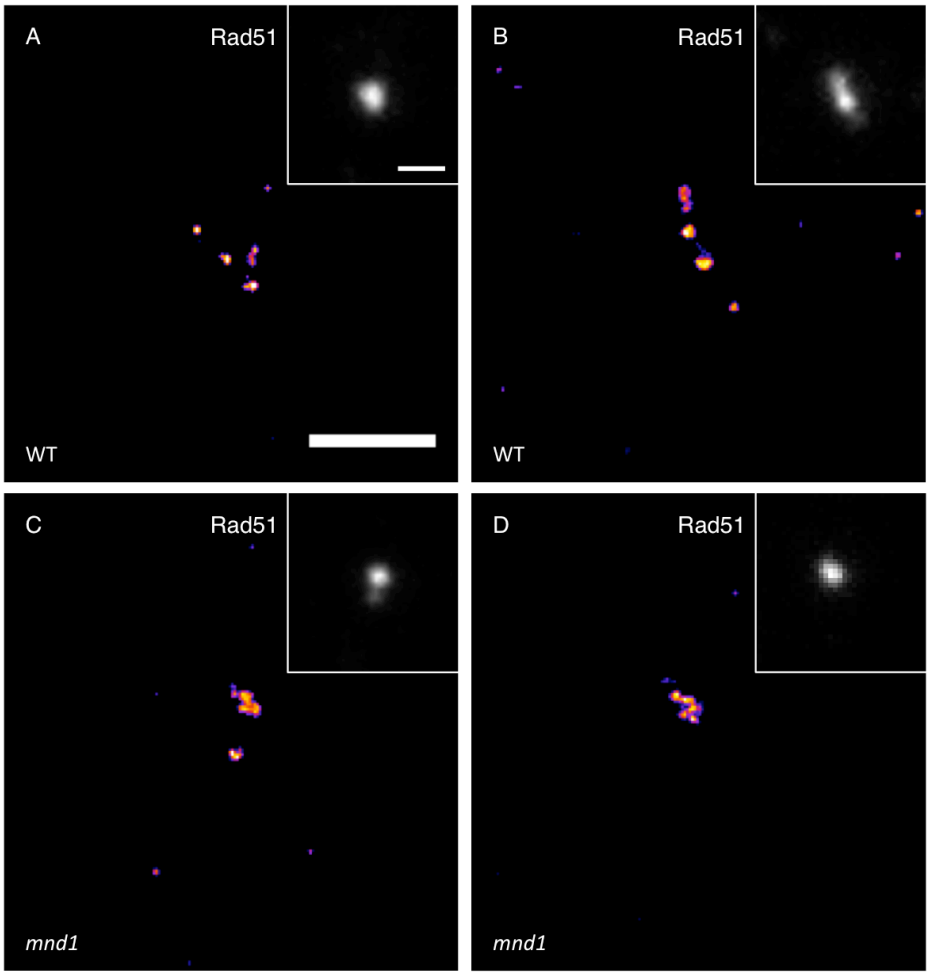

Figure 3.10 dSTORM reveals additional sub-diffraction organization of Rad51 foci in *spo11* VDE cut site heterozygous strains. (**A-D**) Example dSTORM micrographs of Rad51 sr foci with corresponding widefield images inset at top right. Micrographs from cultures 4 hours after meiotic induction. All strains are *spo11* VDE cut site heterozygotes. (**A,B**) are otherwise wild type and (**C,D**) are *mnd1*. Scale bar is 1 μ m wide. Note that there are more than four Rad51 sr foci revealed by dSTORM in each image and that these structures are not elongated.

are greater than the resolution of the technique, the images of sr foci are only slightly elongated with aspect ratios of 1.27 ± 0.25 and 1.31 ± 0.23 (Fig 3.5P). The small size of sr foci suggests only a portion of the ssDNA formed by resection of a DSB is bound by Rad51 or Dmc1 (see Discussion).

We next asked if Rad51 and Dmc1 sr foci were altered when strand exchange is blocked. In wild type cells, Dmc1 foci are present and strand exchange occurs between 3 and 6 hours (Bishop, 1994; Bishop et al., 1992; Schwacha and Kleckner, 1997); foci disappear and strand exchange is complete before 8 hours. If strand exchange is blocked in an *mnd1* or a *dmc1* mutant, DSB-associated ssDNA tracts become much longer than normal by 8 hours (Bishop et al., 1992; Schwacha and Kleckner, 1997; Zierhut et al., 2004). dSTORM microscopy of 3.5 hour *mnd1* nuclei revealed a punctate Dmc1staining pattern very similar to that seen in wild type (Fig 3.5H,P). However, the Dmc1 staining patterns seen in 8-hour *mnd1* nuclei were dramatically different; they contained numerous elongated structures with contour lengths often reaching 250 nm (Fig 3.11A-D). This result indicates that elongation of Dmc1-containing structures is limited by Mnd1 function, likely because completion of Hop2-Mnd1-dependent strand exchange is associated with Dmc1 disassembly, as has been argued for Rad51 based on biochemical observations (Li and Heyer, 2008). Importantly, no corresponding elongated Dmc1 structures have been observed in strand exchange-proficient cells (for example, Fig 3.5F,P). Like Dmc1 staining, little or no difference in the Rad51 staining was seen in either *mnd1* or *dmc1* mutants, as compared to wild type, at 3.5 hours (Fig 3.5G,P; 3.11E-H). However, at 8 hours, *mnd1* nuclei frequently displayed clusters of about 3-7 poorly resolved Rad51 sr foci (Fig 3.11I-L). These clusters lacked obvious elongated structure, in dramatic contrast to the fibrous staining patterns seen for Dmc1 using duplicate slides from the same cultures and time points (compare Fig 3.11A

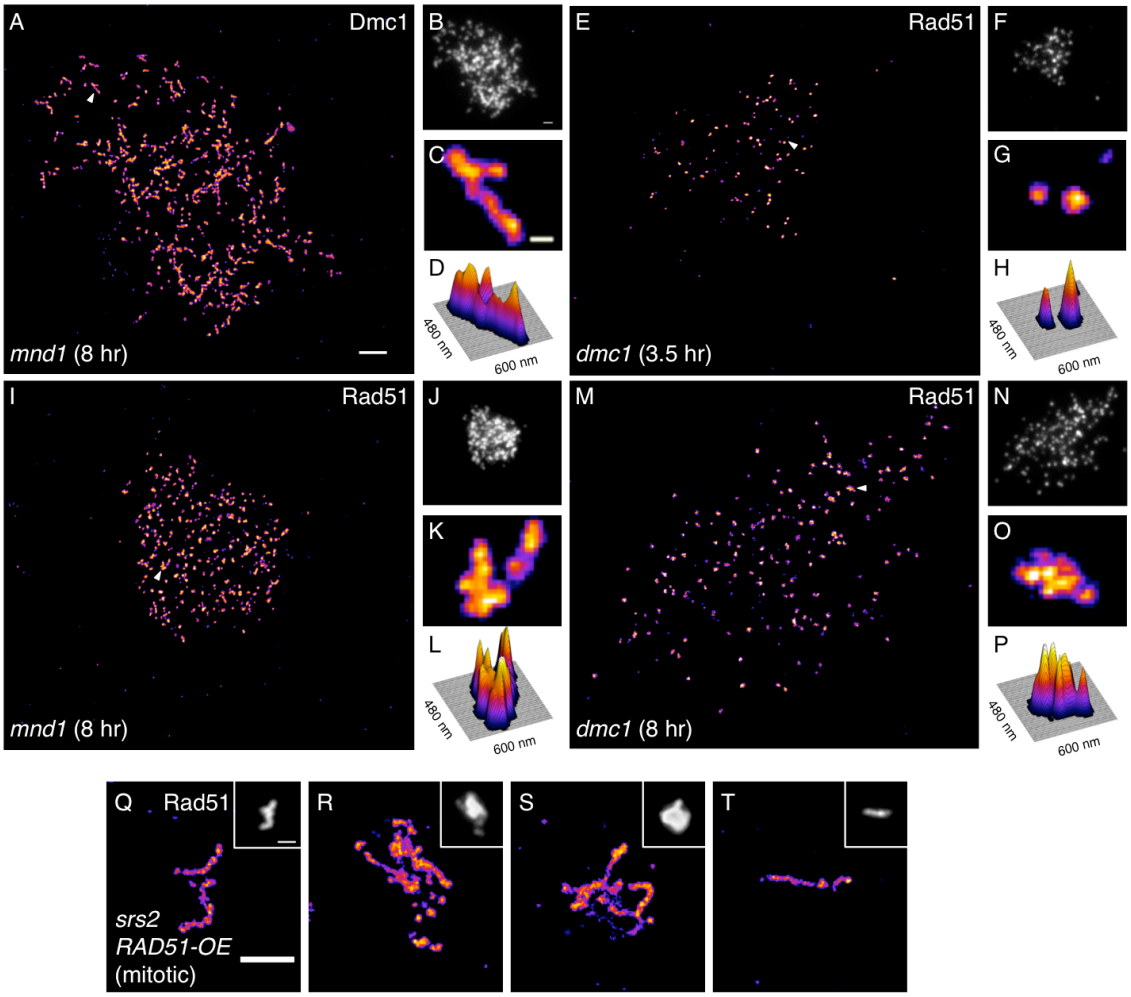

Figure 3.11 Elongated Dmc1 structures and higher order clustered Rad51 structures accumulate in strand exchange mutants at late times. (**A-D**) 8 hr *mnd1* nucleus stained for Dmc1. (**A**) dSTORM and (**B**) widefield micrographs each with 1 μ m scale bars. (**C**) Magnified region from (A) indicated by arrowhead, highlighting elongated Dmc1 structure. Scale bar is 100 nm wide. (**D**) Surface plot of (C). (**E-H**) 3.5 hr *dmc1* nucleus stained for Rad51, highlighting a common pair (low order cluster) of sr foci. (**I-L**) 8 hr *mnd1* nucleus and (**M-P**) 8 hr *dmc1* nucleus stained for Rad51, highlighting higher order clusters of Rad51 sr foci. (**Q-T**) dSTORM micrographs of elongated Rad51 structures observed in spread nuclei of mitotic *srs2* mutants overexpressing Rad51. Scale bar is 1 μm.

to 3.11I). Similar clustering of Rad51 sr foci was seen at 8 hours in *dmc1* cells (Fig 5M-P), suggesting Dmc1 does not influence formation of Rad51 clusters when strand exchange is blocked. The Rad51 staining results are in agreement with previous low resolution studies showing Rad51 focus staining intensity increases with time in *dmc1* and *mnd1* mutants (Bishop, 1994; Tsubouchi and Roeder, 2002).

The observation that elongated Dmc1 structures are seen at 8 hours in *mnd1* mutants indicates that the small dimensions of sr foci in strand exchange-proficient cells truly reflect the dimensions of underlying structures in living cells, rather than a shortcoming of the chromosome spreading or staining methods. To further address this issue, we examined mitotic *srs2* mutant cells overexpressing Rad51. These mutant cells had previously been shown to form elongated structures by widefield microscopy (Shah, 2008). In these cells, spread nuclei stained for Rad51 and imaged by dSTORM revealed filamentous structures with contour lengths of up to 1.5 μm (Fig 3.11Q-T). Thus, we have observed highly elongated Dmc1 structures (Fig 3.11A-D) and Rad51 structures (Fig 3.11Q-T) *in vivo* with dSTORM imaging. Importantly, the widths of these elongated Rad51 and Dmc1 structures match the 70 nm width of the images of Rad51 filaments assembled *in vitro* and imaged under identical conditions (Fig 3.5A-D). These results strongly suggest that the small Rad51 and Dmc1 sr foci observed in meiotic nuclei are indeed very short filaments. Furthermore, we can rule out several potential explanations for the size and arrangement of *in vivo* sr foci including disruption of filaments by the spreading procedure and incomplete antibody labeling. Finally, the clear contrast between elongated structures/filaments and clustered sr foci strengthens the conclusion that clustered sr foci associated with hyper-resected tracts of ssDNA represent distinct filamentous entities rather than an artifact of dSTORM imaging. In summary, dSTORM easily detects elongated Rad51 and Dmc1 filaments

under our experimental conditions. Given this, we conclude that the Rad51 and Dmc1 sr foci observed in wild type meiosis represent underlying structures that are shorter than 40 protomers on average.

3.4 Discussion

3.4.1 A single DSB end is bound by short, often multiple, Rad51- and Dmc1-containing structures

Assuming that Rad51 and Dmc1 sr foci represent the DNA bound helical filaments that promote strand exchange *in vitro*, the sr foci we observed by dSTORM suggest that the Rad51 and Dmc1 filaments that promote recombination *in vivo* are extremely short and that more than one Rad51 and/or Dmc1 filament can form on the same ssDNA tract. Images of Rad51 and Dmc1 sr foci are only about 115 nm long. Since the diameter of Rad51 and Dmc1 filaments are known to be 10 nm (Sheridan et al., 2008), but sr foci are 70 nm wide, the images of sr foci observed with super-resolution microscopy following indirect immunostaining are likely about 60 nm larger in each dimension than the underlying protein complex. This difference can be accounted for by considering the size of the primary and secondary antibodies decorating the structure. Thus, assuming that RecA homolog structures represent the canonical nucleoprotein filaments (Sheridan et al., 2008), they are about 55 nm long. Given that Rad51 and Dmc1 filaments contain about 2 nt per nm (Chen et al., 2008b; Ogawa et al., 1993; Sheridan et al., 2008), this corresponds to roughly 100 nt, 33 protomers of Rad51 (or Dmc1), and 5 turns of the helical nucleoprotein filament. This length estimate suggests that an individual Rad51 or Dmc1 filament typically occupies less than 15% of a typical 800 nt ssDNA tract (Bishop et al., 1992; Zakharyevich et al., 2010). An alternative, but in our view less likely, interpretation, is that RecA

homologs coat a more substantial fraction of each ssDNA tract in a previously unknown compact configuration. Additionally, a significant fraction of the closely spaced (<200 nm apart) Rad51 sr foci likely represent loading of distinct filaments on the same tract of ssDNA as evidenced by detection of nuclei with more than 4 Rad51 sr foci in VDE cut site heterozygote nuclei and the accumulation of clustered Rad51 sr foci at late time points in strand exchange mutants. Although 100 nt filaments are quite small relative to those that have been studied in many biochemical experiments (Roca et al., 1990), both ensemble and single molecule experiments have shown that only 8 nt is sufficient for recognition of homology by RecA-like strand exchange proteins (Hsieh et al., 1992; Qi et al., 2015). Thus, the size of the structures we observe is more than sufficient to promote efficient recombination. The finding that Rad51 and Dmc1 structures are small relative to the average length of ssDNA tracts is in agreement with previous observations indicating that Rad51 foci display offset colocalization with foci formed by the recombination proteins RPA and Rad52. These observations suggest that RPA and Rad52 can simultaneously occupy ssDNA segments adjacent to regions bound by Rad51 and Dmc1 (Gasior et al., 1998). Furthermore, the lack of an inverse relationship between Rad51 and Dmc1 staining intensity in a single co-focus supports the hypothesis that ssDNA tracts are not completely bound by RecA homologs. All of these observations suggest that the protein composition and organization of a tract of ssDNA associated with a meiotic DSB is highly heterogeneous (Fig 3.12, top).

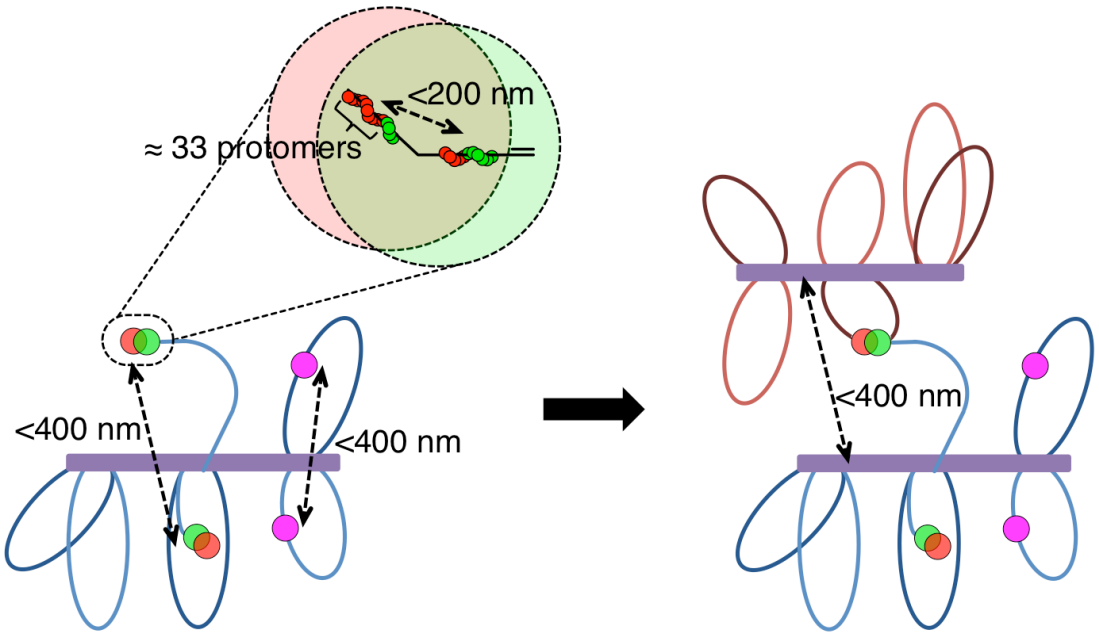

Figure 3.12 Recombinosome Model: Rad51 and Dmc1 each form short filaments on both spatially separated ends of a DSB. (**Top**) Short helical Rad51 and Dmc1 nucleoprotein homofilaments (green and red, respectively) form on adjacent segments of a single DSB-associated ssDNA tract. Each of these filaments is on the order of 100 nt or 33 protomers long and more than one Rad51-Dmc1 structure can form on a single tract of ssDNA. This single end of the DSB manifests itself cytologically as a side-by-side Rad51-Dmc1 co-focus (represented by the offset transparent red and green circles). (**Left**) Both Rad51 and Dmc1 similarly occupy the second end of the DSB. Prior to strand exchange, the two ends of the DSB are separated by 400 nm or less, resulting in focus pairing. The two ends of the DSB are both tethered to the axial element (purple box) by chromatin arms of variable length. Sister chromatids (pink circles) are often split in a DSB-independent manner. (**Right**) This architecture is maintained after strand exchange tethers the homolog at the predetermined distance of 400 nm or less.

3.4.2 Rad51 and Dmc1 occupancy does not functionally differentiate the 1st and 2nd ends of a DSB

The evidence presented here for loading of both Rad51 and Dmc1 on both DSB ends suggests that the two ends may be functionally identical with respect to homology search and strand exchange activity. The observed paired co-focus structure also suggests a simple molecular mechanism through which Rad51 could mediate Dmc1 assembly (Brown and Bishop, 2015). Binding of Rad51 to a ssDNA tract could enhance the efficiency of nearby Dmc1 filament

initiation on that same tract (Bishop, 1994; Hayase et al., 2004; Shinohara et al., 2003a; Tsubouchi and Roeder, 2004). Furthermore, although the two DSB ends engage the homolog in temporal succession (Hunter and Kleckner, 2001), the first invading end need not be predetermined. Rather, the two ends of a DSB might both be released from the tethered loop complex in which they are formed (Fig 3.12, left) (Blat et al., 2002). It is possible that both ends then compete to locate and invade a homolog chromatid with the "winner" maturing into the stable single end invasion intermediate (Hunter and Kleckner, 2001). Indeed, the presence of Dmc1—and thus its homology search and strand exchange activity—on both ends of a single DSB accounts for the existence of joint molecules connecting more than two chromatids (Oh et al., 2007). These multichromatid joint molecules are not readily accounted for by the model positing loading of Rad51 and Dmc1 on opposite DSB ends, because the ability of Rad51 to form homology-dependent joint molecules is inhibited by Hed1 protein during meiotic prophase (Tsubouchi and Roeder, 2006).

While our data argue that a large fraction of DSBs load both Rad51 and Dmc1 on both ends, a subset of structures in our micrographs do not fit into this class. At standard resolution, about 15% of Rad51 foci do not colocalize with Dmc1 foci (and vice versa), representing at least one ssDNA tract lacking Dmc1 (or Rad51). At super-resolution, about 21% of Rad51 sr foci lack a neighboring Rad51 sr focus within 400 nm, indicating a Rad51-coated ssDNA end unaccompanied by another Rad51-coated ssDNA tract within 400 nm. These results could be explained by a number of non-mutually exclusive possibilities. First, some focus pairs may be too close together to be resolved, even by dSTORM. Second, it is likely that a substantial fraction of structures formed by Rad51 and Dmc1 are too small to be detected by our methods. Consistent with this, focus staining intensities vary dramatically with some foci being only

barely detectable above background. Third, the spread nuclei analyzed represent static snapshots of a possibly dynamic and undefined recombinosome assembly and disassembly process that ultimately passes through a stage where both Rad51 and Dmc1 occupy both DSB ends. Fourth, some DSBs may be processed by alternate pathways that do not require Rad51 and Dmc1 loading on both ends, as observed in a *rad51* mutant for example (Schwacha and Kleckner, 1997; Shinohara et al., 2003a).

3.4.3 The two ends of a meiotic DSB separate

Despite the proposed molecular symmetry, our results suggest that DSB ends can separate to distances of up to, and only rarely longer than, 400 nm. This distance is reminiscent of the conserved distance of 400 nm or less at which homologs are initially aligned (Zickler and Kleckner, 1999). Homolog alignment occurs at sites of nascent strand exchange intermediates—called axial association sites—prior to engagement of the second end of the DSB (Börner et al., 2004; Storlazzi et al., 2010; Sym et al., 1993). Thus, we interpret Rad51-Dmc1 co-foci paired at distances up to 400 nm as representing the structures responsible for the strand exchange-dependent component of homolog alignment (Fig 3.12, right). This cytological pattern of spatial separation between pairs of foci composed of recombination proteins Rad51 and Mer3, has previously been observed during leptotene/zygotene in *Zea mays* and *Sordaria macrospora*, respectively (Franklin et al., 1999; Storlazzi et al., 2010). Yet, surprisingly, the paired Rad51-Dmc1 co-focus architecture depends on neither strand exchange nor synapsis in *S. cerevisiae*. Thus, we conclude that the two ends of a DSB are separated by up to 400 nm prior to and after strand exchange (Fig 3.12). In other words, we propose that the structure of a pre-strand exchange intermediate determines the distance at which homolog axes will be aligned.

What determines the distance at which the two ends of a DSB are separated? The variability up to 400 nm suggests that this length is not strictly determined by a fixed proteinacious scaffold, such as the Zip1 protein, which is responsible for the defined 100 nm spacing of lateral elements in the synaptonemal complex (Sym and Roeder, 1995). Instead, we propose that DSB formation within a chromatin loop (Blat et al., 2002), followed by release of the two flexible chromatin arms anchored at sites of sister chromatid cohesion along developing axial elements, allows the two DSB ends to separate as observed. The distribution of sister chromatid splitting distances rarely exceeds 600 nm, suggesting that chromatin loops are about 600 nm in length, similar to estimates of loop size obtained by electron microscopy (Moens and Pearlman, 1988). If this loop size is correct, the lengths of the two released chromatin arms sum to about 600 nm, a distance in reasonable agreement with the separation distances detected for pairs of Rad51 or Dmc1 foci. We note that the DSB-independence of the sister chromatid splitting favors our hypothesis that the ends passively separate and does not provide support for the idea that meiotic recombination events involve local loss of sister chromatid cohesion or disassembly of chromatin to form a long homology-searching tentacle capable of searching the nuclear volume without associated movement of chromosome axes (Kim et al., 2010). It is also in agreement with the alternative possibility that the searching entity is a chromatin "arm," rarely longer than 400 nm, that extends from the axial element (Kim et al., 2010). It is also important to note that although the ≤400 nm axis alignment distance is conserved in diverse organisms, meiotic chromatin loop size is not (Zickler and Kleckner, 1999). Thus, the similarity between focus separation distances and chromatin loop size could be unique to *S. cerevisiae*.

Chapter 4

Live cell imaging of recombination proteins

*Matt Goodsmith contributed to the Rad52 experiments in this chapter. Ivy Fitzgerald and Ben Glick contributed GFP fusion constructs and strains.

4.1 Chapter overview

Although recombination complex structure has been extensively characterized in non-living cytological preparations, initial live cell imaging experiments have provided a dramatically different perspective on these structures. Specifically, the examination of GFP-tagged recombination proteins led to the "recombination factory" hypothesis that multiple DSBs coalesce into a single compartment specialized for DNA repair. In this chapter, we generate and functionally characterize fusions between recombination proteins (Rad52, Rad51, and Dmc1) and either fluorescent proteins (EGFP and msGFP) or tetracysteine tags. Furthermore, the structures of recombination complexes observed in live cells are compared to those observed fixed cells and chromosome spreads. The results suggest that relatively few recombination complexes are observed in live cells because they are often too small to exceed background fluorescence—not because they coalesce into "recombination factories".

4.2 Introduction

In contrast to other fields of cell biology, live cell imaging of the DNA repair machinery has lagged behind. There are particularly few live cell imaging studies in meiotic cells, and they

are generally restricted to studies of chromosome architecture (Conrad et al., 2008; Koszul et al., 2008; Rog and Dernburg, 2015). Greater efforts have been committed to live cell imaging of recombination proteins in mitotic cells (Essers et al., 2002; Lesterlin et al., 2013; Lisby et al., 2001; 2004; 2003). These studies have thus far failed to coalesce around a unifying view of recombination complex architecture and dynamics *in vivo*. The main questions of interest are: what are the dynamics of recombination complex assembly/disassembly and do multiple DSBs occupy a single "recombination factory"?

Examination of recombination complex assembly/disassembly dynamics is the primary reason for live cell imaging. Existing cytological methods are limited to indirect inferences regarding dynamics. The fluorescent protein tagging approach utilized by Lisby et al. has been applied to monitor the assembly and disassembly of a large number of recombination enzymes (Lisby et al., 2004). While this approach seems to accurately report on the genetic requirements for recombination protein assembly or disassembly, interpretations of the timing of these events are intimately connected to the interpretation of the machinery underlying a focus.

The idea that multiple DSBs simultaneously co-occupy a single "recombination factory" is often cited but based on disputed interpretations (Lisby et al., 2001; 2003). The evidence was essentially three pronged and depended to a large extent on the visualization of GFP-tagged proteins. First, fewer Rad52-YFP foci were observed than the predicted number of DSBs present following irradiation. In this context, it should be noted that—although not emphasized—Lisby et al. frequently observed numerous Rad52-YFP foci in a single nucleus (Lisby et al., 2001). Second, the number of Rad52-YFP foci formed after a low irradiation dose does not increase dramatically following a subsequent, much larger irradiation dose. Finally, DSB induction at two distant chromosome loci causes the loci to juxtapose, in strains where no recombination proteins

are tagged. These simple observations form the basis for the "recombination factory" model, but contrast with previous observations indicating a correspondence between the number of DSBs and the number of recombination complexes (Gasior et al., 1998; Miyazaki et al., 2004). However, there are alternative explanations for these data that do not require that DSBs cluster into "recombination factories". One possibility is that recombination complexes are often too small to be observed above background fluorescence. Another possibility is that GFP-mediated oligomerization and increased chromatin mobility following DSB formation are responsible for the range of observations described above (Dion and Gasser, 2013; Pédelacq et al., 2006). Given the importance of understanding recombination complex architecture and kinetics, these alternative explanations need to be addressed.

Live cell imaging of individual recombination complexes may revolutionize the DNA repair field one day, but there are many technical hurdles to overcome in the meantime. Our immediate goals are two-fold. First, the relationship between structures observed in fixed cells and those observed in live cells needs to be established. Second, Rad51 and Dmc1 proteins that are both functional and observable in live cells need to be generated.

4.3 GFP-tagged Rad52

To evaluate the hypothesis that GFP-mediated oligomerization is responsible for the "recombination factory" paradigm, EGFP- and msGFP-tagged Rad52 fusions were compared. The Glick lab designed msGFP to avoid the aggregation caused by hydrophobic surfaces and poor polypeptide folding (Aronson et al., 2011; Fitzgerald and Glick, 2014; Pédelacq et al., 2006). As shown previously for *RAD52-YFP* (Lisby et al., 2004), *RAD52-EGFP* and *RAD52-msGFP* cells both largely complement the survival defect of *rad52* cells following gamma

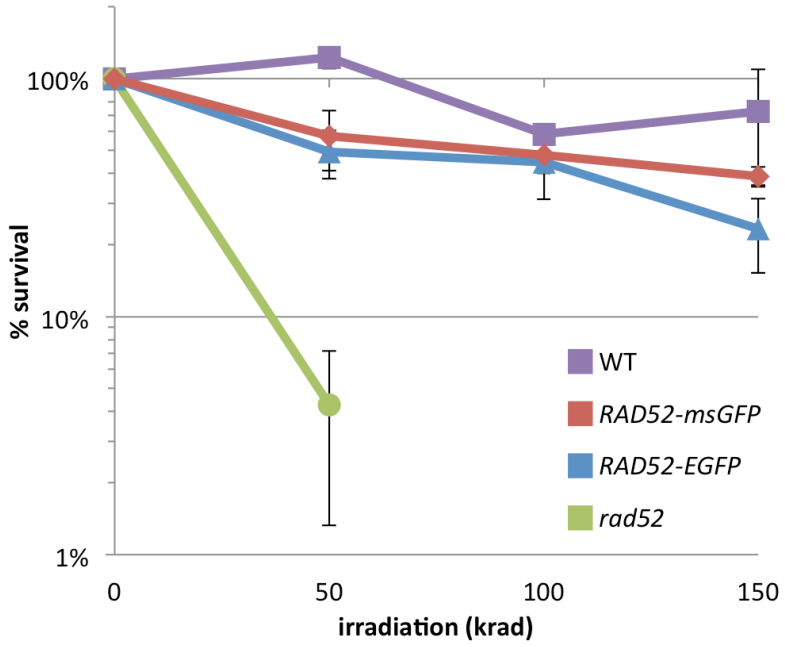

Figure 4.1 msGFP and EGFP-Rad52 remain largely functional. Kill curves in response to gamma irradiation. Percentage survival plotted on a logarithmic scale against irradiation dose (krads). WT (purple), RAD52-msGFP (red), RAD52-EGFP (blue), and rad52 (green) strains shown. Error bars are standard error, n=3.

irradiation (Fig 4.1). Cells with one or, frequently, numerous Rad52 foci were observed in live cells following irradiation (Fig 4.2A-C). Both the fraction of focus-positive cells and the average number of foci per cell increased in an irradiation dose-dependent manner (Fig 4.2D,E). It should be noted that a wide range of focus intensities were observed. There was no apparent difference between Rad52-EGFP and Rad52-msGFP, so GFP aggregation is unlikely contributing to the structures observed in live cells.

Only a small fraction of Rad52 complexes are observable by live cell imaging. While an average of around 3.4 and 3.5 Rad52-EGFP and Rad52-msGFP foci were observed in live cells following 80 krad of gamma irradiation, averages of 13.6 and 12.6 foci were observed when the same cells were spread and immunostained with an anti-GFP antibody (Fig 4.2F-G). Forty DSBs

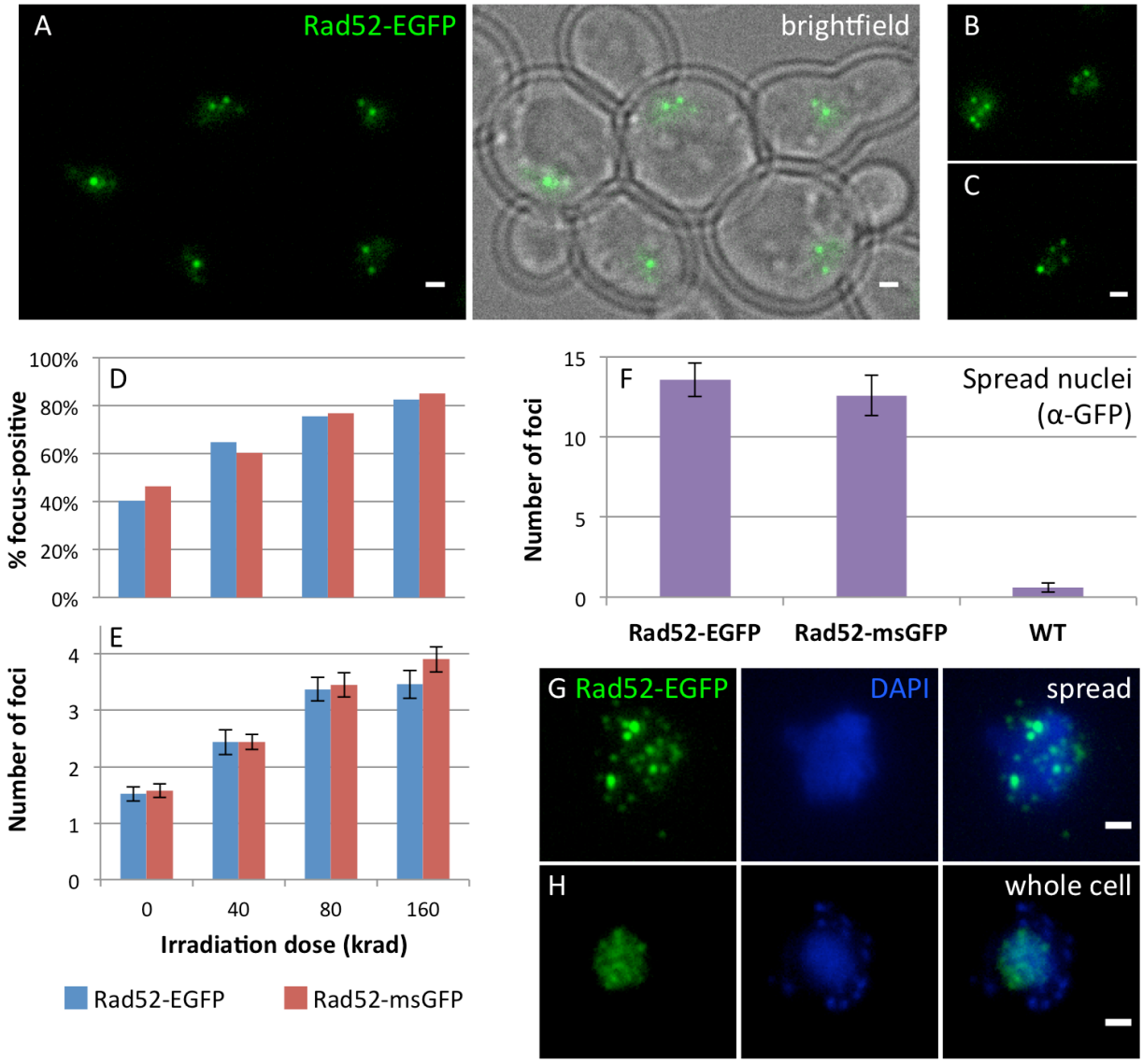

Figure 4.2 Rad52 forms multiple irradiation-induced foci in live cells and even more foci in spread nuclei. (**A-C**) Micrographs of live cells expressing Rad52-EGFP often displaying multiple Rad52 foci following gamma irradiation. (**D,E**) Both the percentage of focus positive cells and the average number of foci in focus positive cells increase in response to increasing doses of gamma irradiation. RAD52-EGFP (blue) and RAD52-msGFP (red) cells shown. (**F**) The average number of GFP foci in spread nuclei immunostained for GFP after 80 krad irradiation. (**G,H**) Micrographs of RAD52-EGFP cells following either chromosome spreading (**G**) or whole cell fixation (**H**) and immunostaining. Scale bars = 1 μm. Error bars are standard errors of the mean, n=3.

per cell are expected to be created by this dose of irradiation (Lisby et al., 2001); however, the ongoing, asynchronous nature of repair and a failure to resolve each individual complex could explain why fewer foci are observed. Still, the number of Rad52 foci observed in spread nuclei better approximates the number of DSBs expected than does the number of Rad52 foci observed in live cells. Similarly, numerous foci were observed when the same samples were fixed without chromosome spreading and immunostained (Fig 4.2H). These results suggest that the majority of Rad52 complexes are too small, and thus too faint, to be observed above background fluorescence in live cells. This notion is supported by the finding that focus intensities appeared to approach (and thus likely dip below) the background fluorescence threshold in live cells. In addition to reducing background by discarding the non-DNA bound Rad52 via chromosome spreading or permeabilization, the signal amplification associated with indirect immunostaining likely makes it easier to detect small complexes. In summary, these results demonstrate that live cell imaging fails to reveal many Rad52 complexes observable in other cytological preparations.

Still, it is difficult to use this data to definitively debunk the "recombination factory" model. First, it can be argued that the additional foci observed in fixed cells or chromosome spreads are artifacts of sample preparation in which DSBs dissociate from each other but Rad52 continues to mark each DSB. Second, definitional discrepancies make it difficult to design experiments and discuss their results in relation to the "recombination factory" model. The commonly held definition is that all DSBs in a given cell coalesce into a single "recombination factory". The more formal, written definition allows for multiple foci or "recombination factories", each with multiple DSBs (Lisby et al., 2001; 2003). While we can definitively rule out the former, more restrictive model, the latter "recombination factory" model is difficult to experimentally disprove.

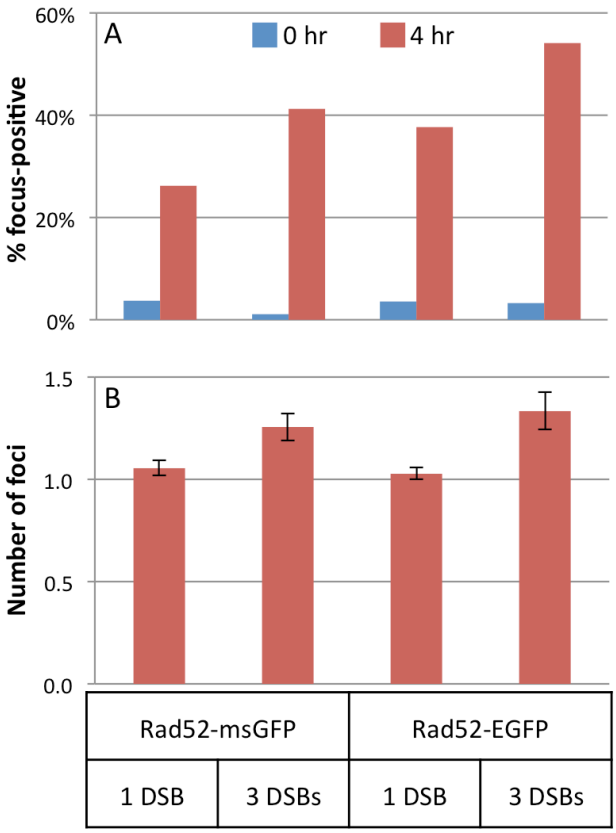

Figure 4.3 There is correlation but not 1:1 correspondence between DSBs and Rad52 foci. Either 1 or 3 irreparable DSBs are induced in RAD52-msGFP and RAD52-EGFP strains. (**A**) The percentage of focus-positive cells before (0 hr; blue) and after (4 hr; red) HO endonuclease induction. (**B**) The average number of GFP foci in focus-positive cells after DSB induction. Error bars are standard errors of the mean, n=3.

The obstacles to definitively debunking the "recombination factory" model are illustrated by an experiment in which a defined number of irreparable DSBs are induced and the number of Rad52 foci determined (Fig 4.3). When a single DSB was induced, a single Rad52 focus was observed. A greater number of Rad52 foci were observed when three DSBs were induced. This correlation between the number of DSBs and the number of Rad52 foci could be used to argue that "recombination factories" do not exist. However, the fact that generally fewer than three foci were observed could be used to argue for the existence of "recombination factories". For

example, cells with two Rad52 foci might have two "recombination factories": one higher order structure containing two DSBs and a spatially separate single DSB.

In summary, we have strong evidence against the notion that all DSBs coalesce into a single "recombination factory" in a live cell. Although we cannot definitively refute the claim that multiple DSBs coalesce into each of multiple "recombination factories" in a single live cell, observations from fixed cells and spread nuclei suggest that recombination complexes associated with individual DSBs do not cluster into higher order structures. The discrepancies between observations in live cells and other cytological preparations likely result from the inability to detect the faint foci (associated with small recombination complexes) above background fluorescence in live cells.

4.4 Tetracysteine-tagged Rad51 and Dmc1

Rad51 and Dmc1 were first tagged with small tetracysteine motifs to facilitate fluorescent labeling of these sensitive proteins. The short six amino acid motif CCPGCC specifically binds to certain molecules—most notably the fluorescein arsenical hairpin binder (FlAsH)—converting the non-fluorescent compound into a fluorescent molecule (Griffin et al., 1998; Hoffmann et al., 2010). The development of spectrally distinct compounds and improved labeling procedures expanded the utility of this technology, allowing two proteins to be simultaneously imaged in different colors (Zürn et al., 2010). In this protocol, CCPGCC and FLNCCPGCCMEP motifs can be orthogonally labeled with FlAsH and ReAsH (Zürn et al., 2010). To this end, a variety of RecA homolog constructs containing tetracysteine tags were constructed by overlap PCR and used to replace the wild type allele.

Tetracysteine tagged Rad51 and Dmc1 alleles largely remained functional. Rad51-TC_6, TC_6-Rad51, Dmc1-TC_6, and Dmc1-TC_{12} all largely retained functionality during meiosis, as demonstrated by 86-99% spore viabilities (Table 4.1A). This data demonstrates that tetracysteine-tagged Dmc1 is strand exchange competent. However, since Rad51's catalytic activity is not required during meiosis (Cloud et al., 2012; Da Ines et al., 2013), the strand exchange proficiencies of these tagged Rad51 alleles were assayed in cell survival assays following gamma irradiation. These assays revealed that Rad51-TC_6 was largely functional, but even small tags were not well tolerated at Rad51's N-terminus (Fig 4.4A). In summary, C-terminal tetracyteine-tagged Rad51 and Dmc1 are functional *in vivo*.

Initial attempts at labeling these functional RecA homologs were unsuccessful *in vivo*. Labeling protocols are most advanced in mammalian cells (Hoffmann et al., 2010), but the presence of a cell wall complicates labeling in yeast. Existing labeling protocols in yeast require either long incubation times (Andresen et al., 2004) or electroporation (Wurm et al., 2010). These protocols might make labeling of Rad51 and Dmc1 difficult due to the relatively short labeling window—the 3-4 hours following meiotic induction when recombinase expression is induced and most recombination complexes are assembled—and the potential sensitivity of sporulating cells to electroporation. An initial attempt to label Rad51 and Dmc1 with ReAsH without electroporation failed, but no positive control was performed. Still, the small size of these tags and demonstrated functionality of the fusion proteins makes this a worthwhile area for future protocol development.

A	viable spores						
	0	1	2	3	4	total	n
WT (*RAD51* targeted)	0%	0%	1%	8%	90%	97%	72
RAD51-TC$_6$	0%	3%	11%	7%	79%	90%	71
TC$_{12}$-Rad51	0%	0%	1%	0%	99%	99%	71
WT (*DMC1* targeted)	0%	1%	0%	6%	93%	98%	72
DMC1-TC$_6$	0%	0%	3%	11%	85%	96%	62
DMC1-TC$_{12}$	4%	4%	8%	10%	73%	86%	71

B	viable spores						
	0	1	2	3	4	total	n
WT	0%	0%	0%	0%	100%	100%	24
msGFP-RAD51	0%	0%	9%	9%	81%	93%	37
msGFP-RAD51 (heterozygote)	0%	0%	4%	2%	93%	97%	45
RAD51-msGFP	0%	6%	28%	33%	32%	72%	45
RAD51-msGFP (heterozygote)	0%	0%	8%	18%	75%	92%	40
msGFP-DMC1	18%	9%	27%	0%	46%	61%	11
msGFP-DMC1 (heterozygote)	0%	0%	8%	17%	75%	92%	12
DMC1-msGFP	does not form tetrads						
DMC1-msGFP (heterozygote)	0%	8%	17%	0%	75%	85%	12

Table 4.1 Spore viabilities of Rad51 and Dmc1 fusion proteins.

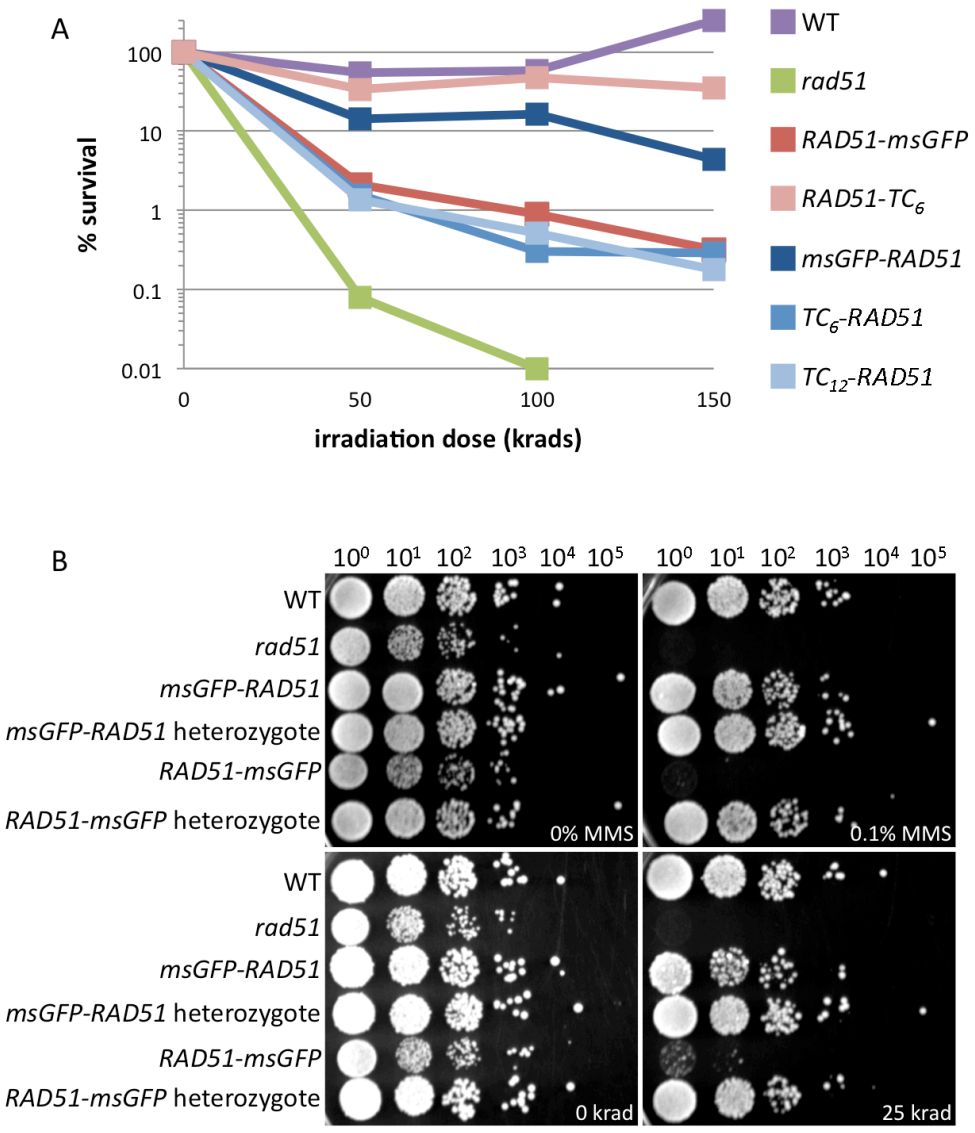

Figure 4.4 Rad51 fusion proteins are partially functional. (**A**) Kill curves in response to gamma irradiation. Percentage survival plotted on a logarithmic scale against irradiation dose (krads). WT (purple), rad51 (green), RAD51-msGFP (red), RAD51-TC6 (pink), msGFP-RAD51 (dark blue), TC6-RAD51 (blue), and TC12-RAD51 (light blue) are shown. (**B**) Serial plating assay after exposure to two different sources of DNA damage (0.1% MMS or 25 krad gamma irradiation).

4.5 msGFP-Tagged Rad51 and Dmc1

Rad51 and Dmc1 were next tagged with monomeric superfolder GFP (msGFP). Previous attempts to fuse the RecA homologs to GFP have largely disrupted recombinase function (Da Ines et al., 2013; Kobayashi et al., 2014; Lesterlin et al., 2013; Lisby et al., 2004; Uringa et al., 2015) (unpublished data). In part, the sensitivity to tagging is likely due to the large size of GFP emanating from the nucleoprotein filament, blocking the second site responsible for homology search and strand exchange (Da Ines et al., 2013; Kobayashi et al., 2014). However, it is also possible that early, poorly behaved versions of GFP are responsible for the loss of function. Two of these problems—poor folding and self-oligomerization due to sticky hydrophobic patches on the molecule's surface—have been mitigated in the msGFP used in this study (Aronson et al., 2011; Fitzgerald and Glick, 2014; Pédelacq et al., 2006).

msGFP-RAD51 is a respectably functional allele. *msGFP-RAD51* and *RAD51-msGFP* strains had 93% and 72% spore viability, respectively, and these figures increased to 97% and 92% when expressed heterozygously (Table 4.1B). While these assays report on the non-strand exchange function of Rad51 required during meiosis, they do not measure strand exchange competency. Strand exchange activity was assayed in irradiation survival assays where Rad51's catalytic activity is essential. By this assay, *RAD51-msGFP* complemented the *rad51* mutation reasonably well. Following 50 krad (500 Gy) of gamma irradiation, 14% of *RAD51-msGFP* cell survived versus 55% of wild type cells (Fig 4.4A). For comparison, the best published Rad51 fusion (*RAD51-YFP*) results in less than 0.1% survival after comparable treatment (Lisby et al., 2004). Only about 2% of *RAD51-msGFP* cells survived (Fig 4.4A). Similarly, the C-terminal fusion was more sensitive to the DNA crosslinking agent MMS (Fig 4.4B). These results suggest that *RAD51-msGFP* is a second site allele like the C-terminal Rad51-GFP fusion in *Arabidopsis*

thaliana (Da Ines et al., 2013; Kobayashi et al., 2014). However, *RAD51-msGFP* homozygous cells appear to have a non-second site defect manifested by decreased spore viability with no apparent homolog disjunction pattern (Table 4.1B). In summary, msGFP-Rad51 is largely functional both catalytically and non-catalytically.

Dmc1 is more sensitive to perturbation by msGFP, but *msGFP-DMC1* is partially functional. *msGFP-DMC1* cells have a modest spore viability defect of 61% compared to 100% in *DMC1*$^{+}$ cells (Table 4.1B). In contrast to the *RAD51* alleles, *msGFP-DMC1*'s spore viability pattern (primarily 4, 2, and 0 viable spores) is specifically consistent with a defect in meiosis I disjunction, which is typical of cells that have an underlying defect in interhomolog recombination, rather than a more general DSB repair defect. Although *DMC1-msGFP* cells enter meiosis (discussed later), they do not form spores. The defects observed in homozygous cells are largely suppressed in heterozygotes (Table 4.1B).

msGFP-tagged Rad51 and Dmc1 do not form visible foci in live cells despite loading at numerous meiotic DSBs. msGFP-Dmc1 and Dmc1-msGFP can be easily detected as an accumulating, bright, and uniform signal in live meiotic nuclei (Fig 4.5B,C). msGFP-Rad51 is expressed at a much lower level, resulting in a fainter nuclear signal with less contrast between the nucleus and cytoplasm (Fig 4.5A). Low contrast, local signal heterogeneity sometimes results in the appearance of focus-like structures. (Rad51-msGFP was not tested in live meiotic cells). Yet, like wild type cells, msGFP-tagged Rad51 and Dmc1 form numerous foci in chromosome spread preparations (Fig 4.6). This finding suggests that these tagged RecA homologs load at the many DSBs in meiotic cells, creating structures too small and thus too faint to be observed above background fluorescence. This interpretation is supported by the finding that foci are

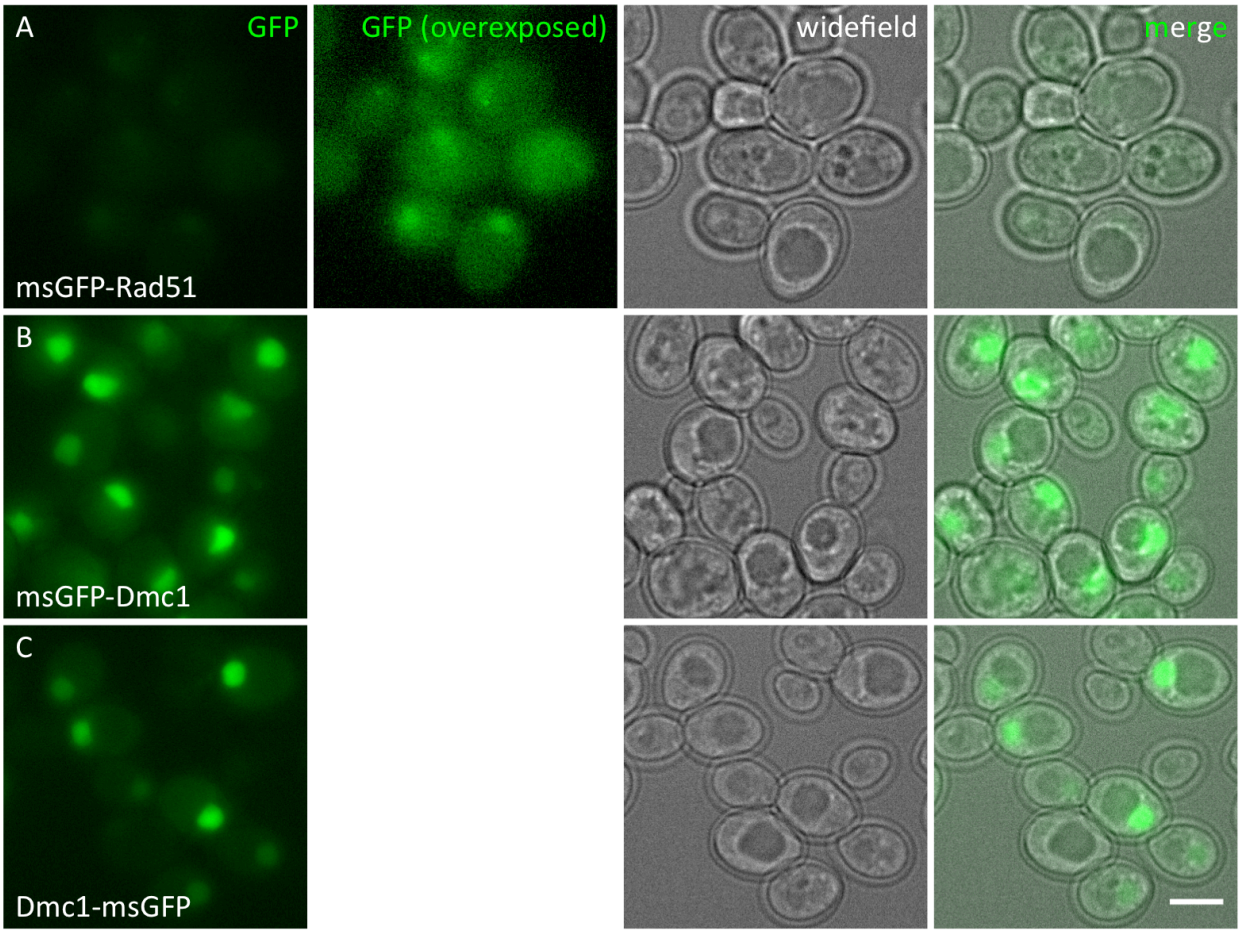

Figure 4.5 GFP-tagged Rad51 and Dmc1 generally do not form observable foci in live meiotic cells. 4-5 hour micrographs of live cells. (**A**) msGFP-Rad51. (**B**) msGFP-Dmc1. (**C**) Dmc1-msGFP. Scale bar = 5 μm.

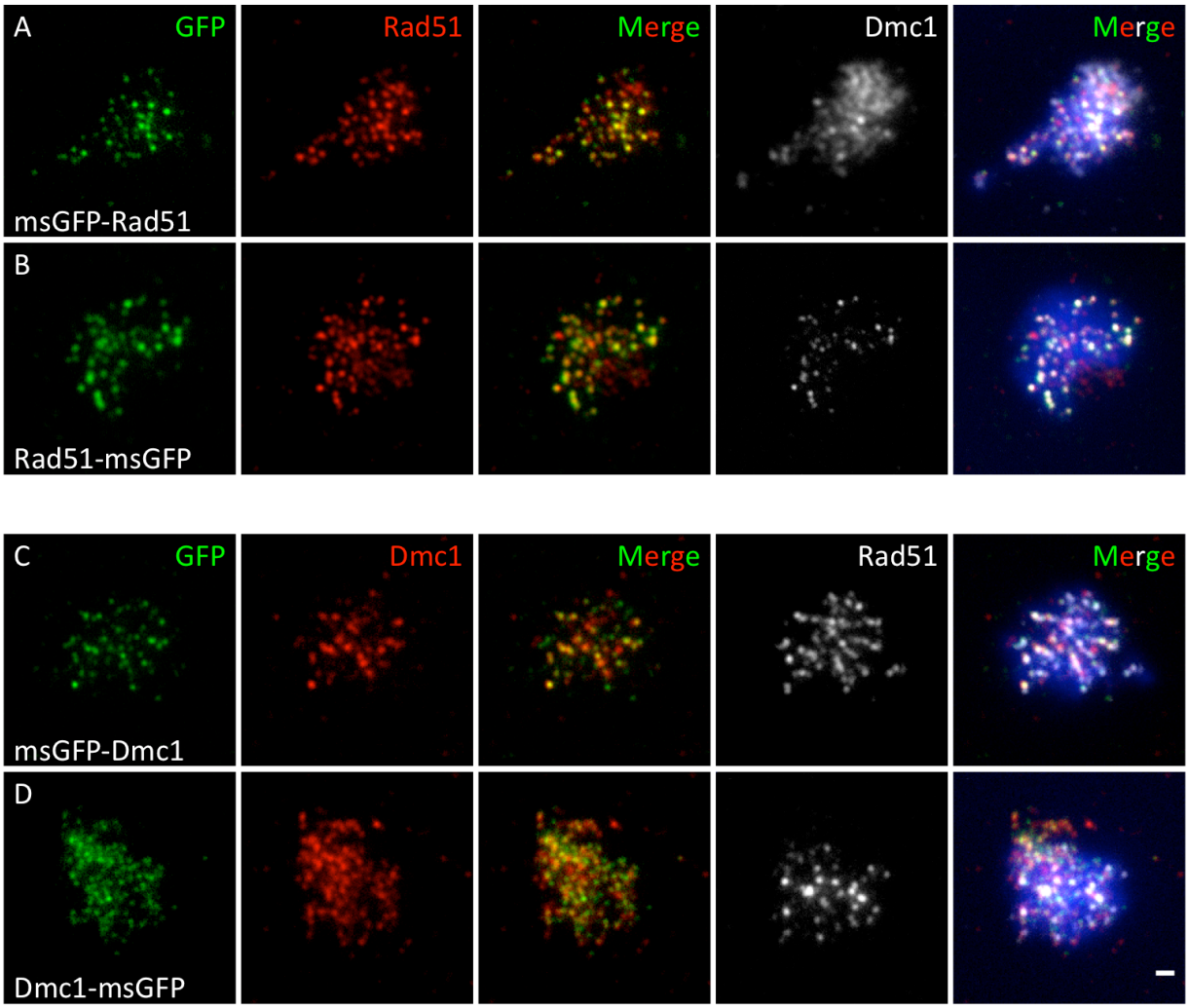

Figure 4.6 GFP-tagged Rad51 and Dmc1 form foci in spread meiotic nuclei. GFP, Rad51, and Dmc1 were each detected by indirect immunostaining of 4-hour nuclei. (**A**) msGFP-Rad51. (**B**) Rad51-msGFP. (**C**) msGFP-Dmc1. (**D**) Dmc1-msGFP. Scale bar = 1 μm.

occasionally observed in *msGFP-RAD51* cells—where background fluorescence is lower than in tagged Dmc1 strains—along with the knowledge that Rad51 and Dmc1 filaments are the same size *in vivo* (Brown et al., 2015). It should be noted that the msGFP tags likely cause some slight defects in Rad51/Dmc1 assembly and/or disassembly, because the pattern of Rad51/Dmc1 colocalization appears to be subtly perturbed (Fig 4.6). Additionally, anti-Rad51 or anti-Dmc1 staining often reveals some fraction of structures not stained by an anti-GFP antibody (Fig 4.6). This observation likely indicates some degree of proteolysis that liberates the msGFP from the RecA homologs, an important consideration in the functional characterization above. Nevertheless, it is clear that msGFP tagged Rad51 and Dmc1 load at DSBs but remain largely invisible in live cells.

4.6 Conclusions

The data in this chapter can be used to build an argument against the existence of "recombination factories". The Rad52 live cell imaging data differ very little from previous reports. However, while few to zero Rad52, Rad51, and Dmc1 foci can be observed in live cells, the presence of many "invisible" foci can be demonstrated indirectly by immunostaining fixed cells or spread chromosomes. The small, packed dimensions of a yeast nucleus will necessitate the utilization of super-resolution and single molecule microscopy approaches to settle this discrepancy once and for all (see next chapter for a discussion of future directions and the associated challenges). The minimally perturbed fusion proteins created and characterized within this chapter will serve as valuable tools in this pursuit.

Chapter 5

Perspectives and future directions

5.1 Chapter overview

The results presented in this thesis reveal new aspects of meiotic DSB architecture at both relatively short and long distances. Super-resolution light microscopy revealed that the pre-strand exchange recombination complex architecture is complex and heterogeneous. At larger scale, relatively long distances separate the two ends of a meiotic DSB. These new organizational features provide mechanistic explanations for several previous observations and chart out paths for future study.

5.2 Structure of the pre-synaptic recombination complex

5.2.1 Mechanism of Rad51-mediated Dmc1 assembly

The role of Rad51 as an accessory factor for Dmc1 assembly is well established. Rad51 is required for normal loading of Dmc1 at DSBs. Specifically, Dmc1 foci are much fainter in a *rad51* mutant relative to wild type (Bishop, 1994; Cloud et al., 2012; Shinohara et al., 2003a). Conversely, Rad51 foci form normally in a *dmc1* mutant (Bishop, 1994). These results formed the basis of a model in which Rad51 loading on ssDNA promotes the assembly of Dmc1 on ssDNA at the same DSB. In the context of the asymmetric loading model, Rad51 loading on one end of the DSB was suggested to mediate assembly of Dmc1 specifically on the other end of the DSB (Shinohara et al., 2000). In other words, Rad51 would be selectively loaded on only one of a pair of ssDNA tracts and then mediate Dmc1 assembly *in trans*.

The results presented here suggest that Rad51 mediates Dmc1 assembly *in cis* (from the same ssDNA molecule)(Brown et al., 2015). There is mechanistic precedent for mediated assembly *in cis*. The best characterized mechanism of mediated assembly is the Rad52-facilitated replacement of RPA by Rad51 (Gibb et al., 2014; Sugiyama et al., 1998; Sugiyama and Kowalczykowski, 2002). Rad52, Rad55/Rad57, and the Shu Complex (Csm2, Psy3, Shu1, and Shu2) all mediate Rad51 assembly in *Saccharomyces cerevisiae* via direct intermolecular contacts (Gaines et al., 2015; Gasior et al., 1998; 2001; Sasanuma et al., 2013b; Sugiyama et al., 1998; Sugiyama and Kowalczykowski, 2002; Sung, 1997) (Fig 5.1). This network of molecular

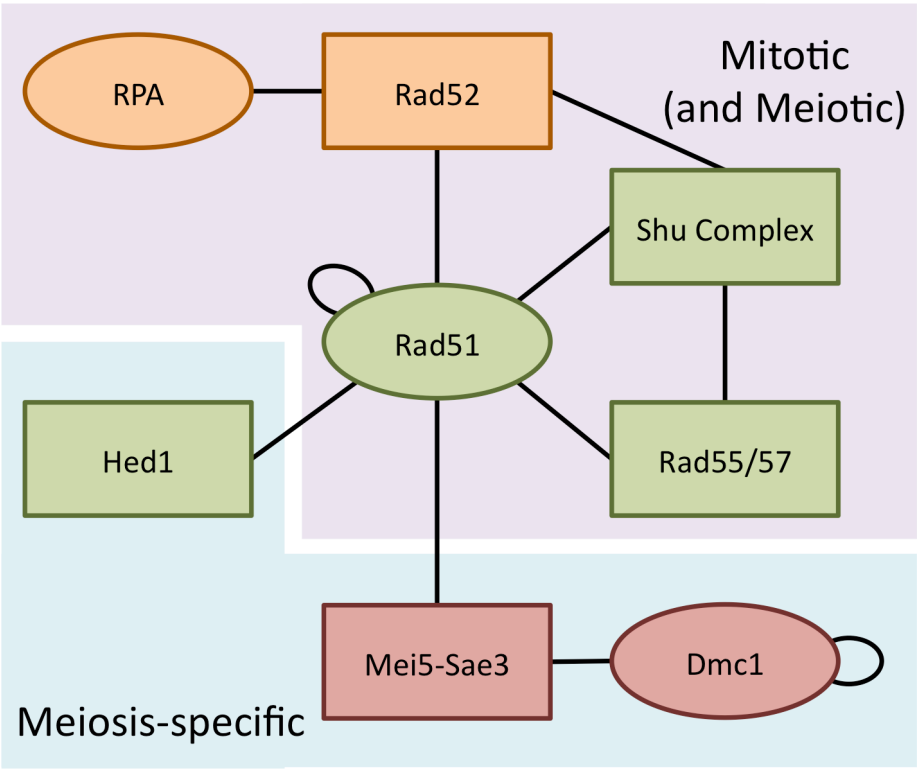

Figure 5.1 Map of biochemical interactions between pre-synaptic recombinosome components. Proteins are divided into a group specifically expressed during meiosis (blue box) and those expressed in both mitosis and meiosis (purple box). They are also divided into those that certainly bind ssDNA tracts in vivo (ovals) and those that may directly bind ssDNA tracts in vivo (rectangles). Each line between proteins represents a direct biochemical interaction. Orange, green, and red shapes represent proven or hypothesized sub-complexes reflected by imperfectly colocalizing (rather than perfectly colocalizing) foci in immunostained meiotic spread nuclei.

interactions within the context of a single tract of ssDNA provides a simple, well-supported mechanism of mediated Rad51 assembly. In contrast, the proposed *in trans* mediation of Dmc1 assembly by Rad51 and Mei5-Sae3 would require a much more convoluted molecular mechanism. The primary piece of evidence for this proposed model is that Rad51 and Dmc1 foci imperfectly colocalize as side-by-side foci (Kurzbauer et al., 2012; Shinohara et al., 2000). However, Rad52 and Rad51 similarly imperfectly colocalize, despite their co-occupancy of a common ssDNA tract (Gasior et al., 1998; Gasior, 1999). Furthermore, Dmc1 interacts with its mediators Mei5-Sae3 and Rad51 via direct intermolecular interactions (Fig 5.1), a simpler feat if all components co-occupy the same tract of ssDNA. Thus, imperfect side-by-side colocalization of recombination foci should not be interpreted as evidence of asymmetric loading, and Dmc1 likely occupies the same tract of ssDNA as its mediators—including Rad51.

What is the mechanism by which Rad51 and Mei5-Sae3 mediate Dmc1 assembly? One model posits that Mei5-Sae3 simultaneously engages one end of a Rad51 filament and one end of a nascent Dmc1 filament, on a spatially juxtaposed region of ssDNA (Brown and Bishop, 2015; Brown et al., 2015)(Fig 1.3). It is based on: the physical interaction of Mei5-Sae3 with both Rad51 and Dmc1 (Hayase et al., 2004; Say et al., 2011), the requirement of Rad51 and Dmc1 for Mei5-Sae3 focus formation (Hayase et al., 2004; Tsubouchi and Roeder, 2004); and the presence of both Rad51 and Dmc1 on a single tract of ssDNA. This model predicts that Mei5-Sae3 sr foci will: 1. colocalize only partially with either Rad51 or Dmc1 sr foci and 2. colocalize equally with both Rad51 and Dmc1 sr foci. An alternative model is that Mei5-Sae3 binds along the length of a Dmc1 filament, stabilizing it but not directly promoting filament formation. This alternative model is supported by two key findings. First, Mei5-Sae3 can stimulate Dmc1-mediated D-loop formation *in vitro* in the absence of Rad51, under certain

conditions (Ferrari et al., 2009). Second, Mei5-Sae3 appears to colocalize more strongly with Dmc1 than with Rad51 at widefield resolution (Tsubouchi and Roeder, 2004). The predictions of this model are clearly distinct from that of the simple "bridging" model (above) and testable (see next section).

Although Rad51 and Dmc1 are both present on a single ssDNA molecule, their spatial relationship remains unclear. One unlikely possibility is that there is a stiff junction between adjacent Rad51 and Dmc1 homofilaments, such that both filaments are maintained in rigid alignment. Preliminary dSTORM micrographs in which both Rad51 and Dmc1 are labeled with a single fluorophore did not reveal the longer, skinny staining patterns expected from this model. Two other possibilities exist in which the Rad51 and Dmc1 homofilaments are not linearly oriented. The differentiating factor is the length of ssDNA between adjacent filaments. In the first possible model, the Rad51 and Dmc1 homofilaments are directly adjacent to each other, with little uncoated ssDNA between them, providing a flexible hinge between the two linear filaments. In the second possibility, Rad51 and Dmc1 homofilaments can form on non-adjacent segments of ssDNA. In this case, Rad51 (and possibly Mei5-Sae3) could mediate Dmc1 assembly on a non-adjacent tract of ssDNA due to the three-dimensional proximity of the two regions. RPA/single strand binding (SSB) protein is known to organize ssDNA in such a conformation (Bell et al., 2015). This property could ensure that a single tract of ssDNA and its associated proteins remain in close spatial proximity but do not interact with other ssDNA tracts present in the same nucleus. These two models can be distinguished *in vitro* utilizing previously described conditions under which Rad51 and Mei5-Sae3 are both required to stimulate Dmc1-mediated D-loop activity (Cloud et al., 2012). Specifically, a ssDNA oligo could be saturated with Rad51 (and possibly stabilized with non-hydrolyzable ATP analogs) before addition of

another ssDNA molecule, Mei5-Sae3, and Dmc1. If Rad51-dependent stimulation of Dmc1's D-loop activity could be demonstrated, this stimulation would be from a non-contiguous ssDNA molecule.

5.2.2 Mapping the architecture of a meiotic recombinosome

A large variety and number of proteins simultaneously occupy a single tract of ssDNA during meiosis. RPA, Rad52, Rad51, Hed1, Mei5-Sae3, and Dmc1 all form largely colocalizing, *SPO11*-dependent foci in meiotic nuclei (Bishop, 1994; Gasior et al., 1998; Hayase et al., 2004; Tsubouchi and Roeder, 2004; 2006). Additionally, Rad55/57 and the Shu complex are likely present in meiotic recombination complex foci (Gaines et al., 2015; Liu et al., 2011; Sasanuma et al., 2013b; Sung, 1997). Varying degrees of ssDNA binding activity have been demonstrated for almost all of these proteins *in vitro*. RPA, Rad51, and Dmc1 certainly bind ssDNA *in vivo*; Rad52, Hed1, Mei5-Sae3, Rad55/57, and the Shu complex may bind ssDNA directly or be indirectly associated through ssDNA-binding proteins. A wealth of biochemical and genetic data has provided some insight into the interactions between recombinosome components (Fig 5.1). However, the lack of an integrated map of meiotic recombination complex architecture has hampered our understanding of this complex molecular machinery.

The procurement of such a map has been hindered by the small size and structural heterogeneity of meiotic recombinosomes. These features of recombination complex architecture have been hidden beneath diffraction-limited foci. Rad51 and Dmc1 filaments are extremely small, only 10 nm wide and likely only about 50 nm long (Brown et al., 2015). The other components of the meiotic recombination complex are possibly even smaller since they do not form extended homopolymeric structures like the RecA homologs. Furthermore, while the

dimensions of diffraction-limited foci are—by definition—almost identical, super-resolution light microscopy revealed that recombinosomes are structurally heterogeneous by several criteria. First, Rad51 and Dmc1 sr foci do not have uniform shapes and sizes (major axis 114 ± 29.9; aspect ratio 1.27 ± 0.245). Second, a single tract of ssDNA can be occupied by a variable number of Rad51 and/or Dmc1 sr foci. Finally, variable distances can separate the Rad51 or Dmc1 sr foci co-occupying a tract of ssDNA. These sources of heterogeneity limit our ability to define a rigid, universal recombinosome structure. However, a multi-level imaging approach combined with more powerful, flexible image analysis programs will lead to the determination of an integrated, *average* recombination complex structure.

Integrating multiple imaging modalities will provide complimentary information about recombinosome structure. There is a tradeoff between spatial resolution and the ability to determine relative positional information in two colors with current imaging methods. Resolving ability increases from widefield microscopy (around 200 nm) to structured illumination microscopy (SIM; 100 nm) to stimulated emission depletion microscopy (STED; around 60 nm) to direct stochastic optical reconstruction microscopy (dSTORM; around 20 nm). Conversely, multi-color imaging capabilities are weakest in dSTORM (1 color) and increasingly stronger in STED (2 colors), SIM (3 colors), and widefield microscopy (4 colors). Multi-color SIM has been demonstrated on *S. cerevisiae* meiotic spread chromosome preparations (Voelkel-Meiman et al., 2013) and is generally considered routine on commercially available microscopes. We have successfully applied 2-color STED microscopy to Rad51 and Dmc1, demonstrating that Rad51 and Dmc1 display almost no colocalization (Fig 5.2; Rad51 and Dmc1 sr foci are generally separated by 50-80 nm; see materials and methods for discussion of different STED setups). The

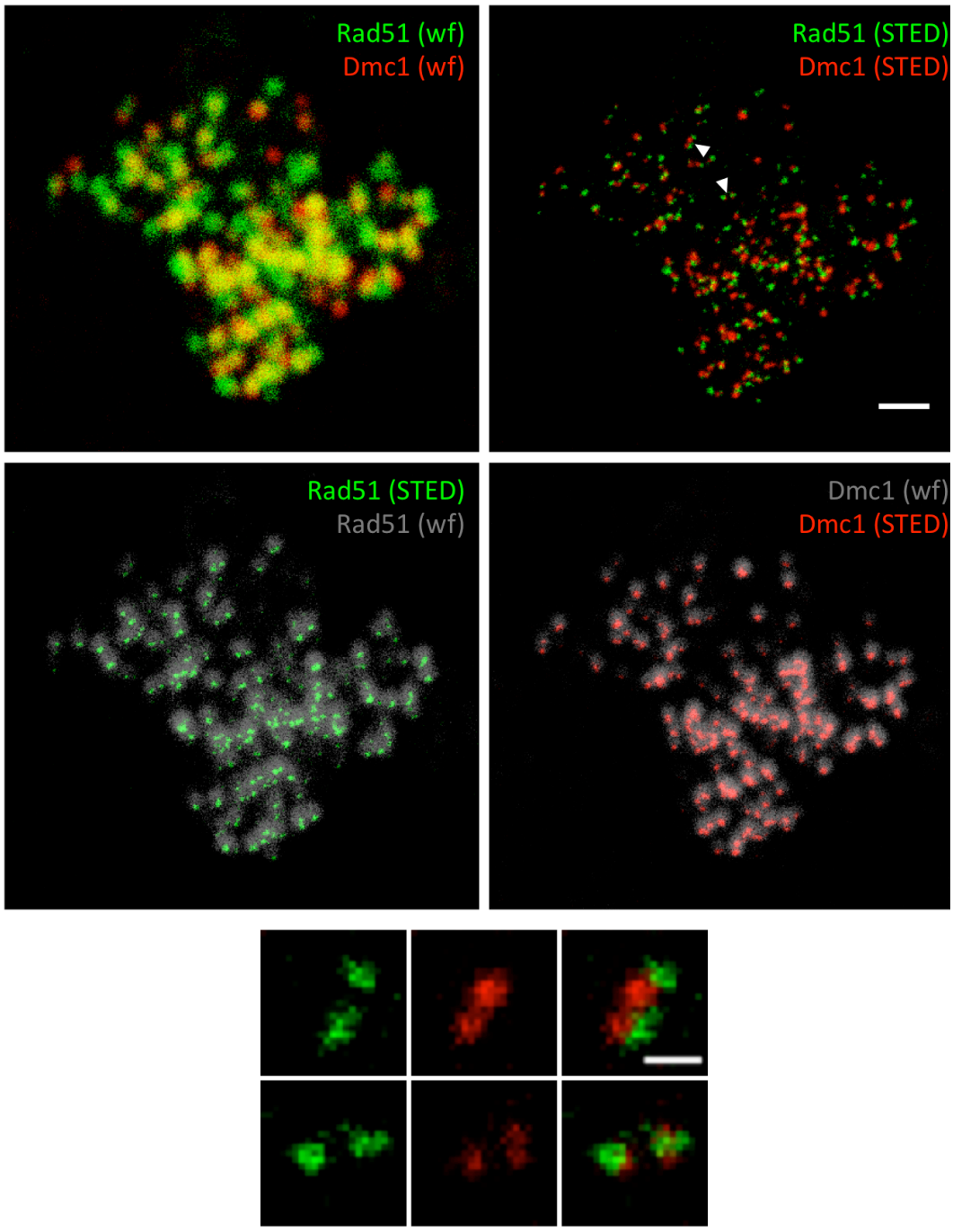

Figure 5.2 Two-color STED microscopy reveals non-colocalizing Rad51 and Dmc1 sr foci. Scale bar = 1 μm or 200 nm for inset. wf stands for widefield.

almost complete lack of colocalization at such high resolution suggests that the underlying Rad51 and Dmc1 filaments are quite far apart. Indeed, simulations of idealized structures—consistent with this and all previous data—demonstrate that most of the information regarding Rad51/Dmc1 colocalization could be gleaned from a lower resolution imaging modality such as SIM (Fig 5.3). The varied capabilities of different tools suggest an integrated imaging approach in which a particular recombinosome component is imaged by itself at the highest possible resolution to determine the dimensions of each individual complex. Then, its position relative to other recombinosome components is determined at lower resolutions. Repeating this process for each individual component and all possible combinations of components will provide the comprehensive data set required to fully characterize the architecture of a recombination complex (Fig 5.4).

More flexible, sophisticated image analysis can likely create an integrated recombinosome structure from this multi-level data set. The particle averaging algorithms most often associated with cryo-EM have now been applied to super-resolution light microscopy. These methods are most powerful when applied to relatively homogeneous structures such as the nuclear pore complex or the synaptonemal complex (Schücker et al., 2015; Szymborska et al., 2013). However, more advanced methods also allow multiple, discrete states to be differentiated (Burns et al., 2015). While it appears that meiotic recombination complexes are significantly more heterogeneous than previously characterized structures, the same principles could be applied to determine one or more representative *average* structures. In this pursuit, *spo11* hypomorphic tetraploids or *spo11* VDE cut site heterozygotes should be utilized to meet the requirement that discrete particles (the recombination complexes associated with single tracts of ssDNA) are well isolated.

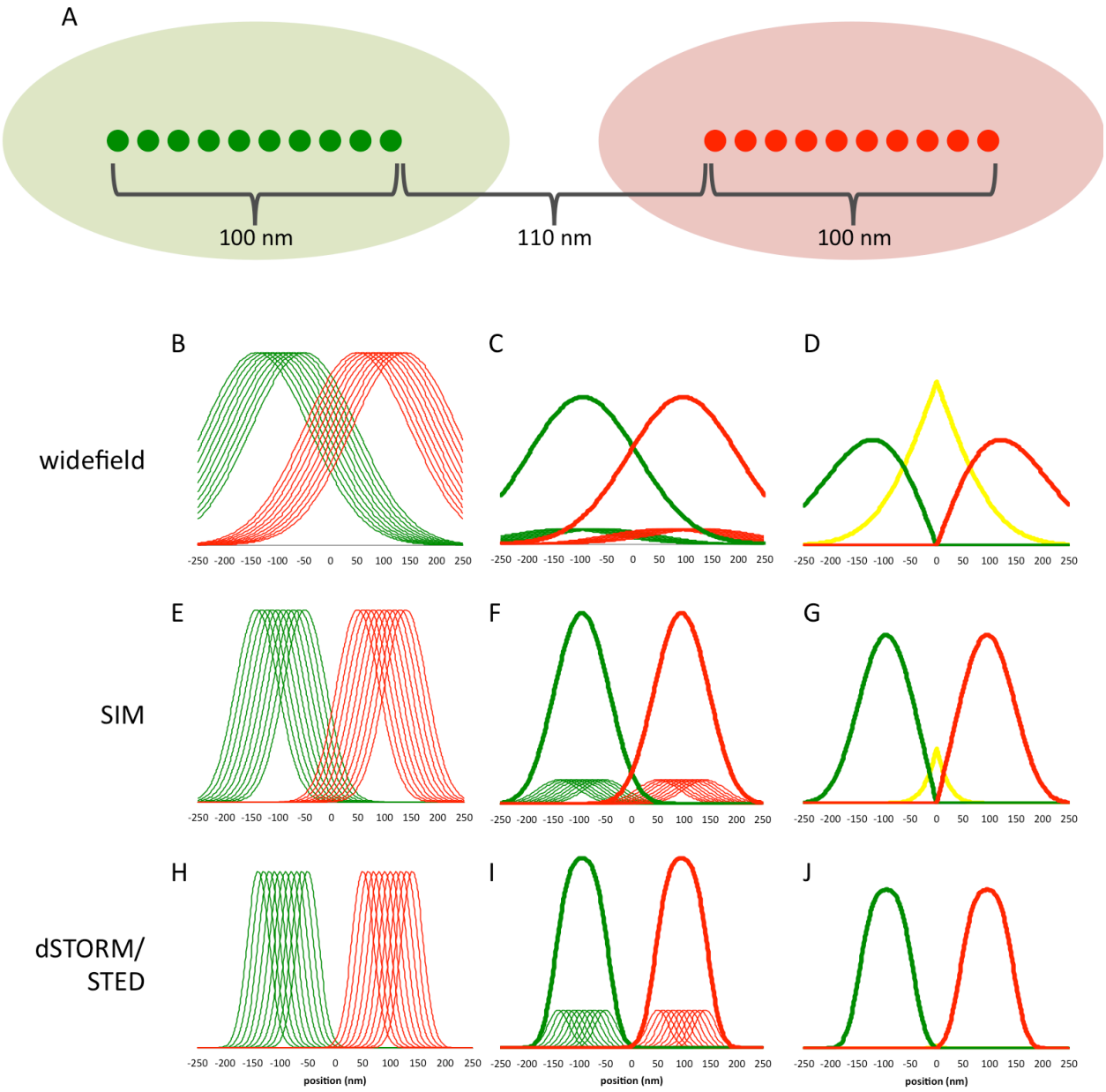

Figure 5.3 Effect of resolution on structural interrogation. (**A**) Hypothetical Rad51/Dmc1 structure where green fluorophores (small dark green circles) decorate a Rad51 filament and red fluorophores (dark red circles) decorate a nearby Dmc1 filament. The filaments are 100 nm long, separated by 110 nm, and assumed to be co-linear. The outline of the sr foci as observed by dSTORM are shown in light green and red. (**B-J**) Idealized fluorescent signal of (**B,E,H**) individual fluorophores each displayed as a single gaussian, (**C,F,I**) superposed signals of individual colors, and (**D,G,J**) superposed signals demonstrating colocalization (yellow). Y-axes are in arbitrary units, approximately normalized to the maximum intensity in each panel. The x-axes are positions along a line through structure portrayed in (A). The idealized distributions of individual fluorophores have standard deviations of 250 nm (B, widefield), 100 nm (E, SIM), and 50 nm (H, dSTORM).

modality	resolution	# colors											
dSTORM	<50 nm	1	Rad51			Dmc1			Mei5-Sae3			RPA	
STED	50 nm	2	Rad51 Dmc1			Rad51 M5S3			Rad51 RPA			Dmc1 M5S3	
			Dmc1 RPA			M5S3 RPA							
SIM	100 nm	3	Rad51 Dmc1 M5S3			Rad51 Dmc1 RPA			Rad51 M5S3 RPA			Dmc1 M5S3 RPA	

Figure 5.4 An integrated, combinatorial approach to recombinosome mapping. Each colored box represents a single imaging experiment. Blue boxes are single color dSTORM experiments. Red boxes are two color STED experiments. Purple boxes are three color SIM experiments. This combinatorial approach would take advantage of the strengths of each imaging modality and provide complimentary information.

En route to the ultimate goal of generating an integrated spatial map of meiotic recombination complex architecture, the above outlined approach will answer many outstanding questions. Are Rad51 and Dmc1 precisely juxtaposed, or is RPA or some other component interspersed? Does Hed1 coat the entire Rad51 filament? Is Mei5-Sae3 only located at the ends of spatially juxtaposed Rad51 and Dmc1 filaments or along the entire length of a Dmc1 filament? Is Rad52 associated tightly with RPA but not Rad51? These are just a few of the most immediately addressable questions answerable by this methodology.

Aside from the advances in imaging and analysis discussed above, improvements in sample preparation and labeling will further enrich our understanding of meiotic recombinosome architecture. First, the effect of chromosome spreading methods on recombination complex architecture should be evaluated. All of the chromosome spreads in this thesis were prepared by the Loidl method (Grubb et al., 2015; Loidl et al., 1991). The Giroux method is generally considered to better preserve cellular structure (Dresser and Giroux, 1988; Rua et al., 2004). Indeed, meiotic chromosome axes (labeled with a mixture of Red1 and Rec8 antibodies) appear

more continuous in Giroux spreads at super-resolution (Fig 5.5). Second, the physical size of antibodies likely makes a significant contribution to the size of sr foci observed by dSTORM or STED microscopy. The contribution of antibody size to sr focus size should be addressed by directly conjugating flurophores to primary antibodies before visualization by super-resolution microscopy. Third, direct labeling of ssDNA will create a point of reference with which to orient recombination complex components. One method involves incorporation of BrdU (requiring integration of thymidine kinase and human equilibrative nucleoside transporter 1 into chromosomes because 2-micron plasmids bearing these genes appear to be selected against) during pre-meiotic DNA replication followed by immunostaining under non-denaturing conditions (Raderschall et al., 1999; Terasawa et al., 2007). This method has proven successful (although easier in mitotic than meiotic cells) but suffers from uncertainties about epitope masking by recombination complex components. A potential alternative method is terminal deoxynucleotidyl transferase-mediated dUTP nick end-labeling (TUNEL). Although TUNEL has been reported to label meiotic DSBs in *Maize* and *C. elegans* (Mets and Meyer, 2009; Pawlowski et al., 2004), my attempts in meiotic yeast chromosome spreads have proven unsuccessful. If optimized, the TUNEL method would facilitate the orientation of recombinosome components relative to ssDNA polarity.

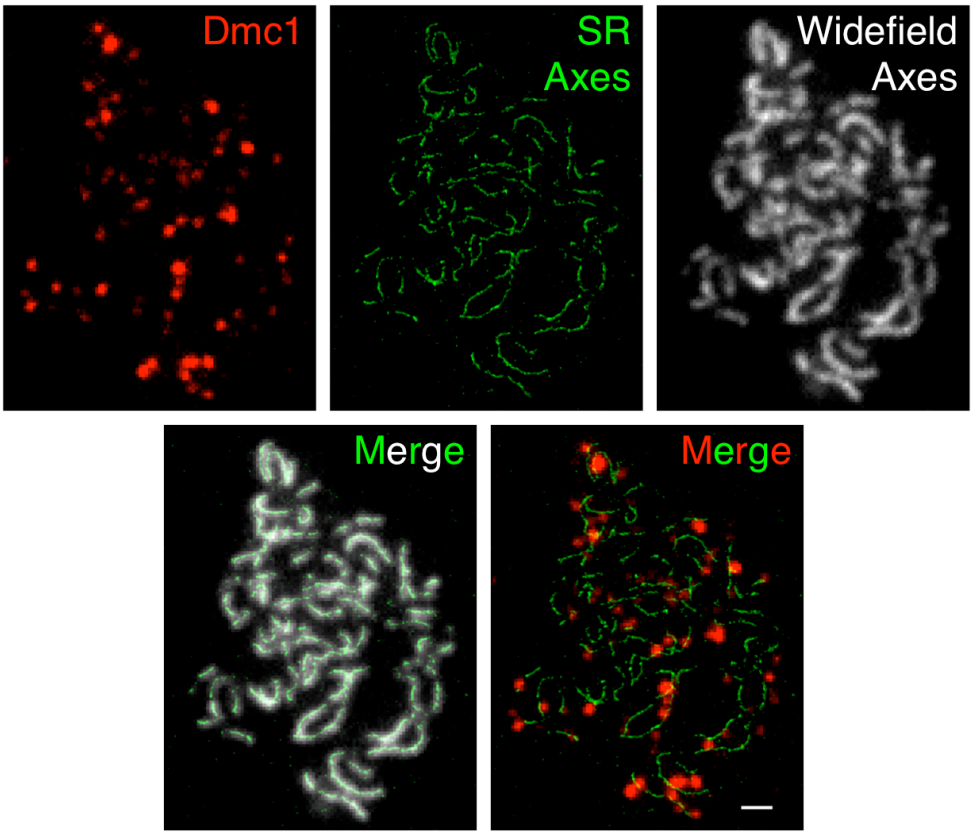

Figure 5.5 dSTORM imaging of axial associations. Dmc1 is imaged at widefield resolution (red). Chromosome axes stained for both Red1 and Rec8 are imaged at super-resolution (SR, green). Scale bar = 1 μm.

5.2.3 What limits the lengths of Rad51 and Dmc1 filaments?

The average meiotic ssDNA tract length is about 800 nt (Zakharyevich et al., 2010), but Rad51 and Dmc1 filaments are only about 100 nt long (Brown et al., 2015). Multiple non-mutually exclusive possibilities can account for this observation. First, simple competition between recombinosome components for ssDNA-binding might be appropriately tuned. Alternatively, the competition between filament stabilization (assembly) and destabilization (disassembly) could be appropriately balanced. Both factors likely contribute to a highly dynamic environment in which Rad51 and Dmc1 are around 100 nt long at any given moment.

Simple competitive binding between recombinosome components and ssDNA likely only partially account for Rad51 and Dmc1 filament length. Simple competition would predict that eliminating any ssDNA-binding component via genetic mutation would increase the fraction of ssDNA bound by any other ssDNA-binding component. To the contrary, no change in Rad51 filament length (as determined by sr focus length) was detected in a *dmc1*Δ mutant. This interpretation is complicated by the facts that ssDNA tract length increases in *dmc1*Δ mutants (Bishop et al., 1992) and that intracellular Rad51 concentration increases as prophase I progresses (AZ, unpublished data). Indeed, at late time points in a *dmc1*Δ mutant, many Rad51 filaments appear to simultaneously occupy a single ssDNA tract. Unfortunately, epistatic relationships—for example, the requirement of Rad51 for Dmc1 loading—make it difficult to test this hypothesis with other null mutants. Overexpression of individual recombinosome components might be the easiest way to evaluate the effect of protein concentration on Rad51 or Dmc1 filament length. Yet, it is unlikely that this hypothesis fully explains the short lengths of Rad51 and Dmc1 filaments.

Rad51 and Dmc1 filaments are likely very dynamic *in vivo*. The literature has often assumed that the appearance and disappearance of foci represent assembly on newly revealed ssDNA and disassembly following successful completion of strand exchange, in a strictly linear pathway. Indeed, live-cell imaging seemed to confirm that Rad51 filaments are very stable (Essers et al., 2002), but this conclusion was later called into question when a more careful functional analysis revealed recombination defects associated with the Rad51-GFP protein used (Uringa et al., 2015). Additionally, several independent lines of evidence suggest that Rad51 and Dmc1 structures on a single ssDNA tract are assembled and disassembled dynamically, until successful strand exchange breaks the cycle. First, like RecA, Rad51 and presumably Dmc1 are

known to assemble and disassemble spontaneously on ssDNA (Ristic, 2005; van der Heijden et al., 2007). Second, Srs2 has been shown to disassemble pre-existing Rad51 filaments *in vivo* (Sasanuma et al., 2013a). This active disassembly process is counteracted by the Rad51 stabilizing Rad55/57 and Shu complexes (Fung et al., 2009; Liu et al., 2011; Malik and Symington, 2008; Sasanuma et al., 2013a; 2013b). Pre-synaptic filament disassembly might similarly be antagonized by other Rad51 and Dmc1 filament stabilizing proteins (Busygina et al., 2012; Chi et al., 2007; Pezza et al., 2007; Sasanuma et al., 2013b; Taylor et al., 2015; Tsai et al., 2012). Third, in several cases, the existence of Rad51 filaments can be inferred (by Dmc1 focus formation) when Rad51 foci are undetectable, suggesting that transient Rad51 filaments were able to mediate Dmc1 assembly but might not be present upon observation (Gasior, 1999; Sasanuma et al., 2013a; 2013b). Finally, Rad51 foci or sr foci can be observed that are unassociated with Dmc1 structures (and vice versa) even in wild type cells, suggesting that Rad51 and Dmc1 filaments do not always co-occupy each ssDNA tract (Brown et al., 2015). While there are alternative explanations for these observations, together they suggest that Rad51 and Dmc1 filaments are unlikely to be stable entities from the time of assembly until strand exchange-triggered disassembly *in vivo*. A better grasp on Rad51 and Dmc1 filament dynamics *in vivo* remains a crucial barrier to better understanding recombinosome structure.

Ideally, RecA homologs tagged with fluorescent proteins could report on recombination complex architecture in live cells. Unfortunately, a combination of technical problems and the nature of the structures under examination will likely continue to thwart these efforts for the foreseeable future. As discussed in Chapter 4, Rad51 and Dmc1 are sensitive to the addition of bulky fluorescent protein fusions. Additionally, during meiosis, a large number of DSBs coexist in a relatively small nuclear volume, exaggerating the crowding problem seen in chromosome

spreads. Furthermore, the small size of the recombination complexes formed make it difficult to detect above the background fluorescence contributed from free protein and other recombination complexes (Chapter 3 and 4). Finally, meiotic chromosomes are known to move very rapidly about the nucleus, presumably carrying recombination complexes with them (Conrad et al., 2008; Koszul et al., 2008). In theory, the crowding and high background problems could be overcome by new single molecule and blurred microscopy methods (Betzig et al., 2006; Etheridge et al., 2014). However, the chromosome movement would need to be halted (perhaps in an *ndj1* mutant) and functional photoactivatable fluorescent protein fusions would need to be created. The *spo11* hypomorphic tetraploid and *spo11* VDE cut site$^{+/-}$ backgrounds would likely be advantageous. Nevertheless, this extensive undertaking could potentially be foiled if Rad51 and Dmc1 filaments are assembled and disassembled too quickly. For these reasons, the characterization of Rad51 and Dmc1 filament dynamics in live cells is not likely to be a near term project.

The partial characterization of Rad51 and Dmc1 filament dynamics indirectly via a combination of genetics and existing chromosome spread methods is a more realistic objective. The ability of super-resolution microscopy to differentiate normal (100 nm long) sr foci and elongated structures provides an experimental endpoint with which filament dynamics can be probed (Brown et al., 2015). This and other work demonstrated that Srs2 is responsible for disassembly of Rad51 filaments associated with ssDNA *in vivo* (Brown et al., 2015; Sasanuma et al., 2013a; 2013b). Importantly, this activity is specific for Rad51, apparently sparing Dmc1, RPA, and Rad52 (Sasanuma et al., 2013a; 2013b). It should be confirmed with dSTORM that longer Rad51 filaments are formed in meiotic *srs2* mutant nuclei. Presumably, an unknown protein is similarly responsible for disassembling Dmc1 filaments from ssDNA *in vivo*. A

candidate gene approach should be used to identify this gene, focusing on helicases expressed during meiosis. Similar to the relationship between Srs2 and Rad51, a knockout of this putative gene should result in longer (200 nm or greater) Dmc1 filaments and overexpression should reduce the total number of Dmc1 structures. Once all of the Rad51 and Dmc1 disassembly enzymes are identified, epistasis analysis will provide a more thorough picture of the competition between assembly/stabilization and disassembly/destabilization *in vivo*. Furthermore, eliminating (or at least slowing) the filament disassembly process will aid in the characterization of the recombinosome state where Rad51 is mediating Dmc1 assembly.

5.3 Relationship between the two ends of a meiotic DSB

5.3.1 Compositional asymmetry of a DSB

Either implicitly or explicitly, models of meiotic recombination universally differentiate the functions of each individual DSB end. While the exact nature of this functional differentiation varies (Hong et al., 2013; Hunter and Kleckner, 2001; Hunter, 2007), these models often rely upon the molecular differentiation of DSB ends via asymmetric loading of Rad51 and Dmc1. This key mechanistic tenant is likely invalid, as demonstrated by the results presented in this thesis (Brown et al., 2015). Thus, either some other molecule differentiates the two ends or they are not molecularly differentiated.

If meiotic DSB ends are molecularly differentiated, what molecule is responsible? Aside from Rad51/Dmc1 asymmetry, only one other molecularly asymmetric mechanism has been proposed. Following DSB formation by Spo11, a DNA oligonucleotide remains covalently attached via 5' linkage to the catalytic site of Spo11. Oligonucleotides of two discrete sizes were found in equivalent proportions (Neale et al., 2005). This finding led to the proposal that the two

ends of a DSB were differentiated by asymmetric cleavage of Spo11-oligos. Furthermore, rather than immediately dissociating, these short Spo11-oligos might remain associated via base pairing with the 3' ends of the ssDNA tracts, continuing to asymmetrically define the two DSB ends (Neale et al., 2005). While this model remains untested, it should be addressable by determining if the 3' end of ssDNA tracts are double stranded. Specifically, nuclease protection assays (using an RNA probe) or primer extension assays could be utilized to map the single versus double stranded nature of specific 3' ends following psoralen crosslinking of meiotic DNA. Another possibility is that phosphorylation or some other post-translational modification could differentiate the two ends of a DSB. For example, Dmc1 could be phosphorylated only on a single end of a DSB but invisible to our immunostaining protocols. Yet again, there is no evidence for this idea. A more subtle idea is that the relative amount of some protein (or some set of proteins) on one end of a DSB versus the other results in a non-binary, graded differentiation of the two DSB ends. This work provided evidence against such a mechanism for Rad51 and Dmc1 (Fig 3.2G).

In theory, any number of mechanisms involving any subset of dozens of proteins could potentially define a compositional asymmetry mechanism. However, aside from historical inertia, there seems to be little reason to focus on searching for such a mechanism. At the very least, any future claim of compositional asymmetry between the two ends of a DSB should be subject to a heavy burden of proof.

5.3.2 Context of a DSB within chromosomal architecture

The structure of meiotic chromosomes layers a rich architectural context onto the study of meiotic DNA recombination. Although ignored in the Watson-Crick DNA strand diagrams

commonly used to represent recombination reactions (Fig 1.1), meiotic DSBs are created and repaired in the context of a complex meiotic chromosome structure. Meiotic chromosomes are arranged in a series of loops joined at their bases by axial elements, and DSBs are catalyzed within the loop. Thus, the two DSB ends are tethered to the underlying chromosome structure by relatively long chromatin arms (Fig 3.12).

Spatial modeling shed light on the consequences of DSB end tethering. To better understand the structural context of DSBs within broken chromatin loops, the distance separating a DSB's two ends were simulated under various conditions and compared to the experimental proxy of DSB end separation (cytological inter-Rad51 and inter-Dmc1 nearest neighbor distributions). Specifically, a simple spatial model was constructed based on several assumptions. First, chromatin loops are roughly 600 nm in circumference. This is based upon the finding that sister chromatid *tetO* foci were split at distances up to 600 nm and is in agreement with previous measurements (Moens and Pearlman, 1988). Second, DSB formation is equally likely to occur at any position along the chromatin loop. This simplifying assumption may or may not be reflective of reality (Blat et al., 2002; Kugou et al., 2009; Panizza et al., 2011; Sommermeyer et al., 2013). (Although this feature of DSB position has never been specifically commented on, the datasets to test this assumption are available.) However, deviations from the uniform distribution employed are unlikely to seriously alter the results discussed below. Finally, it assumes that the two chromatin arms emanate from the same point. Under these assumptions and one of four different structural constraints, the separation between the two ends of a DSB was simulated (Fig 5.6). Of the simulated inter-end distributions, the only reasonable match with experimentally determined inter-Rad51 or inter-Dmc1 nearest neighbor distance distributions was the model in which both chromatin arms were flexible and free. (This model assumes that

each end is equally likely to fall on any point within its reach—defined by the length of their chromatin arms—and thus ignores any entropic considerations of chromatin arm conformation.) This is the only of the four models that yields an inter-end distribution with a local maximum. Furthermore, the local maximum occurs at a distance reminiscent of the maxima in Rad51-Rad51 and Dmc1-Dmc1 nearest neighbor distance distributions. By contrast, if both arms are rigid, a distribution without a local maximum and weighted heavily towards long distances is expected. If one end is held closely to the axial element (MacQueen, 2015; Storlazzi et al., 2010), the inter-end distributions also fail to achieve any resemblance to the experimentally observed distribution between Rad51 or Dmc1 foci. Additionally, paired Dmc1 foci do not appear to be preferentially oriented with a single focus associated with an axial element as predicted by the models where only one end is free (Fig 5.5 and Fig 5.6A,C). In summary, simple geometric modeling strongly suggests that the spatial relationship between the two ends of a meiotic DSB can be explained if both chromatin arms are flexible and free to independently explore the space defined by their lengths.

This architectural model potentially also has implications for the interpretation of interhomolog bias. To illustrate the implications, consider a DSB that forms one sixth of the way into a chromatin loop. A 100 nm and a 500 nm chromatin arm will be released, and the 500 nm arm will be free to explore a volume 125 times greater than the short arm. This dramatic difference in searchable space will likely mean that the 500 nm arm locates a homologous target first, making it the *de facto* first end. In fact, sister chromatids are often separated by 400 nm, significantly out of the reach of the shorter chromatin arm. Early in meiosis when homologs are unlinked by recombination, the homolog chromatids will very often be out of reach of even the

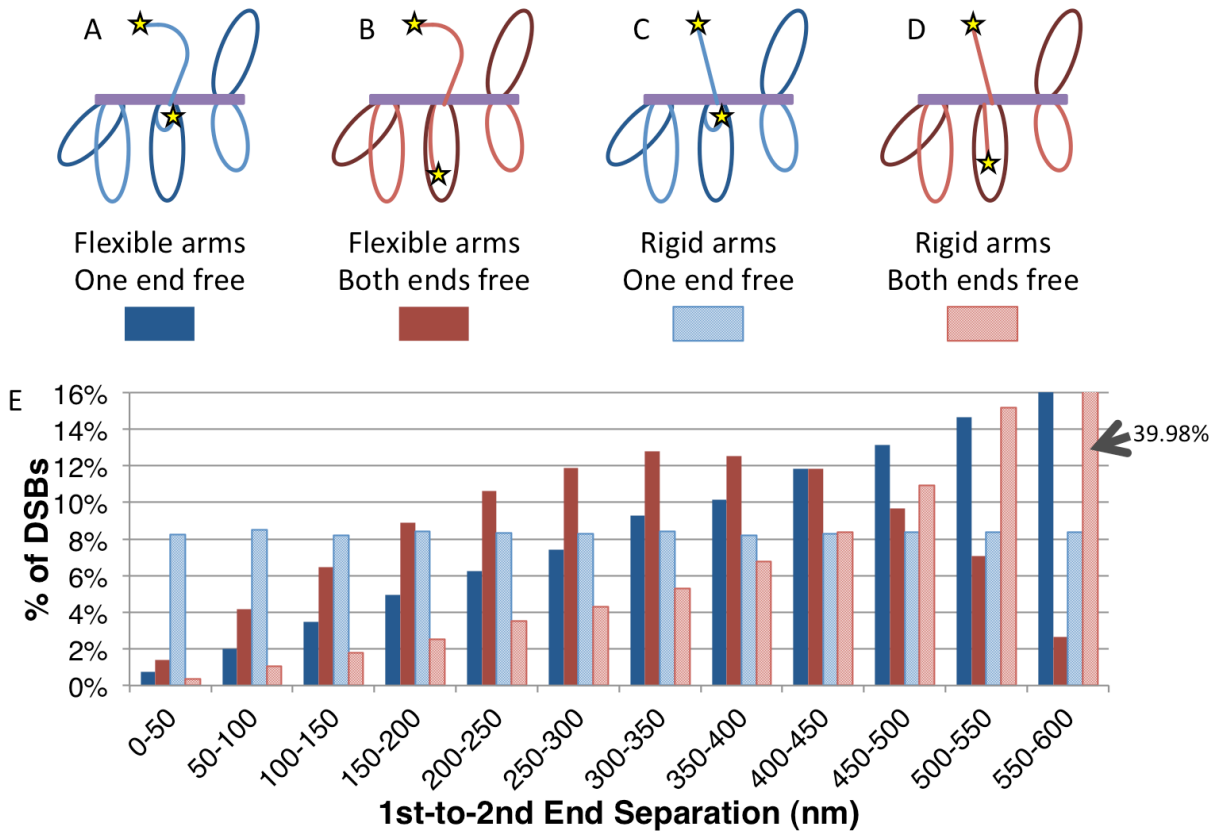

Figure 5.6 Modeling of chromatin arms suggests both arms liberated by a DSB are free and flexible. The position of both ends of a single DSB were modeled under the following assumptions. First, DSB occurs within a chromatin loop 600 nm long, anchored at a single point at the base of the loop. Second, the DSB is equally likely to occur at any position along the loop. Third, the model is strictly geometric. No physical properties like entropy are considered. Many DSBs meeting these criteria were simulated under four different criteria: (**A**) flexible arms, one end free; (**B**) flexible arms, both ends free; (**C**) rigid arms, one end free; (**D**) rigid arms, both ends free. When an arm is flexible, the DSB end is free and equally likely to occupy any position within the maximum reach of the chromatin arm. When an arm is rigid, the DSB end is restricted to locations along the perimeter defined by the length of the chromatin arm. When only one arm is free, the non-free DSB end is held at the base of the chromatin loop. (**E**) The simulated distribution of distances between the DSB ends under each of these four scenarios.

longer chromatin arm, resulting in a low probability of interhomolog repair. However, as recombination progressively aligns homologs, the 500 nm arm will have roughly equivalent probabilities of encountering any of the three available chromatids. Thus, this architectural context could at least partially account for the apparent propensity of intersister repair in early, "scout" DSBs and the progressive implementation of interhomolog bias throughout a meiotic time course (Joshi et al., 2015). If a DSB were to occur exactly in the middle of the chromatin loop, releasing two 300 nm arms with equivalent reaches, either end would be equally likely to be the invading first end, but the temporal change in partner choice would still occur. It should be emphasized that this is a probabilistic model in which neither the invading end nor the donor template is pre-determined; rather, these outcomes are only governed by the probability of a donor template passing through the reach of a DSB end's chromatin arm in a highly simplified system. It should be noted that this first-principles discussion cannot fully explain the interhomolog bias of meiotic recombination. Instead, it suggests that architectural context should be added to other well-known contributors including *MEK1* signaling as well as the cooperation between Rad51 and Dmc1 (Callender and Hollingsworth, 2010; Goldfarb and Lichten, 2010; Hong et al., 2013; Kim et al., 2010; Schwacha and Kleckner, 1997; Wan et al., 2004).

This architectural model of partner choice predicts that longer chromatin arms have a greater ability to invade a homolog chromatid. Natural variation in chromatin loop size and DSB position within chromatin loops can be exploited to probe this hypothesis. This architectural model predicts that the interhomolog bias of a DSB will positively correlate with chromatin loop size, because larger loops will release longer chromatin loops with greater reach. Additionally, within any individual loop, the deviation of DSB position from the center of the loop will positively correlate with interhomolog bias, because off center DSBs will release one long

chromatin arm. These analyses could be performed on pre-existing data sets (Blat et al., 2002; Buhler et al., 2007; Chen et al., 2008a; Liu et al., 2014; Pan et al., 2011; Panizza et al., 2011), using gene conversion frequency divided by DSB frequency as a proxy of interhomolog bias. Since the proposed architectural component of interhomolog bias would only be a part of the partner choice mechanism, the correlations sought in this analysis might be modest. Significant results would need to be carefully controlled through simulations or shuffling datasets.

An ultrastructural perspective of meiotic chromosomes could also provide additional insight into the possible differentiation of DSB ends. Kim et al. have previously suggested that the release of Rec8-mediated cohesion could liberate a long chromatin arm of the type discussed above, differentiating the two DSB ends (Kim et al., 2010). However, no evidence of DSB-dependent remodeling of sister chromatid cohesion was observed in this work, casting doubt on the existence of this proposed pre-strand exchange symmetry breaking mechanism. Again, I reiterate that there is no need for the two ends to be differentiated prior to strand exchange. Instead, I propose that the two ends of a DSB are only differentiated by post-strand exchange mechanisms. In other words, the first end is not defined prior to strand exchange; rather, strand exchange defines the first end.

There are two primary candidates to break the symmetry between the DSB ends by stabilizing the nascent strand exchange intermediate. First, the ZMM proteins (Zip1-4, Msh4/5, and Mer3) collectively fit the criteria for this activity. They are not required for strand exchange but are required for the subsequent stabilization of nascent strand exchange intermediates into stable single end invasion intermediates (Börner et al., 2004). All of these components form foci at the positions of SEIs—axial associations cytologically—in spread nuclei (Lynn et al., 2007). Msh4/5 has been reported to bind branched DNA molecules (SEIs and dHJs) biochemically by

encircling DNA duplexes (Rakshambikai et al., 2013; Snowden et al., 2004). Mer3 is a 3'-to-5' helicase that extends heteroduplex DNA, stabilizing strand exchange intermediates *in vitro* (Mazina et al., 2004). The mechanism of joint molecule stabilization by Zip1-4 is less clear but might reflect the mechanical strength conferred by synaptonemal complex assembly. A second candidate for the stabilization of nascent strand exchange intermediates is cohesin. A complicated epistasis analysis revealed that *rec8* mutants display normal interhomolog bias at the SEI stage but subsequently lose this bias at the SEI-to-dHJ transition (Hong et al., 2013; Kim et al., 2010). An alternative interpretation of the relevant data introduces the possibility that Rec8-mediated cohesion can stabilize strand exchange intermediates by encircling non-sister chromatids, similar to the proposed Msh4/5 mechanism. This proposed mechanism is supported by the finding that Rec8 is required for meiotic joint molecule formation in cells that fail to undergo pre-meiotic DNA synthesis and thus lack sister chromatids (*pMCD1-CDC6*) (Hong et al., 2013). While the establishment of sister chromatid cohesion during pre-meiotic S-phase is well established, the DSB repair-dependent establishment of cohesion (particularly between non-sister chromatids) is generally not considered. Yet, DSB repair in mitotic cells results in the local deposition of cohesin and establishment of cohesion (Sjögren and Nasmyth, 2001; Strom et al., 2007; Ström et al., 2004; Unal et al., 2007). In summary, the ZMM proteins and/or Rec8-mediated interhomolog cohesion could break the molecular symmetry between DSB ends by stabilizing the first nascent strand exchange intermediate.

The hypothesis that newly deposited cohesin stabilizes interhomolog strand exchange intermediates can be tested. First, strand exchange-dependent Rec8 deposition must be observed following completion of pre-meiotic DNA synthesis. To this end, a transcriptionally inducible epitope-tagged *REC8* allele must be introduced into a *REC8*$^{+}$ strain. Expression of the tagged

allele will only be induced after DNA replication. Second, chromosome spreads from wild type, *spo11*, and *dmc1* strains will be stained for the tagged protein to look for Rec8 foci that form in a DSB- and strand exchange-dependent manner. Such foci are predicted to be located at the site of axial associations. This localization pattern could be evidenced by colocalization with ZMM foci or at sites where axial elements meet. Third, ChIP-SEQ experiments could provide higher resolution information on Rec8 localization. Prior work has demonstrated that Rec8 primarily occupies periodic chromosomal domains that correspond with the bases of chromatin loops (Glynn et al., 2004; Panizza et al., 2011) and DSBs are located within the chromatin loops (Blat et al., 2002; Kugou et al., 2009). In the Rec8 deposition model being interrogated, the tagged Rec8 would occupy DSB hotspots, in sharp contrast to the normal Rec8 binding domains. An alternative version of this experiment would use untagged Rec8 and look for *SPO11*- and *DMC1*-dependent bumps in the chromatin binding profile that again correlates with DSB hotspot locations. An important caveat to this experiment is that it relies upon new Rec8 deposition and is blind to pre-loaded Rec8 becoming newly cohesive. However, the well-established paradigm of cohesin loading in mitotic DSB repair suggests that an analogous mechanism could exist in meiotic recombination (and is perhaps adapted to meet its unique interhomolog requirements) (Kleckner et al., 2004; Sjögren and Nasmyth, 2001; Strom et al., 2007; Ström et al., 2004; Unal et al., 2007). One additional piece of evidence supporting such a role in meiosis is that Rec8 localizes to polycomplexes. The ZMM proteins are all known to localize to this pathological aggregate structure that forms when meiotic recombination is perturbed (Chua and Roeder, 1998; Shinohara et al., 2015; Sym and Roeder, 1995; Tsubouchi et al., 2006). This similarity suggests that, like the ZMM proteins, Rec8 could stabilize interhomolog joint molecules during meiosis.

References

Akamatsu, Y., Tsutsui, Y., Morishita, T., Siddique, M.S.P., Kurokawa, Y., Ikeguchi, M., Yamao, F., Arcangioli, B., and Iwasaki, H. (2007). Fission yeast Swi5/Sfr1 and Rhp55/Rhp57 differentially regulate Rhp51-dependent recombination outcomes. The EMBO Journal *26*, 1352–1362.

Alexeev, A., Mazin, A., and Kowalczykowski, S.C. (2003). Rad54 protein possesses chromatin-remodeling activity stimulated by the Rad51-ssDNA nucleoprotein filament. Nat Struct Biol *10*, 182–186.

Anderson, L.K., Reeves, A., Webb, L.M., and Ashley, T. (1999). Distribution of crossing over on mouse synaptonemal complexes using immunofluorescent localization of MLH1 protein. Genetics *151*, 1569–1579.

Andresen, M., Schmitz-Salue, R., and Jakobs, S. (2004). Short tetracysteine tags to beta-tubulin demonstrate the significance of small labels for live cell imaging. Mol Biol Cell *15*, 5616–5622.

Argunhan, B., Farmer, S., Leung, W.-K., Terentyev, Y., Humphryes, N., Tsubouchi, T., Toyoizumi, H., and Tsubouchi, H. (2013). Direct and indirect control of the initiation of meiotic recombination by DNA damage checkpoint mechanisms in budding yeast. PLoS ONE *8*, e65875.

Aronson, D.E., Costantini, L.M., and Snapp, E.L. (2011). Superfolder GFP is fluorescent in oxidizing environments when targeted via the Sec translocon. Traffic *12*, 543–548.

Baumann, P., Benson, F.E., and West, S.C. (1996). Human Rad51 protein promotes ATP-dependent homologous pairing and strand transfer reactions in vitro. Cell *87*, 757–766.

Bell, J.C., Liu, B., and Kowalczykowski, S.C. (2015). Imaging and energetics of single SSB-ssDNA molecules reveal intramolecular condensation and insight into RecOR function. Elife *4*.

Benson, F.E., Baumann, P., and West, S.C. (1998). Synergistic actions of Rad51 and Rad52 in recombination and DNA repair. Nature *391*, 401–404.

Bergerat, A., de Massy, B., Gadelle, D., Varoutas, P.C., Nicolas, A., and Forterre, P. (1997). An atypical topoisomerase II from Archaea with implications for meiotic recombination. Nature *386*, 414–417.

Betzig, E., Patterson, G.H., Sougrat, R., Lindwasser, O.W., Olenych, S., Bonifacino, J.S., Davidson, M.W., Lippincott-Schwartz, J., and Hess, H.F. (2006). Imaging intracellular fluorescent proteins at nanometer resolution. Science *313*, 1642–1645.

Bishop, D.K. (1994). RecA homologs Dmc1 and Rad51 interact to form multiple nuclear complexes prior to meiotic chromosome synapsis. Cell *79*, 1081–1092.

Bishop, D.K., Ear, U., Bhattacharyya, A., Calderone, C., Beckett, M., Weichselbaum, R.R., and

Shinohara, A. (1998). Xrcc3 is required for assembly of Rad51 complexes in vivo. Journal of Biological Chemistry *273*, 21482–21488.

Bishop, D.K., Park, D., Xu, L., and Kleckner, N. (1992). *DMC1*: a meiosis-specific yeast homolog of *E. coli recA* required for recombination, synaptonemal complex formation, and cell cycle progression. Cell *69*, 439–456.

Blat, Y., Protacio, R.U., Hunter, N., and Kleckner, N. (2002). Physical and Functional Interactions among Basic Chromosome Organizational Features Govern Early Steps of Meiotic Chiasma Formation. Cell *111*, 791–802.

Börner, G.V., Kleckner, N., and Hunter, N. (2004). Crossover/noncrossover differentiation, synaptonemal complex formation, and regulatory surveillance at the leptotene/zygotene transition of meiosis. Cell *117*, 29–45.

Brown, M.S., and Bishop, D.K. (2015). DNA strand exchange and RecA homologs in meiosis. Cold Spring Harb Perspect Biol *7*, a016659.

Brown, M.S., Grubb, J., Zhang, A., Rust, M.J., and Bishop, D.K. (2015). Small Rad51 and Dmc1 Complexes Often Co-occupy Both Ends of a Meiotic DNA Double Strand Break. PLoS Genet *11*, e1005653.

Bugreev, D.V., and Mazin, A.V. (2004). Ca2+ activates human homologous recombination protein Rad51 by modulating its ATPase activity. Proc Natl Acad Sci U S A *101*, 9988–9993.

Bugreev, D.V., Golub, E.I., Stasiak, A.Z., Stasiak, A., and Mazin, A.V. (2005). Activation of human meiosis-specific recombinase Dmc1 by Ca2+. J. Biol. Chem. *280*, 26886–26895.

Bugreev, D.V., Pezza, R.J., Mazina, O.M., Voloshin, O.N., Camerini-Otero, R.D., and Mazin, A.V. (2011). The resistance of DMC1 D-loops to dissociation may account for the DMC1 requirement in meiosis. Nat Struct Mol Biol *18*, 56–60.

Buhler, C., Borde, V., and Lichten, M. (2007). Mapping meiotic single-strand DNA reveals a new landscape of DNA double-strand breaks in Saccharomyces cerevisiae. PLoS Biol *5*, e324.

Burns, S., Avena, J.S., Unruh, J.R., Yu, Z., Smith, S.E., Slaughter, B.D., Winey, M., and Jaspersen, S.L. (2015). Structured illumination with particle averaging reveals novel roles for yeast centrosome components during duplication. Elife *4*.

Busygina, V., Saro, D., Williams, G., Leung, W.-K., Say, A.F., Sehorn, M.G., Sung, P., and Tsubouchi, H. (2012). Novel Attributes of Hed1 Affect Dynamics and Activity of the Rad51 Presynaptic Filament during Meiotic Recombination. Journal of Biological Chemistry *287*, 1566–1575.

Busygina, V., Sehorn, M.G., Shi, I.Y., Tsubouchi, H., Roeder, G.S., and Sung, P. (2008). Hed1 regulates Rad51-mediated recombination via a novel mechanism. Genes & Development *22*, 786–795.

Bzymek, M., Thayer, N.H., Oh, S.D., Kleckner, N., and Hunter, N. (2010). Double Holliday junctions are intermediates of DNA break repair. Nature *464*, 937–941.

Callender, T.L., and Hollingsworth, N.M. (2010). Mek1 suppression of meiotic double-strand break repair is specific to sister chromatids, chromosome autonomous and independent of Rec8 cohesin complexes. Genetics *185*, 771–782.

Cao, L., Alani, E., and Kleckner, N. (1990). A pathway for generation and processing of double-strand breaks during meiotic recombination in S. cerevisiae. Cell *61*, 1089–1101.

Carballo, J.A., Johnson, A.L., Sedgwick, S.G., and Cha, R.S. (2008). Phosphorylation of the axial element protein Hop1 by Mec1/Tel1 ensures meiotic interhomolog recombination. Cell *132*, 758–770.

Ceballos, S.J., and Heyer, W.-D. (2011). Functions of the Snf2/Swi2 family Rad54 motor protein in homologous recombination. Biochim. Biophys. Acta *1809*, 509–523.

Chan, Y.-L., Brown, M.S., Qin, D., Handa, N., and Bishop, D.K. (2014). The third exon of the budding yeast meiotic recombination gene HOP2 is required for calcium-dependent and recombinase Dmc1-specific stimulation of homologous strand assimilation. Journal of Biological Chemistry *289*, 18076–18086.

Chen, S.Y., Tsubouchi, T., Rockmill, B., Sandler, J.S., Richards, D.R., Vader, G., Hochwagen, A., Roeder, G.S., and Fung, J.C. (2008a). Global analysis of the meiotic crossover landscape. Developmental Cell *15*, 401–415.

Chen, Y.K., Leng, C.H., Olivares, H., Lee, M.H., Chang, Y.C., Kung, W.M., Ti, S.C., Lo, Y.H., Wang, A.H.J., Chang, C.S., et al. (2004). Heterodimeric complexes of Hop2 and Mnd1 function with Dmc1 to promote meiotic homolog juxtaposition and strand assimilation. Proc Natl Acad Sci U S A *101*, 10572–10577.

Chen, Z., Yang, H., and Pavletich, N.P. (2008b). Mechanism of homologous recombination from the RecA-ssDNA/dsDNA structures. Nature *453*, 489–484.

Chi, P., San Filippo, J., Sehorn, M.G., Petukhova, G.V., and Sung, P. (2007). Bipartite stimulatory action of the Hop2-Mnd1 complex on the Rad51 recombinase. Genes & Development *21*, 1747–1757.

Chua, P.R., and Roeder, G.S. (1998). Zip2, a meiosis-specific protein required for the initiation of chromosome synapsis. Cell *93*, 349–359.

Cloud, V., Chan, Y.L., Grubb, J., Budke, B., and Bishop, D.K. (2012). Rad51 Is an Accessory Factor for Dmc1-Mediated Joint Molecule Formation During Meiosis. Science *337*, 1222–1225.

Colaiacovo, M.P., MacQueen, A.J., Martinez-Perez, E., McDonald, K., Adamo, A., La Volpe, A., and Villeneuve, A.M. (2003). Synaptonemal Complex Assembly in C. elegans Is Dispensable for Loading Strand-Exchange Proteins but Critical for Proper Completion of Recombination. Developmental Cell *5*, 463–474.

Cole, F. (2014). The sense and sensibility of strand exchange in recombination homeostasis. PLoS Genet *10*, e1004104.

Cole, F., Kauppi, L., Lange, J., Roig, I., Wang, R., Keeney, S., and Jasin, M. (2012). Homeostatic control of recombination is implemented progressively in mouse meiosis. Nat. Cell Biol. *14*, 424–430.

Conrad, M.N., Lee, C.-Y., Chao, G., Shinohara, M., Kosaka, H., Shinohara, A., Conchello, J.-A., and Dresser, M.E. (2008). Rapid telomere movement in meiotic prophase is promoted by NDJ1, MPS3, and CSM4 and is modulated by recombination. Cell *133*, 1175–1187.

Couteau, F., Belzile, F., Horlow, C., Grandjean, O., Vezon, D., and Doutriaux, M.P. (1999). Random chromosome segregation without meiotic arrest in both male and female meiocytes of a dmc1 mutant of Arabidopsis. Plant Cell *11*, 1623–1634.

Cromie, G.A., Hyppa, R.W., Taylor, A.F., Zakharyevich, K., Hunter, N., and Smith, G.R. (2006). Single Holliday junctions are intermediates of meiotic recombination. Cell *127*, 1167–1178.

Da Ines, O., Abe, K., Goubely, C., Gallego, M.E., and White, C.I. (2012). Differing requirements for RAD51 and DMC1 in meiotic pairing of centromeres and chromosome arms in Arabidopsis thaliana. PLoS Genet *8*, e1002636.

Da Ines, O., Degroote, F., Goubely, C., Amiard, S., Gallego, M.E., and White, C.I. (2013). Meiotic Recombination in Arabidopsis Is Catalysed by DMC1, with RAD51 Playing a Supporting Role. PLoS Genet *9*, e1003787.

Daley, J.M., Gaines, W.A., Kwon, Y., and Sung, P. (2014). Regulation of DNA pairing in homologous recombination. Cold Spring Harb Perspect Biol *6*, a017954.

Danilowicz, C., Peacock-Villada, A., Vlassakis, J., Facon, A., Feinstein, E., Kleckner, N., and Prentiss, M. (2013). The differential extension in dsDNA bound to Rad51 filaments may play important roles in homology recognition and strand exchange. Nucleic Acids Research *42*, 526–533.

Danilowicz, C., Feinstein, E., Conover, A., Coljee, V.W., Vlassakis, J., Chan, Y.-L., Bishop, D.K., and Prentiss, M. (2012). RecA homology search is promoted by mechanical stress along the scanned duplex DNA. Nucleic Acids Research *40*, 1717–1727.

De Massy, B., Baudat, F., and Nicolas, A. (1994). Initiation of Recombination in Saccharomyces cerevisiae Haploid Meiosis. Proc Natl Acad Sci U S A *91*, 11929–11933.

Dernburg, A.F., McDonald, K., Moulder, G., Barstead, R., Dresser, M., and Villeneuve, A.M. (1998). Meiotic Recombination in C. elegans Initiates by a Conserved Mechanism and Is Dispensable for Homologous Chromosome Synapsis. Cell *94*, 387–398.

Dion, V., and Gasser, S.M. (2013). Chromatin Movement in the Maintenance of Genome Stability. Cell *152*, 1355–1364.

Domenichini, S., Raynaud, C., Ni, D.-A., Henry, Y., and Bergounioux, C. (2006). Atmnd1-delta1 is sensitive to gamma-irradiation and defective in meiotic DNA repair. DNA Repair (Amst.) *5*, 455–464.

Dresser, M.E., and Giroux, C.N. (1988). Meiotic chromosome behavior in spread preparations of yeast. J. Cell Biol. *106*, 567–573.

Dresser, M.E., Ewing, D.J., Conrad, M.N., Dominguez, A.M., Barstead, R., Jiang, H., and Kodadek, T. (1997). DMC1 functions in a Saccharomyces cerevisiae meiotic pathway that is largely independent of the RAD51 pathway. Genetics *147*, 533–544.

Enomoto, R., Kinebuchi, T., Sato, M., Yagi, H., Kurumizaka, H., and Yokoyama, S. (2006). Stimulation of DNA strand exchange by the human TBPIP/Hop2-Mnd1 complex. J. Biol. Chem. *281*, 5575–5581.

Essers, J., Houtsmuller, A.B., van Veelen, L., Paulusma, C., Nigg, A.L., Pastink, A., Vermeulen, W., Hoeijmakers, J.H.J., and Kanaar, R. (2002). Nuclear dynamics of RAD52 group homologous recombination proteins in response to DNA damage. The EMBO Journal *21*, 2030–2037.

Etheridge, T.J., Boulineau, R.L., Herbert, A., Watson, A.T., Daigaku, Y., Tucker, J., George, S., Jönsson, P., Palayret, M., Lando, D., et al. (2014). Quantification of DNA-associated proteins inside eukaryotic cells using single-molecule localization microscopy. Nucleic Acids Research *42*, e146.

Ferrari, S.R., Grubb, J., and Bishop, D.K. (2009). The Mei5-Sae3 Protein Complex Mediates Dmc1 Activity in Saccharomyces cerevisiae. J. Biol. Chem. *284*, 11766–11770.

Fitzgerald, I., and Glick, B.S. (2014). Secretion of a foreign protein from budding yeasts is enhanced by cotranslational translocation and by suppression of vacuolar targeting. Microb. Cell Fact. *13*, 125.

Fölling, J., Bossi, M., Bock, H., Medda, R., Wurm, C.A., Hein, B., Jakobs, S., Eggeling, C., and Hell, S.W. (2008). Fluorescence nanoscopy by ground-state depletion and single-molecule return. Nat. Methods *5*, 943–945.

Franklin, A.E., McElver, J., Sunjevaric, I., Rothstein, R., Bowen, B., and Cande, W.Z. (1999). Three-dimensional microscopy of the Rad51 recombination protein during meiotic prophase. Plant Cell *11*, 809–824.

Fukuda, T., Nogami, S., and Ohya, Y. (2003). VDE-initiated intein homing in Saccharomyces cerevisiae proceeds in a meiotic recombination-like manner. Genes to Cells *8*, 587–602.

Fung, C.W., Mozlin, A.M., and Symington, L.S. (2009). Suppression of the double-strand-break-repair defect of the Saccharomyces cerevisiae rad57 mutant. Genetics *181*, 1195–1206.

Gaines, W.A., Godin, S.K., Kabbinavar, F.F., Rao, T., VanDemark, A.P., Sung, P., and Bernstein, K.A. (2015). Promotion of presynaptic filament assembly by the ensemble of S. cerevisiae Rad51 paralogues with Rad52. Nat Comms *6*, 7834.

Game, J.C., and Mortimer, R.K. (1974). A genetic study of x-ray sensitive mutants in yeast. Mutat. Res. *24*, 281–292.

Game, J.C., Zamb, T.J., Braun, R.J., Resnick, M., and Roth, R.M. (1980). The Role of Radiation (rad) Genes in Meiotic Recombination in Yeast. Genetics *94*, 51–68.

Gasior, S.L., Olivares, H., Ear, U., Hari, D.M., Weichselbaum, R., and Bishop, D.K. (2001). Assembly of RecA-like recombinases: Distinct roles for mediator proteins in mitosis and meiosis. Proc Natl Acad Sci U S A *98*, 8411–8418.

Gasior, S.L., Wong, A.K., Kora, Y., Shinohara, A., and Bishop, D.K. (1998). Rad52 associates with RPA and functions with Rad55 and Rad57 to assemble meiotic recombination complexes. Genes & Development *12*, 2208–2221.

Gasior, S. (1999). Assembly of recombination complexes in Saccharomyces cerevisiae. Dissertation.

Gerton, J.L., and DeRisi, J.L. (2002). Mnd1p: An evolutionarily conserved protein required for meiotic recombination. Proc Natl Acad Sci U S A *99*, 6895–6900.

Gibb, B., Ye, L.F., Kwon, Y., Niu, H., Sung, P., and Greene, E.C. (2014). Protein dynamics during presynaptic-complex assembly on individual single-stranded DNA molecules. Nat Struct Mol Biol *21*, 893–900.

Glynn, E.F., Megee, P.C., Yu, H.-G., Mistrot, C., Unal, E., Koshland, D.E., DeRisi, J.L., and Gerton, J.L. (2004). Genome-wide mapping of the cohesin complex in the yeast Saccharomyces cerevisiae. PLoS Biol *2*, E259.

Goldfarb, T., and Lichten, M. (2010). Frequent and efficient use of the sister chromatid for DNA double-strand break repair during budding yeast meiosis. PLoS Biol *8*, e1000520.

Govin, J., Dorsey, J., Gaucher, J., Rousseaux, S., Khochbin, S., and Berger, S.L. (2010). Systematic screen reveals new functional dynamics of histones H3 and H4 during gametogenesis. Genes & Development *24*, 1772–1786.

Gray, S., Allison, R.M., Garcia, V., Goldman, A.S.H., and Neale, M.J. (2013). Positive regulation of meiotic DNA double-strand break formation by activation of the DNA damage checkpoint kinase Mec1(ATR). Open Biol *3*, 130019.

Griffin, B.A., Adams, S.R., and Tsien, R.Y. (1998). Specific covalent labeling of recombinant protein molecules inside live cells. Science *281*, 269–272.

Grubb, J., Brown, M.S., and Bishop, D.K. (2015). Surface Spreading and Immunostaining of Yeast Chromosomes. J Vis Exp e53081.

Grushcow, J.M., Holzen, T.M., Park, K.J., Weinert, T., Lichten, M., and Bishop, D.K. (1999). Saccharomyces cerevisiae checkpoint genes MEC1, RAD17 and RAD24 are required for normal meiotic recombination partner choice. Genetics *153*, 607–620.

Gupta, R.C., Bazemore, L.R., Golub, E.I., and Radding, C.M. (1997). Activities of human recombination protein Rad51. Proc Natl Acad Sci U S A *94*, 463–468.

Gupta, R.C., Golub, E., Bi, B., and Radding, C.M. (2001). The synaptic activity of HsDmc1, a human recombination protein specific to meiosis. Proc Natl Acad Sci U S A *98*, 8433–8439.

Haaf, T., Golub, E.I., Reddy, G., Radding, C.M., and Ward, D.C. (1995). Nuclear foci of mammalian Rad51 recombination protein in somatic cells after DNA damage and its localization in synaptonemal complexes. Proc Natl Acad Sci U S A *92*, 2298–2302.

Haruta, N., Akamatsu, Y., Tsutsui, Y., Kurokawa, Y., Murayama, Y., Arcangioli, B., and Iwasaki, H. (2008). Fission yeast Swi5 protein, a novel DNA recombination mediator. DNA Repair (Amst.) *7*, 1–9.

Haruta, N., Kurokawa, Y., Murayama, Y., Akamatsu, Y., Unzai, S., Tsutsui, Y., and Iwasaki, H. (2006). The Swi5–Sfr1 complex stimulates Rhp51/Rad51 - and Dmc1-mediated DNA strand exchange in vitro. Nat Struct Mol Biol *13*, 823–830.

Hayase, A., Takagi, M., Miyazaki, T., Oshiumi, H., Shinohara, M., and Shinohara, A. (2004). A Protein Complex Containing Mei5 and Sae3 Promotes the Assembly of the Meiosis-Specific RecA Homolog Dmc1. Cell *119*, 927–940.

Heilemann, M., van de Linde, S., Schüttpelz, M., Kasper, R., Seefeldt, B., Mukherjee, A., Tinnefeld, P., and Sauer, M. (2008). Subdiffraction-Resolution Fluorescence Imaging with Conventional Fluorescent Probes. Angew. Chem. Int. Ed. *47*, 6172–6176.

Henderson, K.A., and Keeney, S. (2004). Tying synaptonemal complex initiation to the formation and programmed repair of DNA double-strand breaks. Proc Natl Acad Sci U S A *101*, 4519–4524.

Henriques, R., Lelek, M., Fornasiero, E.F., Valtorta, F., Zimmer, C., and Mhlanga, M.M. (2010). QuickPALM: 3D real-time photoactivation nanoscopy image processing in ImageJ. Nat. Methods *7*, 339–340.

Henry, J.M., Camahort, R., Rice, D.A., Florens, L., Swanson, S.K., Washburn, M.P., and Gerton, J.L. (2006). Mnd1/Hop2 Facilitates Dmc1-Dependent Interhomolog Crossover Formation in Meiosis of Budding Yeast. Mol Cell Biol *26*, 2913–2923.

Hicks, W.M., Yamaguchi, M., and Haber, J.E. (2011). Real-time analysis of double-strand DNA break repair by homologous recombination. Proc Natl Acad Sci U S A *108*, 3108–3115.

Hochwagen, A., and Amon, A. (2006). Checking your breaks: surveillance mechanisms of meiotic recombination. Curr. Biol. *16*, R217–R228.

Hoffmann, C., Gaietta, G., Zürn, A., Adams, S.R., Terrillon, S., Ellisman, M.H., Tsien, R.Y., and Lohse, M.J. (2010). Fluorescent labeling of tetracysteine-tagged proteins in intact cells. Nat Protoc *5*, 1666–1677.

Holzen, T.M., Shah, P.P., Olivares, H.A., and Bishop, D.K. (2006). Tid1/Rdh54 promotes dissociation of Dmc1 from nonrecombinogenic sites on meiotic chromatin. Genes & Development *20*, 2593–2604.

Hong, E.L., Shinohara, A., and Bishop, D.K. (2001). Saccharomyces cerevisiae Dmc1 protein promotes renaturation of single-strand DNA (ssDNA) and assimilation of ssDNA into homologous super-coiled duplex DNA. J. Biol. Chem. *276*, 41906–41912.

Hong, S., Sung, Y., Yu, M., Lee, M., Kleckner, N., and Kim, K.P. (2013). The logic and mechanism of homologous recombination partner choice. Mol Cell *51*, 440–453.

Hotta, Y., Furukawa, K., and Tabata, S. (1995). Meiosis specific transcription and functional proteins. Adv. Biophys. *31*, 101–115.

Hsieh, P., Camerini-Otero, C.S., and Camerini-Otero, R.D. (1992). The synapsis event in the homologous pairing of DNAs: RecA recognizes and pairs less than one helical repeat of DNA. Proc Natl Acad Sci U S A *89*, 6492–6496.

Hunter, N., and Kleckner, N. (2001). The single-end invasion: an asymmetric intermediate at the double-strand break to double-holliday junction transition of meiotic recombination. Cell *106*, 59–70.

Hunter, N. (2007). Meiotic recombination. In Molecular Genetics of Recombination, (Berlin, Heidelberg: Springer Berlin Heidelberg), pp. 381–442.

Hyppa, R.W., and Smith, G.R. (2010). Crossover Invariance Determined by Partner Choice for Meiotic DNA Break Repair. Cell *142*, 243–255.

Ishishita, S., Inui, T., Matsuda, Y., Serikawa, T., and Kitada, K. (2013). Infertility Associated with Meiotic Failure in the tremor Rat (tm/tm) is Caused by the Deletion of Spermatogenesis Associated 22. Exp. Anim. *62*, 219–227.

Jackson, J.A., and Fink, G.R. (1985). Meiotic recombination between duplicated genetic elements in Saccharomyces cerevisiae. Genetics *109*, 303–332.

Jang, Y.K., Jin, Y.H., Kim, E.M., Fabre, F., Hong, S.H., and Park, S.D. (1994). Cloning and sequence analysis of rhp51+, a Schizosaccharomyces pombe homolog of the Saccharomyces cerevisiae RAD51 gene. Gene *142*, 207–211.

Johnson, R., Borde, V., Neale, M.J., Bishop-Bailey, A., North, M., Harris, S., Nicolas, A., and Goldman, A.S.H. (2007). Excess single-stranded DNA inhibits meiotic double-strand break repair. PLoS Genet *3*, e223.

Joo, C., and Ha, T. (2012). Single-molecule FRET with total internal reflection microscopy. Cold Spring Harb Protoc *2012*.

Joshi, N., Brown, M.S., Bishop, D.K., and Börner, G.V. (2015). Gradual implementation of the meiotic recombination program via checkpoint pathways controlled by global DSB levels. Mol

Cell *57*, 797–811.

Kadyk, L.C., and Hartwell, L.H. (1992). Sister chromatids are preferred over homologs as substrates for recombinational repair in Saccharomyces cerevisiae. Genetics *132*, 387–402.

Keeney, S., Giroux, C.N., and Kleckner, N. (1997). Meiosis-Specific DNA Double-Strand Breaks Are Catalyzed by Spo11, a Member of a Widely Conserved Protein Family. Cell *88*, 375–384.

Kerzendorfer, C., Vignard, J., Pedrosa-Harand, A., Siwiec, T., Akimcheva, S., Jolivet, S., Sablowski, R., Armstrong, S., Schweizer, D., Mercier, R., et al. (2006). The Arabidopsis thaliana MND1 homologue plays a key role in meiotic homologous pairing, synapsis and recombination. J. Cell. Sci. *119*, 2486–2496.

Kiianitsa, K., Solinger, J.A., and Heyer, W.-D. (2006). Terminal association of Rad54 protein with the Rad51-dsDNA filament. Proc Natl Acad Sci U S A *103*, 9767–9772.

Kim, K.P., Weiner, B.M., Zhang, L., Jordan, A., Dekker, J., and Kleckner, N. (2010). Sister Cohesion and Structural Axis Components Mediate Homolog Bias of Meiotic Recombination. Cell *143*, 924–937.

Kinebuchi, T.T., Kagawa, W.W., Enomoto, R.R., Tanaka, K.K., Miyagawa, K.K., Shibata, T.T., Kurumizaka, H.H., and Yokoyama, S.S. (2004). Structural basis for octameric ring formation and DNA interaction of the human homologous-pairing protein Dmc1. Mol Cell *14*, 363–374.

Kleckner, N., Zickler, D., Jones, G.H., Dekker, J., Padmore, R., Henle, J., and Hutchinson, J. (2004). A mechanical basis for chromosome function. Proc Natl Acad Sci U S A *101*, 12592–12597.

Kobayashi, T., Kobayashi, E., Sato, S., Hotta, Y., Miyajima, N., Tanaka, A., and Tabata, S. (1994). Characterization of cDNAs Induced in Meiotic Prophase in Lily Microsporocytes. DNA Research *1*, 15–26.

Kobayashi, W., Sekine, S., Machida, S., and Kurumizaka, H. (2014). Green fluorescent protein fused to the C terminus of RAD51 specifically interferes with secondary DNA binding by the RAD51-ssDNA complex. Genes Genet. Syst. *89*, 169–179.

Kokabu, Y., Murayama, Y., Kuwabara, N., Oroguchi, T., Hashimoto, H., Tsutsui, Y., Nozaki, N., Akashi, S., Unzai, S., Shimizu, T., et al. (2011). Fission yeast Swi5-Sfr1 protein complex, an activator of Rad51 recombinase, forms an extremely elongated dogleg-shaped structure. J. Biol. Chem. *286*, 43569–43576.

Koszul, R., Kim, K.P., Prentiss, M., Kleckner, N., and Kameoka, S. (2008). Meiotic Chromosomes Move by Linkage to Dynamic Actin Cables with Transduction of Force through the Nuclear Envelope. Cell *133*, 1188–1201.

Kugou, K., Fukuda, T., Yamada, S., Ito, M., Sasanuma, H., Mori, S., Katou, Y., Itoh, T., Matsumoto, K., Shibata, T., et al. (2009). Rec8 guides canonical Spo11 distribution along yeast

meiotic chromosomes. Mol Biol Cell *20*, 3064–3076.

Kurokawa, Y., Murayama, Y., Haruta-Takahashi, N., Urabe, I., and Iwasaki, H. (2008). Reconstitution of DNA strand exchange mediated by Rhp51 recombinase and two mediators. PLoS Biol *6*, e88.

Kurzbauer, M.-T., Uanschou, C., Chen, D., and Schlögelhofer, P. (2012). The recombinases DMC1 and RAD51 are functionally and spatially separated during meiosis in *Arabidopsis*. Plant Cell *24*, 2058–2070.

Kuwabara, N., Hashimoto, H., Yamada, N., Unzai, S., Ikeguchi, M., Sato, M., Murayama, Y., Iwasaki, H., and Shimizu, T. (2010). Expression, purification and crystallization of Swi5 and the Swi5–Sfr1 complex from fission yeast. Acta Crystallogr. Sect. F Struct. Biol. Cryst. Commun. *66*, 1124–1126.

Kuwabara, N., Murayama, Y., Hashimoto, H., Kokabu, Y., Ikeguchi, M., Sato, M., Mayanagi, K., Tsutsui, Y., Iwasaki, H., and Shimizu, T. (2012). Mechanistic insights into the activation of Rad51-mediated strand exchange from the structure of a recombination activator, the Swi5-Sfr1 complex. Structure *20*, 440–449.

La Salle, S., Palmer, K., O'Brien, M., Schimenti, J.C., Eppig, J., and Handel, M.A. (2012). Spata22, a novel vertebrate-specific gene, is required for meiotic progress in mouse germ cells. Biol. Reprod. *86*, 45.

Lam, I., and Keeney, S. (2015). Mechanism and regulation of meiotic recombination initiation. Cold Spring Harb Perspect Biol *7*, a016634.

Lange, J., Pan, J., Cole, F., Thelen, M.P., Jasin, M., and Keeney, S. (2011). ATM controls meiotic double-strand-break formation. Nature *479*, 237–240.

Lao, J.P., and Hunter, N. (2010). Trying to avoid your sister. PLoS Biol *8*, e1000519.

Lao, J.P., Cloud, V., Huang, C.-C., Grubb, J., Thacker, D., Lee, C.-Y., Dresser, M.E., Hunter, N., and Bishop, D.K. (2013). Meiotic crossover control by concerted action of Rad51-Dmc1 in homolog template bias and robust homeostatic regulation. PLoS Genet *9*, e1003978.

Lao, J.P., Oh, S.D., Shinohara, M., Shinohara, A., and Hunter, N. (2008). Rad52 promotes postinvasion steps of meiotic double-strand-break repair. Mol Cell *29*, 517–524.

Lee, M.-H., Chang, Y.-C., Hong, E.L., Grubb, J., Chang, C.-S., Bishop, D.K., and Wang, T.-F. (2005). Calcium ion promotes yeast Dmc1 activity via formation of long and fine helical filaments with single-stranded DNA. J. Biol. Chem. *280*, 40980–40984.

Lesterlin, C., Ball, G., Schermelleh, L., and Sherratt, D.J. (2013). RecA bundles mediate homology pairing between distant sisters during DNA break repair. Nature *506*, 249–253.

Leu, J.Y., Chua, P.R., and Roeder, G.S. (1998). The meiosis-specific Hop2 protein of S. cerevisiae ensures synapsis between homologous chromosomes. Cell *94*, 375–386.

Li, W., Chen, C., Markmann-Mulisch, U., Timofejeva, L., Schmelzer, E., Ma, H., and Reiss, B. (2004). The Arabidopsis AtRAD51 gene is dispensable for vegetative development but required for meiosis. Proc Natl Acad Sci U S A *101*, 10596–10601.

Li, X., and Heyer, W.D. (2008). RAD54 controls access to the invading 3'-OH end after RAD51-mediated DNA strand invasion in homologous recombination in Saccharomyces cerevisiae. Nucleic Acids Research *37*, 638–646.

Li, Z., Golub, E.I., Gupta, R., and Radding, C.M. (1997). Recombination activities of HsDmc1 protein, the meiotic human homolog of RecA protein. Proc Natl Acad Sci U S A *94*, 11221–11226.

Lindsley, J.E., and Cox, M.M. (1990). Assembly and disassembly of RecA protein filaments occur at opposite filament ends. Relationship to DNA strand exchange. J. Biol. Chem. *265*, 9043–9054.

Lisby, M., Rothstein, R., and Mortensen, U.H. (2001). Rad52 forms DNA repair and recombination centers during S phase. Proc Natl Acad Sci U S A *98*, 8276–8282.

Lisby, M., Barlow, J.H., Burgess, R.C., and Rothstein, R. (2004). Choreography of the DNA Damage Response. Cell *118*, 699–713.

Lisby, M., Mortensen, U.H., and Rothstein, R. (2003). Colocalization of multiple DNA double-strand breaks at a single Rad52 repair centre. Nat. Cell Biol. *5*, 572–577.

Liu, J., Renault, L., Veaute, X., Fabre, F., Stahlberg, H., and Heyer, W.-D. (2011). Rad51 paralogues Rad55–Rad57 balance the antirecombinase Srs2 in Rad51 filament formation. Nature *479*, 245–248.

Liu, Y., Gaines, W.A., Callender, T., Busygina, V., Oke, A., Sung, P., Fung, J.C., and Hollingsworth, N.M. (2014). Down-regulation of Rad51 activity during meiosis in yeast prevents competition with Dmc1 for repair of double-strand breaks. PLoS Genet *10*, e1004005.

Loidl, J., Nairz, K., and Klein, F. (1991). Meiotic chromosome synapsis in a haploid yeast. Chromosoma *100*, 221–228.

Luo, M., Yang, F., Leu, N.A., Landaiche, J., Handel, M.A., Benavente, R., La Salle, S., and Wang, P.J. (2013). MEIOB exhibits single-stranded DNA-binding and exonuclease activities and is essential for meiotic recombination. Nat Comms *4*, 2788.

Lydall, D., Nikolsky, Y., Bishop, D.K., and Weinert, T. (1996). A meiotic recombination checkpoint controlled by mitotic checkpoint genes. Nature *383*, 840–843.

Lynn, A., Soucek, R., and Börner, G.V. (2007). ZMM proteins during meiosis: crossover artists at work. Chromosome Res *15*, 591–605.

MacQueen, A.J. (2015). Catching a (Double-Strand) Break: The Rad51 and Dmc1 Strand Exchange Proteins Can Co-occupy Both Ends of a Meiotic DNA Double-Strand Break. PLoS

Genet *11*, e1005741.

MacQueen, A.J., Colaiacovo, M.P., McDonald, K., and Villeneuve, A.M. (2002). Synapsis-dependent and -independent mechanisms stabilize homolog pairing during meiotic prophase in C. elegans. Genes & Development *16*, 2428–2442.

Malik, P.S., and Symington, L.S. (2008). Rad51 gain-of-function mutants that exhibit high affinity DNA binding cause DNA damage sensitivity in the absence of Srs2. Nucleic Acids Research *36*, 6504–6510.

Martini, E., Diaz, R.L., Hunter, N., and Keeney, S. (2006). Crossover homeostasis in yeast meiosis. Cell *126*, 285–295.

Masson, J.-Y., Davies, A.A., Hajibagheri, N., Van Dyck, E., Benson, F.E., Stasiak, A.Z., Stasiak, A., and West, S.C. (1999). The meiosis-specific recombinase hDmc1 forms ring structures and interacts with hRad51. The EMBO Journal *18*, 6552–6560.

Mazin, A.V., and Kowalczykowski, S.C. (1996). The specificity of the secondary DNA binding site of RecA protein defines its role in DNA strand exchange. Proc Natl Acad Sci U S A *93*, 10673–10678.

Mazin, A.V., and Kowalczykowski, S.C. (1998). The function of the secondary DNA-binding site of RecA protein during DNA strand exchange. The EMBO Journal *17*, 1161–1168.

Mazina, O.M., Mazin, A.V., Nakagawa, T., Kolodner, R.D., and Kowalczykowski, S.C. (2004). Saccharomyces cerevisiae Mer3 helicase stimulates 3“-5” heteroduplex extension by Rad51; implications for crossover control in meiotic recombination. Cell *117*, 47–56.

McKim, K.S., Green-Marroquin, B.L., Sekelsky, J.J., Chin, G., Steinberg, C., Khodosh, R., and Hawley, R.S. (1998). Meiotic synapsis in the absence of recombination. Science *279*, 876–878.

McMahill, M.S., Sham, C.W., and Bishop, D.K. (2007). Synthesis-Dependent Strand Annealing in Meiosis. PLoS Biol *5*, e299.

Menetski, J.P., Bear, D.G., and Kowalczykowski, S.C. (1990). Stable DNA heteroduplex formation catalyzed by the Escherichia coli RecA protein in the absence of ATP hydrolysis. Proc Natl Acad Sci U S A *87*, 21–25.

Mets, D.G., and Meyer, B.J. (2009). Condensins regulate meiotic DNA break distribution, thus crossover frequency, by controlling chromosome structure. Cell *139*, 73–86.

Miyazaki, T., Bressan, D.A., Shinohara, M., Haber, J.E., and Shinohara, A. (2004). In vivo assembly and disassembly of Rad51 and Rad52 complexes during double-strand break repair. The EMBO Journal *23*, 939–949.

Moens, P.B., and Pearlman, R.E. (1988). Chromatin organization at meiosis. Bioessays *9*, 151–153.

Morrical, S.W. (2015). DNA-pairing and annealing processes in homologous recombination and homology-directed repair. Cold Spring Harb Perspect Biol *7*, a016444.

Murayama, Y., Tsutsui, Y., and Iwasaki, H. (2011). The fission yeast meiosis-specific Dmc1 recombinase mediates formation and branch migration of Holliday junctions by preferentially promoting strand exchange in a direction opposite to that of Rad51. Genes & Development *25*, 516–527.

Nabeshima, K., Kakihara, Y., Hiraoka, Y., and Nojima, H. (2001). A novel meiosis-specific protein of fission yeast, Meu13p, promotes homologous pairing independently of homologous recombination. The EMBO Journal *20*, 3871–3881.

Neale, M.J., Pan, J., and Keeney, S. (2005). Endonucleolytic processing of covalent protein-linked DNA double-strand breaks. Nature *436*, 1053–1057.

New, J.H., Sugiyama, T., Zaitseva, E., and Kowalczykowski, S.C. (1998). Rad52 protein stimulates DNA strand exchange by Rad51 and replication protein A. Nature *391*, 407–410.

Nimonkar, A.V., Dombrowski, C.C., Siino, J.S., Stasiak, A.Z., Stasiak, A., and Kowalczykowski, S.C. (2012). Saccharomyces cerevisiae Dmc1 and Rad51 proteins preferentially function with Tid1 and Rad54 proteins, respectively, to promote DNA strand invasion during genetic recombination. J. Biol. Chem. *287*, 28727–28737.

Niu, H., Li, X., Job, E., Park, C., Moazed, D., Gygi, S.P., and Hollingsworth, N.M. (2007). Mek1 kinase is regulated to suppress double-strand break repair between sister chromatids during budding yeast meiosis. Mol Cell Biol *27*, 5456–5467.

Niu, H., Wan, L., Baumgartner, B., Schaefer, D., Loidl, J., and Hollingsworth, N.M. (2005). Partner choice during meiosis is regulated by Hop1-promoted dimerization of Mek1. Mol Biol Cell *16*, 5804–5818.

Niu, H., Wan, L., Busygina, V., Kwon, Y., Allen, J.A., Li, X., Kunz, R.C., Kubota, K., Wang, B., Sung, P., et al. (2009). Regulation of meiotic recombination via Mek1-mediated Rad54 phosphorylation. Mol Cell *36*, 393–404.

Ogawa, T., Yu, X., Shinohara, A., and Egelman, E.H. (1993). Similarity of the yeast RAD51 filament to the bacterial RecA filament. Science *259*, 1896–1899.

Oh, S.D., Lao, J.P., Hwang, P.Y.-H., Taylor, A.F., Smith, G.R., and Hunter, N. (2007). BLM Ortholog, Sgs1, Prevents Aberrant Crossing-over by Suppressing Formation of Multichromatid Joint Molecules. Cell *130*, 259–272.

Okorokov, A.L., Chaban, Y.L., Bugreev, D.V., Hodgkinson, J., Mazin, A.V., and Orlova, E.V. (2010). Structure of the hDmc1-ssDNA filament reveals the principles of its architecture. PLoS ONE *5*, e8586.

Page, S.L., and Hawley, R.S. (2001). c(3)G encodes a Drosophila synaptonemal complex protein. Genes & Development *15*, 3130–3143.

Pan, J., Sasaki, M., Kniewel, R., Murakami, H., Blitzblau, H.G., Tischfield, S.E., Zhu, X., Neale, M.J., Jasin, M., Socci, N.D., et al. (2011). A Hierarchical Combination of Factors Shapes the Genome-wide Topography of Yeast Meiotic Recombination Initiation. Cell *144*, 719–731.

Panizza, S., Mendoza, M.A., Berlinger, M., Huang, L., Nicolas, A., Shirahige, K., and Klein, F. (2011). Spo11-Accessory Proteins Link Double-Strand Break Sites to the Chromosome Axis in Early Meiotic Recombination. Cell *146*, 372–383.

Panoli, A.P., Ravi, M., Sebastian, J., Nishal, B., Reddy, T.V., Marimuthu, M.P.A., Subbiah, V., Vijaybhaskar, V., and Siddiqi, I. (2006). AtMND1 is required for homologous pairing during meiosis in Arabidopsis. BMC Mol. Biol. *7*, 24.

Passy, S.I., Yu, X., Li, Z., Radding, C.M., Masson, J.Y., West, S.C., and Egelman, E.H. (1999). Human Dmc1 protein binds DNA as an octameric ring. Proc Natl Acad Sci U S A *96*, 10684–10688.

Pawlowski, W.P., Golubovskaya, I.N., Timofejeva, L., Meeley, R.B., Sheridan, W.F., and Cande, W.Z. (2004). Coordination of meiotic recombination, pairing, and synapsis by PHS1. Science *303*, 89–92.

Peacock-Villada, A., Yang, D., Danilowicz, C., Feinstein, E., Pollock, N., McShan, S., Coljee, V., and Prentiss, M. (2012). Complementary strand relocation may play vital roles in RecA-based homology recognition. Nucleic Acids Research *40*, 10441–10451.

Petukhova, G., Stratton, S., and Sung, P. (1998). Catalysis of homologous DNA pairing by yeast Rad51 and Rad54 proteins. Nature *393*, 91–94.

Petukhova, G.V., Pezza, R.J., Vanevski, F., Ploquin, M., Masson, J.-Y., and Camerini-Otero, R.D. (2005). The Hop2 and Mnd1 proteins act in concert with Rad51 and Dmc1 in meiotic recombination. Nat Struct Mol Biol *12*, 449–453.

Petukhova, G.V., Romanienko, P.J., and Camerini-Otero, R.D. (2003). The Hop2 protein has a direct role in promoting interhomolog interactions during mouse meiosis. Developmental Cell *5*, 927–936.

Pezza, R.J., Petukhova, G.V., Ghirlando, R., and Camerini-Otero, R.D. (2006). Molecular Activities of Meiosis-specific Proteins Hop2, Mnd1, and the Hop2-Mnd1 Complex. J. Biol. Chem. *281*, 18426–18434.

Pezza, R.J., Voloshin, O.N., Vanevski, F., and Camerini-Otero, R.D. (2007). Hop2/Mnd1 acts on two critical steps in Dmc1-promoted homologous pairing. Genes & Development *21*, 1758–1766.

Pezza, R.J., Camerini-Otero, R.D., and Bianco, P.R. (2010). Hop2-Mnd1 condenses DNA to stimulate the synapsis phase of DNA strand exchange. Biophys. J. *99*, 3763–3772.

Pezza, R.J., Voloshin, O.N., Volodin, A.A., Boateng, K.A., Bellani, M.A., Mazin, A.V., and Camerini-Otero, R.D. (2014). The dual role of HOP2 in mammalian meiotic homologous recombination. Nucleic Acids Research *42*, 2346–2357.

Pédelacq, J.-D., Cabantous, S., Tran, T., Terwilliger, T.C., and Waldo, G.S. (2006). Engineering and characterization of a superfolder green fluorescent protein. Nat. Biotechnol. *24*, 79–88.

Ploquin, M., Petukhova, G.V., Morneau, D., Déry, U., Bransi, A., Stasiak, A., Camerini-Otero, R.D., and Masson, J.-Y. (2007). Stimulation of fission yeast and mouse Hop2-Mnd1 of the Dmc1 and Rad51 recombinases. Nucleic Acids Research *35*, 2719–2733.

Qi, Z., Redding, S., Lee, J.Y., Gibb, B., Kwon, Y., Niu, H., Gaines, W.A., Sung, P., and Greene, E.C. (2015). DNA Sequence Alignment by Microhomology Sampling during Homologous Recombination. Cell *160*, 856–869.

Qian, X., He, Y., Ma, X., Fodje, M.N., Grochulski, P., and Luo, Y. (2006). Calcium Stiffens Archaeal Rad51 Recombinase from Methanococcus voltae for Homologous Recombination. Journal of Biological Chemistry *281*, 39380–39387.

Rabitsch, K.P., Tóth, A., Gálová, M., Schleiffer, A., Schaffner, G., Aigner, E., Rupp, C., Penkner, A.M., Moreno-Borchart, A.C., Primig, M., et al. (2001). A screen for genes required for meiosis and spore formation based on whole-genome expression. Current Biology *11*, 1001–1009.

Raderschall, E., Golub, E.I., and Haaf, T. (1999). Nuclear foci of mammalian recombination proteins are located at single-stranded DNA regions formed after DNA damage. Proc Natl Acad Sci U S A *96*, 1921–1926.

Rakshambikai, R., Srinivasan, N., and Nishant, K.T. (2013). Structural insights into Saccharomyces cerevisiae Msh4-Msh5 complex function using homology modeling. PLoS ONE *8*, e78753.

Ramesh, M.A., Malik, S.-B., and Logsdon, J.M., Jr. (2005). A Phylogenomic Inventory of Meiotic Genes. Current Biology *15*, 185–191.

Register, J.C., and Griffith, J. (1985). The direction of RecA protein assembly onto single strand DNA is the same as the direction of strand assimilation during strand exchange. J. Biol. Chem. *260*, 12308–12312.

Ristic, D. (2005). Human Rad51 filaments on double- and single-stranded DNA: correlating regular and irregular forms with recombination function. Nucleic Acids Research *33*, 3292–3302.

Roca, A.I., Cox, M.M., and Brenner, S.L. (1990). The RecA Protein: Structure and Function. Crit. Rev. Biochem. Mol. Biol. *25*, 415–456.

Rockmill, B., and Roeder, G.S. (1990). Meiosis in asynaptic yeast. Genetics *126*, 563–574.

Rockmill, B., and Roeder, G.S. (1991). A meiosis-specific protein kinase homolog required for chromosome synapsis and recombination. Genes & Development *5*, 2392–2404.

Rockmill, B., Sym, M., Scherthan, H., and Roeder, G.S. (1995). Roles for two RecA homologs in promoting meiotic chromosome synapsis. Genes & Development *9*, 2684–2695.

Rog, O., and Dernburg, A.F. (2015). Direct Visualization Reveals Kinetics of Meiotic Chromosome Synapsis. Cell Rep.

Rohner, S., Gasser, S.M., and Meister, P. (2008). Modules for cloning-free chromatin tagging in *Saccharomyces cerevisae*. Yeast *25*, 235–239.

Rosu, S., Libuda, D.E., and Villeneuve, A.M. (2011). Robust Crossover Assurance and Regulated Interhomolog Access Maintain Meiotic Crossover Number. Science *334*, 1286–1289.

Rua, D., Holzen, T., Glick, B.S., Kron, S.J., and Bishop, D.K. (2004). Monitoring changes in the subcellular location of proteins in S. cerevisiae. Methods Mol. Biol. *241*, 299–311.

Saito, T.T. (2004). Mcp7, a meiosis-specific coiled-coil protein of fission yeast, associates with Meu13 and is required for meiotic recombination. Nucleic Acids Research *32*, 3325–3339.

San Filippo, J., Sung, P., and Klein, H. (2008). Mechanism of eukaryotic homologous recombination. Annu. Rev. Biochem. *77*, 229–257.

Sasanuma, H., Furihata, Y., Shinohara, M., and Shinohara, A. (2013a). Remodeling of the Rad51 DNA strand-exchange protein by the Srs2 helicase. Genetics *194*, 859–872.

Sasanuma, H., Tawaramoto, M.S., Lao, J.P., Hosaka, H., Sanda, E., Suzuki, M., Yamashita, E., Hunter, N., Shinohara, M., Nakagawa, A., et al. (2013b). A new protein complex promoting the assembly of Rad51 filaments. Nat Comms *4*, 1676.

Sauvageau, S., Stasiak, A.Z., Banville, I., Ploquin, M., Stasiak, A., and Masson, J.-Y. (2005). Fission yeast Rad51 and Dmc1, two efficient DNA recombinases forming helical nucleoprotein filaments. Mol Cell Biol *25*, 4377–4387.

Say, A.F., Ledford, L.L., Sharma, D., Singh, A.K., Leung, W.-K., Sehorn, H.A., Tsubouchi, H., Sung, P., and Sehorn, M.G. (2011). The budding yeast Mei5-Sae3 complex interacts with Rad51 and preferentially binds a DNA fork structure. DNA Repair (Amst.) *10*, 586–594.

Schmuckli-Maurer, J., and Heyer, W.-D. (2000). Meiotic recombination in RAD54 mutants of Saccharomyces cerevisiae. Chromosoma *109*, 86–93.

Schommer, C., Beven, A., Lawrenson, T., Shaw, P., and Sablowski, R. (2003). AHP2 is required for bivalent formation and for segregation of homologous chromosomes in Arabidopsis meiosis. Plant J *36*, 1–11.

Schücker, K., Holm, T., Franke, C., Sauer, M., and Benavente, R. (2015). Elucidation of synaptonemal complex organization by super-resolution imaging with isotropic resolution. Proceedings of the National Academy of Sciences *112*, 2029–2033.

Schwacha, A., and Kleckner, N. (1994). Identification of joint molecules that form frequently between homologs but rarely between sister chromatids during yeast meiosis. Cell *76*, 51–63.

Schwacha, A., and Kleckner, N. (1995). Identification of double Holliday junctions as

intermediates in meiotic recombination. Cell *83*, 783–791.

Schwacha, A., and Kleckner, N. (1997). Interhomolog bias during meiotic recombination: meiotic functions promote a highly differentiated interhomolog-only pathway. Cell *90*, 1123–1135.

Sehorn, M.G., Sigurdsson, S., Bussen, W., Unger, V.M., and Sung, P. (2004). Human meiotic recombinase Dmc1 promotes ATP-dependent homologous DNA strand exchange. Nature *429*, 433–437.

Shah, P.P. (2008). Characterization of in vivo recombinase dynamics in *S. cerevisiae* and *E. coli*. Dissertation.

Shah, P.P., Zheng, X., Epshtein, A., Carey, J.N., Bishop, D.K., and Klein, H.L. (2010). Swi2/Snf2-Related Translocases Prevent Accumulation of Toxic Rad51 Complexes during Mitotic Growth. Mol Cell *39*, 862–872.

Sheridan, S., and Bishop, D.K. (2006). Red-Hed regulation: recombinase Rad51, though capable of playing the leading role, may be relegated to supporting Dmc1 in budding yeast meiosis. Genes & Development *20*, 1685–1691.

Sheridan, S.D., Yu, X., Roth, R., Heuser, J.E., Sehorn, M.G., Sung, P., Egelman, E.H., and Bishop, D.K. (2008). A comparative analysis of Dmc1 and Rad51 nucleoprotein filaments. Nucleic Acids Research *36*, 4057–4066.

Shinohara, A., and Ogawa, T. (1998). Stimulation by Rad52 of yeast Rad51-mediated recombination. Nature *391*, 404–407.

Shinohara, A., Ogawa, H., and Ogawa, T. (1992). Rad51 protein involved in repair and recombination in S. cerevisiae is a RecA-like protein. Cell *69*, 457–470.

Shinohara, A., Gasior, S., Ogawa, T., Kleckner, N., and Bishop, D.K. (2003a). *Saccharomyces cerevisiae recA* homologues *RAD51* and *DMC1* have both distinct and overlapping roles in meiotic recombination. Genes to Cells *2*, 615–629.

Shinohara, M., Gasior, S.L., Bishop, D.K., and Shinohara, A. (2000). Tid1/Rdh54 promotes colocalization of Rad51 and Dmc1 during meiotic recombination. Proc Natl Acad Sci U S A *97*, 10814–10819.

Shinohara, M., Shita-Yamaguchi, E., Buerstedde, J.M., Shinagawa, H., Ogawa, H., and Shinohara, A. (1997). Characterization of the roles of the Saccharomyces cerevisiae RAD54 gene and a homologue of RAD54, RDH54/TID1, in mitosis and meiosis. Genetics *147*, 1545–1556.

Shinohara, M., Hayashihara, K., Grubb, J.T., Bishop, D.K., and Shinohara, A. (2015). DNA damage response clamp 9-1-1 promotes assembly of ZMM proteins for formation of crossovers and synaptonemal complex. J. Cell. Sci. *128*, 1494–1506.

Shinohara, M., Sakai, K., Shinohara, A., and Bishop, D.K. (2003b). Crossover interference in Saccharomyces cerevisiae requires a TID1/RDH54-and DMC1-dependent pathway. Genetics *163*, 1273–1286.

Sjögren, C., and Nasmyth, K. (2001). Sister chromatid cohesion is required for postreplicative double-strand break repair in Saccharomyces cerevisiae. Current Biology *11*, 991–995.

Snowden, T., Acharya, S., Butz, C., Berardini, M., and Fishel, R. (2004). hMSH4-hMSH5 recognizes Holliday Junctions and forms a meiosis-specific sliding clamp that embraces homologous chromosomes. Mol Cell *15*, 437–451.

Sommermeyer, V., Béneut, C., Chaplais, E., Serrentino, M.E., and Borde, V. (2013). Spp1, a member of the Set1 Complex, promotes meiotic DSB formation in promoters by tethering histone H3K4 methylation sites to chromosome axes. Mol Cell *49*, 43–54.

Souquet, B., Abby, E., Hervé, R., Finsterbusch, F., Tourpin, S., Le Bouffant, R., Duquenne, C., Messiaen, S., Martini, E., Bernardino-Sgherri, J., et al. (2013). MEIOB targets single-strand DNA and is necessary for meiotic recombination. PLoS Genet *9*, e1003784.

Staeva-Vieira, E., Yoo, S., and Lehmann, R. (2003). An essential role of DmRad51/SpnA in DNA repair and meiotic checkpoint control. The EMBO Journal *22*, 5863–5874.

Stassen, N.Y., Logsdon, J.M., Jr, Vora, G.J., Offenberg, H.H., Palmer, J.D., and Zolan, M.E. (1997). Isolation and characterization of rad51 orthologs from Coprinus cinereus and Lycopersicon esculentum, and phylogenetic analysis of eukaryotic recA homologs. Current Genetics *31*, 144–157.

Storchová, Z., Breneman, A., Cande, J., Dunn, J., Burbank, K., O'Toole, E., and Pellman, D. (2006). Genome-wide genetic analysis of polyploidy in yeast. Nature *443*, 541–547.

Storlazzi, A., Gargano, S., Ruprich-Robert, G., Falque, M., David, M., Kleckner, N., and Zickler, D. (2010). Recombination proteins mediate meiotic spatial chromosome organization and pairing. Cell *141*, 94–106.

Storlazzi, A., Tessé, S., Gargano, S., James, F., Kleckner, N., and Zickler, D. (2003). Meiotic double-strand breaks at the interface of chromosome movement, chromosome remodeling, and reductional division. Genes & Development *17*, 2675–2687.

Strom, L., Karlsson, C., Lindroos, H.B., Wedahl, S., Katou, Y., Shirahige, K., and Sjogren, C. (2007). Postreplicative Formation of Cohesion Is Required for Repair and Induced by a Single DNA Break. Science *317*, 242–245.

Ström, L., Lindroos, H.B., Shirahige, K., and Sjögren, C. (2004). Postreplicative Recruitment of Cohesin to Double-Strand Breaks Is Required for DNA Repair. Mol Cell *16*, 1003–1015.

Sugiyama, T., New, J.H., and Kowalczykowski, S.C. (1998). DNA annealing by RAD52 protein is stimulated by specific interaction with the complex of replication protein A and single-stranded DNA. Proc Natl Acad Sci U S A *95*, 6049–6054.

Sugiyama, T., and Kowalczykowski, S.C. (2002). Rad52 protein associates with replication protein A (RPA)-single-stranded DNA to accelerate Rad51-mediated displacement of RPA and presynaptic complex formation. J. Biol. Chem. *277*, 31663–31672.

Sun, H., Treco, D., and Szostak, J.W. (1991). Extensive 3'-overhanging, single-stranded DNA associated with the meiosis-specific double-strand breaks at the ARG4 recombination initiation site. Cell *64*, 1155–1161.

Sung, P. (1994). Catalysis of ATP-dependent homologous DNA pairing and strand exchange by yeast RAD51 protein. Science *265*, 1241–1243.

Sung, P. (1997). Yeast Rad55 and Rad57 proteins form a heterodimer that functions with replication protein A to promote DNA strand exchange by Rad51 recombinase. Genes & Development *11*, 1111–1121.

Sung, P., and Robberson, D.L. (1995). DNA strand exchange mediated by a RAD51-ssDNA nucleoprotein filament with polarity opposite to that of RecA. Cell *82*, 453–461.

Sym, M., and Roeder, G.S. (1995). Zip1-induced changes in synaptonemal complex structure and polycomplex assembly. J. Cell Biol. *128*, 455–466.

Sym, M., Engebrecht, J.A., and Roeder, G.S. (1993). ZIP1 is a synaptonemal complex protein required for meiotic chromosome synapsis. Cell *72*, 365–378.

Szymborska, A., de Marco, A., Daigle, N., Cordes, V.C., Briggs, J.A.G., and Ellenberg, J. (2013). Nuclear pore scaffold structure analyzed by super-resolution microscopy and particle averaging. Science *341*, 655–658.

Tarsounas, M., Morita, T., Pearlman, R.E., and Moens, P.B. (1999). RAD51 and DMC1 form mixed complexes associated with mouse meiotic chromosome cores and synaptonemal complexes. J. Cell Biol. *147*, 207–220.

Taylor, M.R.G., Špírek, M., Chaurasiya, K.R., Ward, J.D., Carzaniga, R., Yu, X., Egelman, E.H., Collinson, L.M., Rueda, D., Krejci, L., et al. (2015). Rad51 Paralogs Remodel Pre-synaptic Rad51 Filaments to Stimulate Homologous Recombination. Cell *162*, 271–286.

Terasawa, M., Ogawa, H., Tsukamoto, Y., Shinohara, M., Shirahige, K., Kleckner, N., and Ogawa, T. (2007). Meiotic recombination-related DNA synthesis and its implications for cross-over and non-cross-over recombinant formation. Proc Natl Acad Sci U S A *104*, 5965–5970.

Thacker, D., Mohibullah, N., Zhu, X., and Keeney, S. (2014). Homologue engagement controls meiotic DNA break number and distribution. Nature *510*, 241–246.

Thompson, D.A., and Stahl, F.W. (1999). Genetic control of recombination partner preference in yeast meiosis. Isolation and characterization of mutants elevated for meiotic unequal sister-chromatid recombination. Genetics *153*, 621–641.

Tsai, S.-P., Su, G.-C., Lin, S.-W., Chung, C.-I., Xue, X., Dunlop, M.H., Akamatsu, Y., Jasin, M.,

Sung, P., and Chi, P. (2012). Rad51 presynaptic filament stabilization function of the mouse Swi5-Sfr1 heterodimeric complex. Nucleic Acids Research *40*, 6558–6569.

Tsubouchi, H., and Roeder, G.S. (2004). The Budding Yeast Mei5 and Sae3 Proteins Act Together With Dmc1 During Meiotic Recombination. Genetics *168*, 1219–1230.

Tsubouchi, H., and Roeder, G.S. (2002). The Mnd1 protein forms a complex with Hop2 to promote homologous chromosome pairing and meiotic double-strand break repair. Mol Cell Biol *22*, 3078–3088.

Tsubouchi, H., and Roeder, G.S. (2003). The Importance of Genetic Recombination for Fidelity of Chromosome Pairing in Meiosis. Developmental Cell *5*, 915–925.

Tsubouchi, H., and Roeder, G.S. (2006). Budding yeast Hed1 down-regulates the mitotic recombination machinery when meiotic recombination is impaired. Genes & Development *20*, 1766–1775.

Tsubouchi, T., Zhao, H., and Roeder, G.S. (2006). The meiosis-specific zip4 protein regulates crossover distribution by promoting synaptonemal complex formation together with zip2. Developmental Cell *10*, 809–819.

Uanschou, C., Ronceret, A., Harder, Von, M., De Muyt, A., Vezon, D., Pereira, L., Chelysheva, L., Kobayashi, W., Kurumizaka, H., Schlögelhofer, P., et al. (2013). Sufficient amounts of functional HOP2/MND1 complex promote interhomolog DNA repair but are dispensable for intersister DNA repair during meiosis in Arabidopsis. Plant Cell *25*, 4924–4940.

Unal, E., Heidinger-Pauli, J.M., and Koshland, D. (2007). DNA double-strand breaks trigger genome-wide sister-chromatid cohesion through Eco1 (Ctf7). Science *317*, 245–248.

Uringa, E.-J., Baldeyron, C., Odijk, H., Wassenaar, E., van Cappellen, W.A., Maas, A., Hoeijmakers, J.H.J., Baarends, W.M., Kanaar, R., and Essers, J. (2015). A mRad51-GFP antimorphic allele affects homologous recombination and DNA damage sensitivity. DNA Repair (Amst.) *25*, 27–40.

van de Linde, S., Wolter, S., Heilemann, M., and Sauer, M. (2010). The effect of photoswitching kinetics and labeling densities on super-resolution fluorescence imaging. *149*, 260–266.

van der Heijden, T., Seidel, R., Modesti, M., Kanaar, R., Wyman, C., and Dekker, C. (2007). Real-time assembly and disassembly of human RAD51 filaments on individual DNA molecules. Nucleic Acids Research *35*, 5646–5657.

Vignard, J., Siwiec, T., Chelysheva, L., Vrielynck, N., Gonord, F., Armstrong, S.J., Schlögelhofer, P., and Mercier, R. (2007). The Interplay of RecA-related Proteins and the MND1–HOP2 Complex during Meiosis in Arabidopsis thaliana. PLoS Genet *3*, e176.

Villeneuve, A.M., and Hillers, K.J. (2001). Whence meiosis? Cell *106*, 647–650.

Voelkel-Meiman, K., Taylor, L.F., Mukherjee, P., Humphryes, N., Tsubouchi, H., and

MacQueen, A.J. (2013). SUMO localizes to the central element of synaptonemal complex and is required for the full synapsis of meiotic chromosomes in budding yeast. PLoS Genet *9*, e1003837.

Wan, L., de los Santos, T., Zhang, C., Shokat, K., and Hollingsworth, N.M. (2004). Mek1 kinase activity functions downstream of RED1 in the regulation of meiotic double strand break repair in budding yeast. Mol Biol Cell *15*, 11–23.

Wittung, P., Ellouze, C., Maraboeuf, F., Takahashi, M., and Nordén, B. (1997). Thermochemical and Kinetic Evidence for Nucleotide-Sequence-Dependent RECA-DNA Interactions. Eur J Biochem *245*, 715–719.

Wright, W.D., and Heyer, W.-D. (2014). Rad54 functions as a heteroduplex DNA pump modulated by its DNA substrates and Rad51 during D loop formation. Mol Cell *53*, 420–432.

Wurm, C.A., Suppanz, I.E., Stoldt, S., and Jakobs, S. (2010). Rapid FlAsH labelling in the budding yeast Saccharomyces cerevisiae. J Microsc *240*, 6–13.

Yu, X., and Egelman, E.H. (2010). Helical Filaments of Human Dmc1 Protein on Single-Stranded DNA: A Cautionary Tale. Journal of Molecular Biology *401*, 544–551.

Yuan, J., and Chen, J. (2011). The role of the human SWI5-MEI5 complex in homologous recombination repair. Journal of Biological Chemistry *286*, 9888–9893.

Zakharyevich, K., Ma, Y., Tang, S., Hwang, P.Y.-H., Boiteux, S., and Hunter, N. (2010). Temporally and biochemically distinct activities of Exo1 during meiosis: double-strand break resection and resolution of double Holliday junctions. Mol Cell *40*, 1001–1015.

Zelensky, A., Kanaar, R., and Wyman, C. (2014). Mediators of homologous DNA pairing. Cold Spring Harb Perspect Biol *6*, a016451.

Zhang, L., Kim, K.P., Kleckner, N.E., and Storlazzi, A. (2011). Meiotic double-strand breaks occur once per pair of (sister) chromatids and, via Mec1/ATR and Tel1/ATM, once per quartet of chromatids. Proc Natl Acad Sci U S A *108*, 20036–20041.

Zhang, Z., Fan, H.-Y., Goldman, J.A., and Kingston, R.E. (2007). Homology-driven chromatin remodeling by human RAD54. Nat Struct Mol Biol *14*, 397–405.

Zhao, W., Saro, D., Hammel, M., Kwon, Y., Xu, Y., Rambo, R.P., Williams, G.J., Chi, P., Lu, L., Pezza, R.J., et al. (2014). Mechanistic insights into the role of Hop2-Mnd1 in meiotic homologous DNA pairing. Nucleic Acids Research *42*, 906–917.

Zickler, D., and Kleckner, N. (1999). Meiotic Chromosomes: Integrating Structure and Function. Annu. Rev. Genet. *33*, 603–754.

Zierhut, C., Berlinger, M., Rupp, C., Shinohara, A., and Klein, F. (2004). Mnd1 Is Required for Meiotic Interhomolog Repair. Current Biology *14*, 752–762.

Zürn, A., Klenk, C., Zabel, U., Reiner, S., Lohse, M.J., and Hoffmann, C. (2010). Site-specific, orthogonal labeling of proteins in intact cells with two small biarsenical fluorophores. Bioconjug. Chem. *21*, 853–859.